TURUN
YLIOPISTO
UNIVERSITY
OF TURKU

SEARCHING ANTIBODIES FOR GELSOLIN AMYLOIDOSIS

Discovery and optimization of anti-AGelD187N antibodies

Laura Leimu

TURUN YLIOPISTON JULKAISUJA – ANNALES UNIVERSITATIS TURKUENSIS
SARJA – SER. D OSA – TOM. 1878 | MEDICA – ODONTOLOGICA | TURKU 2025

TURUN
YLIOPISTO
UNIVERSITY
OF TURKU

SEARCHING ANTIBODIES FOR GELSOLIN AMYLOIDOSIS

Discovery and optimization of anti-AGelD187N antibodies

Laura Leimu

TURUN YLIOPISTON JULKAISUJA – ANNALES UNIVERSITATIS TURKUENSIS
SARJA – SER. D OSA – TOM. 1878 | MEDICA – ODONTOLOGICA | TURKU 2025

University of Turku

Faculty of Medicine
Institute of Biomedicine
Pharmacology, Drug Development and Therapeutics
Drug Research Doctoral Programme

Supervised by

Professor Ullamari Pesonen, PhD
Institute of Biomedicine
Integrative Physiology and
Pharmacology Research
University of Turku
Turku, Finland

Professor Antti Haapalinna, PhD
External Science and Partnering
Research and Development
Orion Pharma
Orion Corporation
Turku, Finland

Reviewed by

Professor Jan Gettemans, PhD
Department of Biomolecular Medicine
Faculty of Medicine and Health Sciences
Ghent University
Ghent, Belgium

Associate Professor Sari Atula, MD, PhD
Department of Clinical Neurosciences
Neurology
University of Helsinki
Helsinki, Finland

Opponent

Professor Timo Myöhänen, PhD
Department of Pharmacology
Faculty of Medicine
University of Helsinki
Helsinki, Finland

ISBN 978-952-02-0146-3 (PRINT)
ISBN 978-952-02-0147-0 (PDF)
ISSN 0355-9483 (Print)
ISSN 2343-3213 (Online)
Painosalama, Turku, Finland 2025

Dedicated to my family

UNIVERSITY OF TURKU
Faculty of Medicine
Institute of Biomedicine
Pharmacology, Drug Development and Therapeutics
LAURA LEIMU: Searching antibodies for gelsolin amyloidosis: discovery and optimization of anti-AGelD187N antibodies
Doctoral Dissertation, 152 pp.
Drug Research Doctoral Programme
May 2025

ABSTRACT

Protein-misfolding diseases comprise a large and growing group of human disorders. Their common feature is that a protein or part of it begins to aggregate unnaturally in the body, causing different clinical manifestations. Gelsolin amyloidosis is a hereditary systemic protein-misfolding disease caused by a point mutation in the gelsolin gene. As a result of the mutation, plasma gelsolin is proteolytically cleaved and an amyloidogenic fragment of plasma gelsolin, AGelD187N, is formed. AGelD187N aggregates in different organs, leading to ophthalmological, neurological, cutaneous, and oral symptoms starting from young adulthood. As with most protein-misfolding diseases, only symptomatic treatments are available for gelsolin amyloidosis, highlighting a significant need for disease-modifying therapy.

In this study, antibody fragments were discovered that inhibited the pathological aggregation of AGelD187 efficiently *in vitro*. First, an aggregation assay was developed, in which the aggregation process of AGelD187N from monomers to amyloid fibrils could be monitored on a scale that allowed the evaluation of the functional impact of potential aggregation inhibitors. Next, AGelD187N-binding antibody fragments isolated from synthetic libraries using phage display technology were evaluated in the assay. All tested antibody fragments reduced AGelD187N aggregation, and two blocked it completely. After converting the most promising antibody fragment into a full-length antibody, the colloidal stability of the antibody was improved using mammalian display technology. The high colloidal stability of the antibody allows it to be developed into a subcutaneous drug product that requires high antibody concentrations.

The fully human and drug-like anti-AGelD187N antibodies presented in this study may provide a promising starting point for a disease-modifying treatment for gelsolin amyloidosis. Before that, the bioavailability and functional effect of the developed antibodies need to be studied in a transgenic mouse model. However, the antibodies presented in this study can already be used in fundamental research on gelsolin amyloidosis and as diagnostic tools for the disease.

KEYWORDS: protein misfolding, gelsolin amyloidosis, therapeutic antibodies, aggregation inhibition, developability

TURUN YLIOPISTO
Lääketieteellinen tiedekunta
Biolääketieteen laitos
Farmakologia, lääkekehitys ja lääkehoito
LAURA LEIMU: Vasta-aineiden etsintä gelsoliiniamyloidoosiin: anti-AGelD187N vasta-aineiden löytäminen ja optimointi
Väitöskirja, 152 s.
Lääketutkimuksen tohtoriohjelma
Toukokuu 2025

TIIVISTELMÄ

Proteiinien laskostumissairaudet muodostavat suuren ja kasvavan joukon ihmisten sairauksia. Niiden yhteinen piirre on, että proteiini tai sen osa alkaa aggregoitua luonnottomasti kehossa aiheuttaen erilaisia kliinisiä ilmenemismuotoja. Gelsoliini-amyloidoosi on perinnöllinen systeeminen proteiinien laskostumissairaus, jonka aiheuttaa gelsoliinigeenin pistemutaatio. Mutaation seurauksena plasman gelsoliini pilkkoutuu ja muodostuu plasman gelsoliinin amyloidogeeninen fragmentti, AGelD187N. AGelD187N aggregoituu eri elimissä, mikä johtaa silmän, hermoston, ihon ja suun oireisiin nuoresta aikuisuudesta alkaen. Kuten useimpiin proteiinien laskostumissairauksiin, myös gelsoliiniamyloidoosiin on saatavilla vain oireen-mukaisia hoitoja, mikä korostaa merkittävää tarvetta sairauden kulkua hidastavalle hoidolle.

Tässä tutkimuksessa löydettiin vasta-ainefragmentteja, jotka estivät AGelD187N:n patologista aggregaatiota tehokkaasti *in vitro*. Ensin kehitettiin menetelmä, jossa AGelD187N:n aggregaatioprosessia monomeereistä amyloidi-säikeiksi voitiin seurata sellaisessa mittakaavassa, joka mahdollisti aggregaatio-inhibittorien toiminnallisten vaikutusten arvioinnin. Seuraavaksi arvioitiin synteettisistä kirjastoista faaginäyttötekniikalla eristettyjä AGelD187N:ään sitoutuvia vasta-ainefragmentteja menetelmässä. Kaikki testatut vasta-ainefragmentit vähensivät AGelD187N:n aggregaatiota, ja kaksi esti sen täysin. Kun lupaavin vasta-aine-fragmentti oli muunnettu kokonaiseksi vasta-aineeksi, vasta-aineen kolloidista sta-biiliutta parannettiin nisäkässolunäyttötekniikalla. Korkea kolloidinen stabiilisuus mahdollistaa sen, että vasta-aineesta voidaan kehittää ihonalaisesti annosteltava lääkevalmiste, joka vaatii korkeita vasta-ainepitoisuuksia.

Tässä tutkimuksessa esitetyt lääkkeenkaltaiset ihmisen anti-AGelD187N-vasta-aineet voivat tarjota lupaavan lähtökohdan gelsoliiniamyloidoosia hidastavalle lääkehoidolle. Tätä ennen kehitettyjen vasta-aineiden biologinen hyötyosuus ja toiminnallinen vaikutus on tutkittava siirtogeenisessä hiirimallissa. Tutkimuksessa esitettyjä vasta-aineita voidaan kuitenkin jo nyt käyttää gelsoliiniamyloidoosin perustutkimuksessa sekä taudin diagnostisina työkaluina.

AVAINSANAT: proteiinien laskostumishäiriö, gelsoliiniamyloidoosi, terapeuttiset vasta-aineet, aggregaation esto, kehitettävyys

Table of Contents

Abbreviations

Aβ	Amyloid beta
AC-SINS	Affinity-capture self-interaction spectroscopy
AGel	Amyloidogenic fragment of plasma gelsolin
AL	Amyloidogenic immunoglobulin light chain
APR	Aggregation-prone region
ATTR	Amyloid transthyretin
BLI	Biolayer interferometry
CDR	Complementarity-determining region
chip CE-SDS	Chip-based capillary gel electrophoresis
CHO	Chinese hamster ovary
DLS	Dynamic light scattering
Fab	Antigen-binding fragment of antibody
FACS	Fluorescence-activated cell sorting
Fc	Crystallizable fragment of antibody
IDP	Intrinsically disordered protein
IgG	Immunoglobulin isotype G
K_D	Equilibrium dissociation constant
mAb	Monoclonal antibody
MALS	Multiangle light scattering
nanoDSF	Nano-differential scanning fluorimetry
PBS	Phosphate-buffered saline
RP-HPLC	Reversed-phase high-performance liquid chromatography
scFv	Single-chain variable fragment
SEC	Size exclusion chromatography
SPR	Surface plasmon resonance
TEM	Transmission electron microscopy
ThT	Thioflavin T
T_m	Temperature midpoint of thermal unfolding
TNF	Tumor necrosis factor
VH	Variable heavy domain of antibody
VL	Variable light domain of antibody

List of Original Publications

This dissertation is based on the following original publications, which are referred to in the text by their Roman numerals:

I Leimu L, Haavisto O, Nesati V, Holm P, Haapalinna A, Salbo R, Pesonen U. Development of an *in vitro* aggregation assay for long synthetic polypeptide, amyloidogenic gelsolin fragment AGelD187N 173-242. *PLoS ONE*, 2023; 18(8): e0290179.

II Leimu L, Holm P, Gąciarz A, Haavisto O, Prince S, Pesonen U, Huovinen T, Lamminmäki U. Epitope-specific antibody fragments block aggregation of AGelD187N, an aberrant peptide in gelsolin amyloidosis. *Journal of Biological Chemistry*, 2024; 300(8): 107507.

III Leimu L, Huhtinen O, Lankinen E, Kulmala A, Vilkman A, Nelson B. Using mammalian display to mature anti-AGelD187N antibody for subcutaneous delivery. *Manuscript.*

1 Introduction

Protein-misfolding diseases are a large group of increasingly common human disorders, including Alzheimer´s and Parkinson´s diseases, type II diabetes, and several systemic amyloidoses.[1] Most protein-misfolding diseases are commonly associated with aging or unhealthy lifestyles, but otherwise, they are poorly understood because of their multifactorial disease etiology and diverse disease course.[2,3]

Gelsolin amyloidosis is a hereditary systemic amyloidosis with a straightforward and well-understood pathophysiology.[4] An autosomal dominant mutation in the gelsolin gene leads to the cleavage of plasma gelsolin and the formation of amyloidogenic fragments in the extracellular matrix. The main amyloidogenic fragment, AGelD187N 173-242, is a 70-residue polypeptide comprising amino acids 173-242 of original plasma gelsolin and that has a substitution of the aspartic acid at position 187 to an asparagine. This intrinsically disordered 8-kDa fragment aggregates in the basement membranes of many epithelial cell types, smooth and striated muscle cells, elastic fibers, and the arterial walls of nearly every organ, including peripheral, autonomic, and central nervous systems.[5-8] Amyloid deposition leads to various ophthalmological, neurological, cutaneous, and oral symptoms starting from young adulthood.[9] Together with repeated surgeries, they cause a clinically significant disease burden for the patients. As for most protein-misfolding diseases, only symptomatic treatments are available, and there is a high unmet medical need for better therapy. Advancements in finding disease-modifying treatments for gelsolin amyloidosis could inspire and guide the efforts of tackling more complex protein-misfolding diseases that affect countless individuals and society as a whole.

A promising strategy for preventing the progression of a misfolding disease is to inhibit the formation of harmful protein aggregates. The ability to imitate the aggregation process of the disease-causing protein is essential for evaluating the functional effect of potential aggregation inhibitors.[10] *In vitro* aggregation assays, where a single protein is monitored in isolation, provide an excellent tool for this purpose. However, one important practical issue in assay development needs to be resolved. Many amyloid proteins aggregate slowly *in vivo*.[11,12] To execute the

aggregation process in a laboratory time scale, amyloid formation can be accelerated by using relatively high protein concentrations. As a result, the amyloidogenic protein is needed in large quantities. This issue is especially emphasized when screening multiple inhibitors at multiple concentrations. Moreover, the quality of the amyloidogenic protein must be high. Monomeric protein must be free not only of other molecular species but also of any small aggregates.[13] Insufficient purity may lead to weak or irreproducible aggregation. The purity requirement further exacerbates the problem of material availability. Although the size of the protein can become a limiting factor, chemical synthesis could solve the material availability problem.[14-16]

Earlier suggested AGelD187N aggregation inhibitors have been small molecules or peptides with limited or nonexistent binding data to AGelD187N.[17-20] Despite promising aggregation inhibition *in vitro,* this raises a concern about their effectiveness *in vivo.* Antibodies have a high specificity and binding affinity to their target and a proven track record as therapeutic agents. A broad array of antibodies has been developed against various proteins and peptides associated with protein misfolding diseases.[21-29] Van Overbeke et al. have generated nanobodies against AGelD187N by immunizing a dromedary.[30] Phage display is an efficient and rapid *in vitro* method for discovering fully human antibody fragments.[31] Phage display libraries can comprise huge diversities exceeding 10^{11} unique antibody clones, which means high-affinity antibody fragments can be readily obtained from universal libraries.[32] Although a well-performed phage display campaign often results in high-affinity antibody fragments, affinity to the target and effective biological function are not the only properties a therapeutic antibody must have.[33] As gelsolin amyloidosis is a lifelong disease beginning at a young age, the antibody's biophysical properties must allow the development of a high-concentration subcutaneous drug product that can be self-administered. Mammalian display is a novel *in vitro* selection technology that features whole antibodies presented on the surface of mammalian cells.[34] Despite the limited library sizes, mammalian display platforms can mimic the antibody selection process *in vivo*, in which high affinity and good biophysical properties are simultaneously achieved.[35,36]

This thesis work was done to find drug-like antibodies that could prevent the aggregation of the amyloidogenic gelsolin fragment AGelD187N. It includes three separate studies: study I describes the development of an *in vitro* aggregation assay for AGelD187N using synthetic polypeptide, study II the discovery of anti-AGelD187N antigen-binding fragments (Fabs) using phage display and demonstration of their ability to inhibit the AGelD187N aggregation, and study III the optimization of anti-AGelD187N antibody for therapeutic purposes using mammalian display.

2 Review of the Literature

2.1 Protein-misfolding diseases

2.1.1 Pathophysiology

Most newly synthesized polypeptide chains fold into well-defined, stable structures that control biological function through precise molecular interactions.[37] According to the original thermodynamic hypothesis, protein folding occurs spontaneously because the native conformation of the protein is the one in which the Gibbs free energy of the whole system is lowest.[38] The protein's amino acid sequence and the cellular environment surrounding the polypeptide chain drive the formation of a unique three-dimensional structure. In reality, a protein molecule can adopt multiple different conformational states during its lifetime within a living system.[1] The folding process is highly complex, involving several intermediate states and rate-limiting steps.[37] The proteostasis network, comprising molecular chaperones, proteolytic machineries, and their regulators, ensures that proteins are correctly folded, conserved, and degraded.[39,40] It has been estimated that 70% of globular proteins in the human proteome possess intrinsically disordered regions (IDRs) that lack long-lived stable structures but still mediate essential cellular interactions.[41] Around 1 % of proteins in the human proteome are entirely unfolded and called intrinsically disordered proteins (IDPs). A suggested role of intrinsically disordered regions and proteins is that they act as interaction hubs, which can bind to several different targets through an induced fit mechanism.[42]

While protein aggregation linked to disease has been found to involve both globular and disordered proteins, IDPs are overrepresented.[1] Aggregation-prone regions (APRs) in protein sequences are short stretches of amino acids with high hydrophobicity, low net charge, and a strong tendency to form homomeric intermolecular β-sheets, thereby driving protein aggregation.[43] APRs are needed in the hydrophobic core formation of globular proteins and protein-protein interaction sites. While globular proteins contain more APRs than IDPs, in IDPs, APRs are not buried inside the hydrophobic core and are therefore particularly susceptible to self-assembly.[44] Many proteins involved in protein-misfolding diseases are expressed beyond their solubility limit in healthy tissues, meaning that they are

supersaturated.[45,46] A Significant amount of metabolic energy is needed to maintain proteostasis. Exposure to intrinsic and extrinsic factors, like aging, alterations in physiology, and environmental stress, challenges the proteostasis network.[39,47,48] Once the proteostasis network is overwhelmed, the metastable proteins can no longer be maintained in a soluble state. Protein aggregation can also occur because of specific mutations within the gene coding for the protein.[1] Disease-causing mutations can destabilize the native conformations, making proteins susceptible to aggregation either directly or following proteolytic cleavage.[4,49-53] Mutations can also cause duplication or triplication of the gene, resulting in a higher concentration of the aggregation-prone protein[54,55] or a change in the stop codon for translation, resulting in aggregation-prone truncations or extensions.[56-58] The fact that all the disease-causing mutations in protein-misfolding diseases increase the aggregation propensity of the protein provides strong evidence that protein aggregation is a primary rather than a secondary event in the pathogenesis of these diseases.[1]

Like protein folding, protein aggregation is a highly complex process involving constant interconversions between aggregated species.[1,37,43,59] Globular proteins need to unfold partially or fully before their aggregation is possible. The first early aggregates, also called oligomers, are relatively disorganized structures with little or no secondary structure. However, soon the APRs of the proteins engage in extended intermolecular parallel or antiparallel β-sheet with identical counterparts in a sequence-specific manner. When the aggregates grow, usually the average β-sheet content of the oligomers increases, suggesting that more organized structures are appearing. Fibrillar morphologies called protofilaments have formed when multiple β-sheets align length-wise and extensively interact through the interdigitation of their sidechains to cross-β structures. (Please refer to Chapter 2.3.1 for more information on amyloid structure). Most deposits associated with protein-misfolding diseases consist of mature amyloid fibrils with several coiled protofilaments, although also native-like and amorphous deposits have links to human disease.[1] All amyloid structures share the highly stable cross-β structure, but otherwise, they exhibit significant polymorphism.[60] Some amyloid proteins are known to adopt different amyloid polymorphs with links to different pathologies and toxicities.[61-63] The gain-of-toxic function related to amyloidogenic proteins is mostly caused by the small soluble oligomers that are present transiently during the fibril assembly.[64-66] Their exposed hydrophobic amino acid residues and unpaired β-strands are harmful to cells as they interact with cellular proteins and membranes.[39] However, mature fibrils can also cause toxicity through mechanical perturbations and sequestration of cellular factors.[67,68] Also, large quantities of insoluble protein can physically disrupt specific organs.[69]

2.1.2 Classification

As clinical manifestations of protein-misfolding diseases are often heterogeneous and may be influenced by several aggregating proteins and genetic and environmental factors, the diseases should be classified based on the fibril protein.[70] According to the recommendations by the Nomenclature Committee of the International Society of Amyloidosis (ISA), the amyloid is termed A (for amyloid) followed by an abbreviation of the precursor protein (e.g., ATTR for transthyretin amyloid protein).[71] Currently, the number of known human amyloid fibril proteins is 42. Of these, 14 appear solely as systemic deposits, 24 are found exclusively in localized amyloid, and 4 can manifest in both types. Around a third of the protein-misfolding diseases have been reported to have a hereditary form of the disease, which is often linked to an autosomal dominant mutation within the gene encoding the protein. ISA recommends that the letter "v" should be used after the fibril protein name to specify the variant fibril protein (e.g., ATTRv for variant transthyretin amyloid protein). Additionally, the variant protein can be further specified according to the mature protein's substitution or deletion (e.g., ATTRV30M, valine to methionine). Sporadic forms of the disease can be specified with "wt" after the fibril protein name to specify the wild-type fibril protein (e.g., ATTRwt).

In the clinical context, the term amyloidosis generally refers to rare, severe, and difficult-to-diagnose systemic conditions in which fibrils deposit in a range of tissues, including the heart, spleen, liver, and kidney, and cause organ dysfunction.[72,73] Light-chain amyloidosis (AL amyloidosis), the most common systemic amyloidosis, is caused by unstable immunoglobulin light chains.[70] Other systemic amyloidosis include serum amyloid protein A amyloidosis (AA amyloidosis) and transthyretin amyloidosis (ATTR amyloidosis). The most common hereditary systemic amyloidosis worldwide is ATTRv amyloidosis, with more than 120 known mutations.[74] Many localized amyloid diseases are neuropathic or endocrine and largely sporadic.[75] Six precursor proteins are associated with neurodegenerative diseases, of which amyloid-β (Aβ) is mostly associated with Alzheimer´s disease, α-synuclein (α-syn) with Parkinson´s disease, and tau (τ) with frontotemporal dementia with Parkinsonism.[71] Islet amyloid polypeptide (IAPP) is associated with the most prevalent non-neuropathic localized amyloid disease, type II diabetes.[76] Certain amyloid diseases originate because of the ingestion or iatrogenic transmission of preformed fibrillar aggregates.[77-79]

In addition to amyloid fibrils, e.g., immunoglobulins or their subunits have been found to form extracellular amorphous deposits (light-chain deposition disease) and native-like structures (Berger disease).[1] In many intracellular inclusions, the structural composition of pathological protein aggregates is not confirmed.[71] These include TAR DNA-binding protein 43 (TDP-43) and huntingtin exon 1 (HttEx1) associated with amyotrophic lateral sclerosis and Huntington´s disease, respectively.

2.1.3 Disease-modifying treatments

In the past, and still in many cases today, the only way to treat protein-misfolding diseases has been limited to preventing and managing complications through symptomatic or supportive therapy.[80-84] Despite high unmet medical needs, the development of disease-modifying pharmacotherapies for protein-misfolding diseases has been slow due to the unknown and complex pathophysiology of the diseases and difficulties in timely diagnosis.[1] For a very long time, organ transplantation was the only option to modify the disease course of systemic amyloidoses.[85-88] However, recently significant progress has been made in treating these diseases with disease-modifying drugs. Currently approved disease-modifying treatments for protein-misfolding diseases are listed in Table 1.

Table 1. Approved disease-modifying treatments for protein-misfolding diseases (May 2025).

Indication	Treatment	Mode of action	First approval
ATTRv-PN ATTR-CM	tafamidis (small molecule)	TTR tetramer stabilization	2011[89] 2019[84,90]
ATTRv-PN	patisiran (siRNA)	prevention of the synthesis of TTR	2018[91]
ATTRv-PN	inotersen (ASO)	prevention of the synthesis of TTR	2018[92,93]
ATTRv-PN	vutrisiran (siRNA)	prevention of the synthesis of TTR	2022[94]
ATTRv-PN	eplontersen (ASO)	prevention of the synthesis of TTR	2023[95]
AL amyloidosis	daratumumab (mAb) with VCD	Killing of plasma cells that produce aberrant light chains	2021[87]
Alzheimer´s disease	aducanumab (mAb)	Aβ deposit clearance in brains by microglial-mediated phagocytosis	2021[96] discontinued
Alzheimer´s disease	lecanemab (mAb)	Neutralization of cytotoxic Aβ oligomers and prevention of plaque formation	2023[97]
Alzheimer´s disease	donanemab (mAb)	Aβ deposit clearance in brains by microglial-mediated phagocytosis	2024[98]

ATTRv-PN, variant transthyretin amyloidosis with polyneuropathy; ATTR-CM, transthyretin amyloidosis with cardiomyopathy; TTR, transthyretin; siRNA, short interfering RNA; ASO, antisense oligonucleotide; AL amyloidosis, light chain amyloidosis; mAb, monoclonal antibody; VCD, bortezomib-cyclophosphamide-dexamethasone combination; Aβ, amyloid-β

The first approved disease-modifying treatment for a protein-misfolding disease was small molecule tafamidis for variant ATTR amyloidosis with polyneuropathy (ATTRv-PN). Tafamidis binds selectively to the two thyroxine-binding sites of the TTR tetramer, kinetically stabilizes the protein, and prevents its dissociation into amyloidogenic monomers.[99] Gene silencers, partisan and inotersen, were approved for the same indication seven years later. Patisiran is a double-stranded RNA fragment (short interfering RNA, siRNA) encapsulated in lipid nanoparticles, and

inotersen is a chemically modified single-strand antisense oligonucleotide (ASO). Both bind to TTR mRNA and inhibit the synthesis of TTR in the liver, thereby slowing down the aggregation of TTR and the progression of the disease.[100-102] These treatments and their successors have improved clinical outcomes for patients with ATTR amyloidosis significantly during the past decade.[90] AL amyloidosis is caused by unstable circulating immunoglobulin light chains produced by an aberrant plasma cell clone in bone marrow.[103] Daratumumab is a high-affinity human monoclonal antibody (mAb) that targets CD38, an antigen found in all plasma cells, leading to plasma cell death through various mechanisms.[104] Daratumumab was the first licensed treatment for AL amyloidosis in combination with cytotoxic agents bortezomib, cyclophosphamide, and dexamethasone. Deep hematological and organ responses were achieved in patients with less-advanced disease, offering a new therapeutic backbone for AL amyloidosis.[87]

Over the past few decades, more than 200 clinical trials have evaluated over 30 anti-Aβ immunotherapies as potential treatments for Alzheimer´s disease.[105] Recently, monoclonal antibodies aducanumab, lecanemab, and donanemab have been approved by the U.S. Food and Drug Administration (FDA). Aducanumab is selective for fibrillar and oligomeric Aβ due to low monovalent affinity and high avidity for epitope-rich aggregates.[106] Donanemab binds selectively to a truncated and modified form of Aβ, $Aβ_{p3-42}$, that is only present in Aβ plaques.[107] Both aducanumab and donanemab induce the Aβ deposit clearance in brains by triggering microglial-mediated phagocytosis and subsequent peptide degradation.[107-109] Lecanemab binds to soluble Aβ oligomers and protofibrils with high selectivity over monomer and insoluble fibrils.[110] Lecanemab neutralizes cytotoxic Aβ protofibrils and prevents plaque formation.[110,111] The clinical benefits of these so-called 3rd generation anti-amyloid immunotherapies are still rather modest and associated with amyloid-related imaging abnormalities (ARIA).[112-115] Biogen discontinued aducanumab in 2024 due to reprioritization. Earlier disease intervention and combination therapy that targets also other pathological mechanisms in Alzheimer´s disease have been suggested as possible solutions to improve the efficacy of anti-Aβ immunotherapies.[116]

These first approvals and an increasing understanding of the pathophysiology of protein-misfolding diseases pave the way for new approvals. The high prevalence of neurodegenerative diseases ensures that the intensive search for disease-modifying therapies continues. Also, for systemic amyloidoses, there are several different treatments, including anti-amyloid immunotherapies and a gene-editing agent, under development.[117-121]

2.2 Gelsolin amyloidosis

2.2.1 History and epidemiology

Jouko Meretoja first described a previously unrecognized heritable syndrome with corneal lattice dystrophy, progressive cranial neuropathy, and skin changes in 1969.[122] This systemic amyloidosis was autosomal dominantly inherited and had a high prevalence in two areas in Finland.[123] From those times on, the disease has been referred to as Meretoja disease or familial amyloidosis of Finnish type (FAF), although after the original report from Finland, cases have been detected worldwide.[124] In 1990, two individual groups demonstrated that the amyloid fibrils in patients´ tissues were composed of fragments of gelsolin.[125,126] The same year, these groups also reported that the primary cause of the disease was a point mutation 640G>A (earlier known as 654G>A) in the gelsolin gene on chromosome 9.[127,128] A few years later, a second mutation at the same locus, 640G>T (earlier 654G>T), was found in Danish and Czech families causing pathogenetically and clinically similar disease.[129,130]

Gelsolin amyloidosis (AGel amyloidosis) is one of the most common inherited diseases in Finland.[124] Patients have been reported primarily from Finland and they all carry the 640G>A mutation.[131] However, to date, kindreds with a known molecular defect have been reported from Holland, Denmark, Czech, USA, Japan, Great Britain, Spain, Portugal, France, Greece, Sweden, Germany, Norway, Brazil, Iran, India, Mexico, Canada, and Argentina.[124,132,133] Due to the lack of a common founder, the presence of two disease-related mutations, and different disease-associated haplotypes in different countries, it seems likely that gelsolin amyloidosis is caused by a sporadic mutation occurring at low frequency in different populations.[124,129] However, it is possible that in some populations, all families descended from a common ancestor who had the mutation. This might be the case in Finland, as the disease-associated haplotypes in unrelated Finnish families are uniform.[129] The true global prevalence of gelsolin amyloidosis is not known, but the estimated number of Finnish patients varies from 600 to 1000.[124,133]

2.2.2 Pathogenesis

Gelsolin is a calcium-activated, actin-modulating multidomain protein present in most human tissues.[134,135] It consists of six conserved copies of so-called gelsolin domains, named G1 to G6 (Figure 1A). Each gelsolin domain is composed of a 5- or 6-stranded β-sheet between one long and one short α-helix and contains a conserved calcium-binding site. Gelsolin is expressed as two main splicing variants: cytoplasmic and plasma gelsolin. Plasma gelsolin is one of the most abundant

proteins in the blood (>200 µg/ml).[136] Its physiological function is to sequester actin filaments released into the circulation due to injured or dead cells and tissues.[135] Plasma gelsolin is identical to its cytoplasmic form, except for an added 24-residue N-terminal extension. Additionally, it has a 27-residue N-terminal signal peptide that facilitates its delivery to the endoplasmic reticulum and that is cleaved before secretion from the cell. In gelsolin amyloidosis, the calcium-binding site in the G2 domain (Figure 1B) is mutated. The more common mutation, 640G>A in the gelsolin gene changes the aspartic acid at position 187 of plasma gelsolin to an asparagine (D187N).[127,128] The other known mutation, 640G>T, changes the aspartic acid to tyrosine in the same position (D187Y).[129] As a result of both mutations, G2 in variant gelsolin cannot bind calcium and is left unstabilized.[137,138]

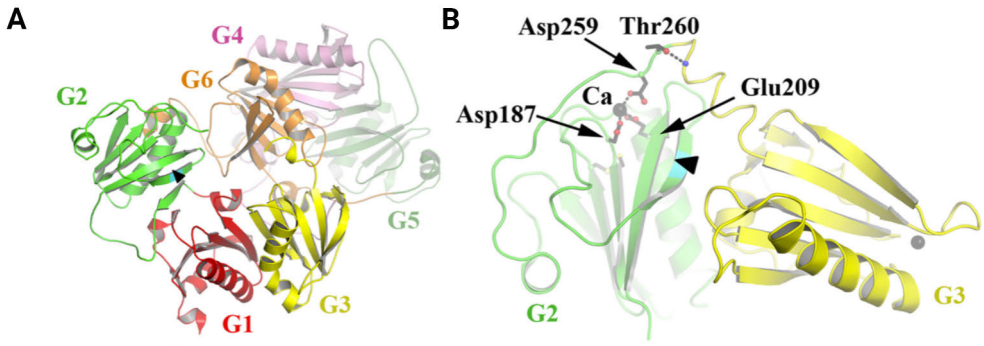

Figure 1. **(A)** The structure of Ca-free human gelsolin. Domains G1-G5 are arranged compactly around the central G6 domain. (**B)** Close-up of the Ca-coordinating residues in the G2 domain from human G1-G3/actin complex. Asp187, Glu209, and Asp259 form the Ca-coordination sphere. Thr260 forms a helix-initiating hydrogen bond that contributes to the close packing of G3 with G2, which protects gelsolin from proteolytic cleavage. The black arrowhead indicates the cleavage site. Modified from [141].

The 81 kDa cytosolic gelsolin is not observed to be affected by the mutations and participate in the amyloidogenesis.[139,140] 83 kDa plasma gelsolin, instead, is directed to secretory compartments of the cell after translation. In the trans-Golgi network, the unstable mutant plasma gelsolin is cleaved between arginine 172 and alanine 173 in G2 by proprotease convertase furin (cleavage site marked by a black arrowhead in Figure 1A and B).[137,141] As a result, a non-amyloidogenic 68 kDa precursor fragment, C68, is formed from the full-length 83 kDa protein. After secretion, this truncated and partly unfolded plasma gelsolin is further cleaved between alanine 242 and methionine 243 in G2 by matrix metalloendoprotease MT1-MMP in the extracellular matrix.[142] This second proteolytic event results in the formation of an 8 kDa amyloidogenic fragment, AGelD187N/Y 173-242, that is the main component of amyloid fibrils in gelsolin amyloidosis patients´ tissues.[125-

[128,143]Also a smaller, 5 kDa fragment AGelD187N 173-225 has been detected from isolated gelsolin amyloid fibrils.[143] It is thought to be formed from the 8 kDa fragment by a second cleavage by MT1-MMP.[142] Domain architecture of the entire plasma gelsolin and the location and amino acid sequences of the aberrant amyloidogenic fragments AGelD187N/Y 173-242 and AGelD187N 173-225 are presented in Figure 2.

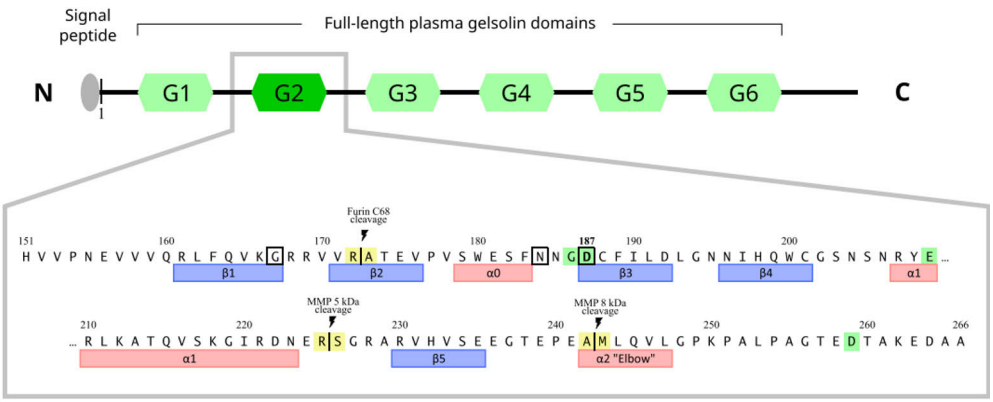

Figure 2. Domain architecture of plasma gelsolin and the location and sequences of amyloidogenic fragments AGelD187N/Y 173-242 and AGelD187N 173-225. Residue numbering excludes the signal peptide. The first vertical bar indicates the first proteolytic cleavage site, which produces the non-amyloidogenic precursor fragment C68 (68 kDa), and the last vertical bar indicates the second proteolytic cleavage site, which produces the major amyloidogenic fragment AGelD187N/Y 173-242 (8 kDa). The vertical bar in the middle indicates the possible third cleavage site that produces the minor amyloidogenic fragment AGelD187N 173-225 (5 kDa). Calcium-coordinating residues of the original G2 domain are marked in green. Also, the secondary structure elements of the original G2 domain are indicated below the sequence, however, both AGelD187N/Y 173-242 and AGelD187N 173-225 are intrinsically disordered. Modified from [138].

The mutations themselves were originally reported to cause the amyloidogenicity of the plasma gelsolin fragments.[144] However, the *in vitro* experiments behind this assumption were made with 7- to 30-residue synthetic peptides resembling only the predicted β-sheet region of the full-length 70-residue fragment. When a recombinant full-length fragment was used, both the wild-type and D187N mutant fragments aggregated, but only in acidic conditions.[145] The amyloid deposition in patients is observed in the basement membrane of the skin, blood vessel walls, central and peripheral nervous system, and the eye.[124] An important finding was that extracellular matrix glycosaminoglycans, especially heparin, accelerated the aggregation of full-length wild-type, D187N, and D187Y gelsolin fragments.[142,146] This study demonstrated that the mutations enable the aberrant proteolytic cleavage of plasma gelsolin, but they do not increase the

aggregation propensity of end-product fragments. Therefore, the gain-of-toxic function is solely caused by the proteolytic cleavage of plasma gelsolin. The tissue-selective deposition of amyloid fibrils observed in gelsolin amyloidosis is likely to be influenced by the cell-type-specific expression of all three: plasma gelsolin, furin, and MT1-MMP, as well as by the extracellular localization of distinct glycosaminoglycans.[137,142,146]

2.2.3 Clinical findings

A national registry for Finnish gelsolin amyloidosis patients (FIN-GAR) was established in 2013-2014 to gather comprehensive information on the symptoms and progression of the disease from as many patients as possible.[133] Information about 227 patients was collected via questionnaires, phone calls, and hospital patient records and was added to the database. Based on FIN-GAR, it was discovered that the first symptoms were typically dry or irritable eyes, followed later by impaired vision, polyneuropathy, facial nerve paresis, and loosening of facial skin (cutis laxa), which developed almost simultaneously. Carpal tunnel syndrome (CTS), cardiac pacemakers, and cardiomyopathy were significantly more common compared to the general population.

The most up-to-date and comprehensive cross-sectional study on AGel amyloidosis, FIN-GAR phase II, started in 2018 and included altogether 261 patients who answered a questionnaire about the known and anticipated symptoms and signs and their time of onset.[9] Also, the lifespan of 478 patients was analyzed using a relative survival (RS) framework. The study showed that patients became symptomatic at the mean age of 39 years and that eye symptoms were the first to appear. The earlier discovered triad of ophthalmological, neurological, and dermatological manifestations was also highly prevalent in this study. The most common symptoms (frequency 75% or more) were dry eyes, corneal lattice amyloidosis, photophobia, impaired vision, drooping eyelids, cutis laxa, dry skin and numbness, tingling, and other paresthesias. Severe cardiac or renal symptoms were uncommon compared to other forms of systemic amyloidosis. However, it is known that patients with AGel amyloidosis can develop severe cardiac or renal amyloidosis, which may result in organ transplantation or even death.[147-149] Although the FIN-GAR phase II study showed that AGel amyloidosis does not shorten the lifespan of the patients at least for the first 75 years, it causes a clinically significant disease burden that can currently be alleviated only with symptomatic or surgical treatment.[9] As many as 65% of the patients had undergone at least one operation, and 45% had multiple skin or soft tissue surgeries.

2.2.4 Suggested disease-modifying treatments

2.2.4.1 Precursor protection

The precursor protein in gelsolin amyloidosis, the C68 fragment, formed after the first intracellular furin cleavage of plasma gelsolin, was found not to be amyloidogenic.[150] Therefore, different strategies to protect C68 from further cleavage to the amyloidogenic 8 kDa fragment were proposed.

Selective MT1-MMP inhibitors, that would inhibit the second proteolytic event in the extracellular matrix, were proposed but never studied for gelsolin amyloidosis.[142,150] Instead of that, chaperone nanobodies that shield C68 or mutant plasma gelsolin from degradation have been studied extensively at Ghent University.[30,151,152] A nanobody is a variable part of a heavy-chain antibody, a specific type of antibody found in camelids that lack light chains.[153] A nanobody consists of a single monomeric variable antibody domain, and it can bind selectively to a specific antigen similar to a common antibody, although it is much smaller (15 kDa compared to 150 kDa). In the first strategy, a dromedary was simultaneously immunized with the G2 domain and the 8 kDa fragment of plasma gelsolin.[30] Discovered nanobodies FAF Nb 1-3 were capable of reducing the formation of 8 kDa fragments by 60-80% *in vitro* by binding to C68. The small size of nanobodies makes them clear rapidly from the blood circulation. Therefore, FAF Nb 1-3 were fused to the albumin-binding nanobody MSA21 to increase the half-lives of the nanobodies before *in vivo* experiments. The D187N gelsolin synthesis and amyloid formation are restricted only to cardiac or striated muscle tissues in the AGel mouse model.[154] Bispecific nanobody FAF Nb2-MSA21 was capable of reducing the amyloid burden by 30% and improving the contractile properties of a certain muscle type (extensor digitorum longus, EDL) in the model.[30]

As nanobodies FAF Nb 1-3 did not completely halt the 8 kDa fragment formation, a second strategy was to target the first step in the proteolytic cascade and shield mutant plasma gelsolin from pathological furin proteolysis with an intrabody.[151] A previously existing gelsolin nanobody Nb11 (GSN Nb11) binding to the G2 was tested for this purpose. It was capable of reducing the formation of C68 fragments by 34% in the furin cleavage assay. It also reduced C68 formation by 80% in HEK293T cells when equipped with an ER signal peptide and co-transfected with mutant plasma gelsolin.[151,155] Developed transgenic mice secreting GSN Nb11 were crossed with AGel mice to generate offspring that express both mutant plasma gelsolin and GSN Nb11. A reduction of amyloid burden by 28% and improvement in EDL contractile properties were observed in double-positive offspring when compared to AGel mice or littermates not expressing GSN Nb11.

To improve the efficacy of the therapy, a third strategy was to combine the earlier two strategies into bispecific nanobodies that were able to simultaneously shield

mutant plasma gelsolin from intracellular furin and extracellular MT1-MMP activity.[152] In a combined furin/MT1-MMP cleavage assay, bivalent Nb11-FAF1-3 nanobodies could reduce the formation of 8 kDa fragments more efficiently than their monovalent counterparts. The *in vivo* study required intracellular delivery of the protective nanobody Nb11-FAF1 by AAV9 gene therapy. A reduction in amyloid burden by 39% in muscle tissue and 43% in heart tissue was observed. EDL contractile properties were indistinguishable from the WT control groups but significantly different from the untreated AGel mice.

2.2.4.2 Aggregation inhibition

Only a few years after the identification of 70-residue AGelD187N/Y 173-242 as the main component of amyloid fibrils in gelsolin amyloidosis patients´ tissues, the so-called amyloidogenic region of AGelD187N 173-242 was defined based on the aggregation propensity of 22 short synthetic peptides resembling the predicted β-sheet forming regions of AGelD187N/Y.[144] The shortest peptide that was capable of forming amyloid-like fibrils was a 9-residue peptide FNNGNCFIL, representing the amino acids 183-191 in AGelD187N 173-242, containing the D187N substitution in its fifth residue. As the wild-type counterpart FNNGDCFIL did not form fibrils, and there was a similar trend observed between other wild-type and mutant peptides investigated, the conclusion was that this sequence motif represented the amyloidogenic region of AGelD187N/Y 173-242.

Based on this study, the aggregation process of a short synthetic stretch of full-length 70-residue AGelD187N 173-242, usually an 11-residue peptide representing amino acids 182-192 (^{182}D187N^{192}), has been monitored in several *in vitro* studies, where the aggregation inhibition has also been attempted.[17-19] Known bioactive compounds, aromatic small molecules curcumin and emetine, have been shown to modulate the aggregation of ^{182}D187N^{192} peptide and produce different types of aggregates compared to each other and to ^{182}D187N^{192} alone.[18] Interestingly, both reduced the cytotoxicity of the ^{82}D187N^{192} aggregates, although curcumin formed rapidly mature fibrils and emetine smaller, off-pathway aggregates. Polylactic-co-glycolic acid (PLGA) nanoparticles were used to improve the solubility of poorly soluble curcumin and emetine.[20] Encapsulating the compounds inside the nanoparticles resulted in lower concentrations needed for aggregation modulation. Methylene blue and epigallocatechin gallate (EGCG) are known modulators of amyloidogenic proteins like amyloid-β or tau.[156-159] They have recently been shown to dissociate aggregates preformed from three different 6- to 10-residue peptides containing the CFILDL motif of AGelD187N 173-242.[17]

In addition to small molecules, peptides have recently been investigated as aggregation inhibitors of ^{182}D187N^{192} peptides.[19] In a structure-based approach Bollati

et al. designed three novel peptides that contain firstly motifs of variable lengths of the ^{182}D187N^{192} peptide and secondly motifs of variable lengths of a presumed flanking sequence spanning residues 194-204 of plasma gelsolin. These two motifs are linked together with a piperidine-pyrrolidine unnatural amino acid that functions as a β-turn inducer. This so-called β-hairpin mimics approach successfully blocked amyloid-β and hIAPP fibril formation.[160,161] The rationale behind this strategy is to interfere with the interactions of the amyloidogenic sequence with a flanking sequence in the native structure of the protein. Two of the peptidomimetics were shown to be effective in inhibiting the aggregation of ^{182}D187N^{192} peptide and the entire G2 domain in a dose-dependent manner. They also counteracted the proteotoxicity of the aggregated ^{182}D187N^{192} peptide in a *Caenorhabditis elegans*-based assay.

2.3 Amyloid formation *in vitro*

2.3.1 Amyloid detection

Amyloid deposits in cells and tissues are composed of long, non-branched fibrous assemblies made up of thousands of protein molecules (Figure 3A).[37] These assemblies have a width of approximately 6-12 nm and can reach lengths of several micrometers. Amyloid fibrils possess a rope-like structure, consisting of one or several protofilaments that are intertwined laterally along the fibril axis (Figure 3B). Similar amyloid structures can also be induced *in vitro* from synthetic or recombinant proteins by diverse experimental systems. All protofilaments share a common secondary conformation called cross-β sheet structure (Figure 3C and D). Polypeptide chains are arranged in a tightly compacted conformation, where intermolecular consecutive β-strands of usually paired β-sheets run perpendicular to the fibril axis.[162,163]

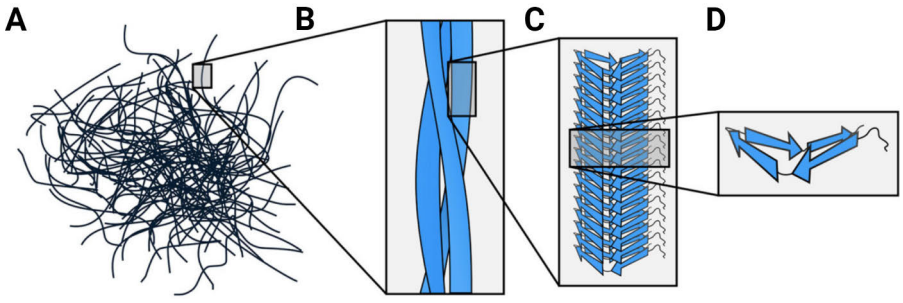

Figure 3. The structure of amyloid fibrils. **(A)** Amyloid deposits are formed of fibrous assemblies called amyloid fibrils. **(B)** Amyloid fibrils are formed by the close lateral association of protofilaments. **(C)** Protofilaments have a characteristic continuous secondary structure called a cross-β structure, where intermolecular β-sheets between monomeric subunits are formed via backbone hydrogen bonding. **(D)** Monomeric subunits contain one or more β-strands that contribute to intermolecular β-sheets. Modified from [163].

The formation of the cross-β motif can be exploited when monitoring the amyloid formation process in real time. Amyloid-specific fluorescent dyes bind to this unique structural entity and change their fluorescence upon binding. Benzathiole dye Thioflavin T (ThT) displays a several orders of magnitude increase in fluorescence intensity when it binds to amyloid fibrils.[164,165] The fluorescence enhancement is due to rotational immobilization of the central C-C bond of ThT (Figure 4A) when it binds to extended channel-like motifs formed by aligned amino acid side chains along solvent-exposed surfaces of fibrils (Figure 4B).[166-169] In solution, free ThT can rotate about its C-C bond. The rotation rapidly quenches excited states, causing low fluorescence emission.[167,170] These photophysical properties of ThT enable real-time in-solution observation of fibril formation and eliminate the need for dye washing. Other advantageous properties of ThT are that it does not affect the aggregation process[171-173] and within an assay system, its fluorescence correlates linearly with amyloid fibril concentration.[165,172] ThT also binds fibrils regardless of the origin of the amyloidogenic protein or state of the aggregation process.[164,165] Due to its sensitivity, universality, and ease of use, ThT has become the most commonly used fluorescent probe to monitor *in vitro* amyloid formation.

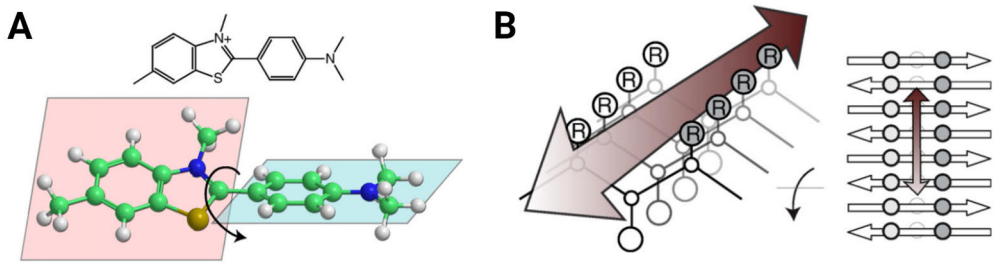

Figure 4. **(A)** The structure of Thioflavin T (ThT). In solution, the benzathiole and benzylamine rings of ThT can rotate freely about their shared C-C bond. **(B)** In amyloid fibrils, ThT binds to the side chain channels along the solvent-exposed surfaces of the fibrils. Binding disables the rotation and preserves the excited state of ThT. Modified from [170].

Despite the advantageous features of ThT, caution is needed when interpreting the results of a ThT-based amyloid formation experiment. The fluorescence brightness varies between fibrils of different amyloidogenic proteins[164,165,172,174] and even between fibrils of different morphologies of the same amyloidogenic protein.[175,176] This is due to more or less favorable ThT binding to different fibril channel types.[168,169,177,178] Experimental conditions and additives can affect ThT fluorescence in various ways. Low pH decreases the ThT fluorescence probably as a result of electrostatic repulsion between the positively charged ThT and the fibril

surface.[179,180] Another amyloid dye, polyethylene glycol, or small molecules investigated as aggregation inhibitors can quench ThT from its binding site on the fibril surface.[177,181,182] Compounds that are spectroscopically active in the ThT fluorescence range, such as certain polyphenols, can interfere with ThT fluorescence.[181] Certain non-fibrillar globular proteins, such as acetylcholinesterase or serum albumins, increase ThT fluorescence via ThT binding to the hydrophobic pockets of the proteins.[183-186]

As a result of the indirectness of ThT as an amyloid reporter, alternative, more direct methods to detect fibrils are needed to validate the results of a ThT-based assay. Transmission electron microscopy (TEM) and atomic force microscopy (AFM) have been used extensively to visualize amyloid fibrils.[187-189] Their nanometre scale resolution allows the detection of the quantity, length, and diameter of the fibrils and prefibrillar structures. The bulk β-sheet content of a sample can be confirmed with circular dichroism (CD) spectroscopy.[190] The existence and size of not-yet-ThT-binding small oligomeric aggregates, which are also recognized as pathogenic species in the aggregation process,[191] can be detected with size exclusion chromatography combined with multiangle light scattering (SEC-MALS).[192,193]

2.3.2 Kinetics of amyloid formation

Despite the complexity involved in protein aggregation, amyloid formation from monomers to mature amyloid fibrils *in vitro* has been observed to follow similar sigmoidal kinetic patterns regardless of the identity of the primary sequence.[1,37] First comes the lag phase, where monomers slowly start forming aggregation-competent nuclei (Figure 5, blue line). At the growth phase, once the critical mass of nuclei has been reached, these nuclei start growing rapidly and form prefibrillar and fibrillar structures. Finally, at the plateau phase, the process of aggregation slows down significantly and finally stops as the soluble monomer has been consumed. Fibrils have an extraordinary ability to proliferate.[163] The addition of pre-formed nuclei of aggregation, so-called seeds, has been observed to shorten the lag phase (Figure 5, red line). This is due to bypassing the rate-limiting nucleation step.

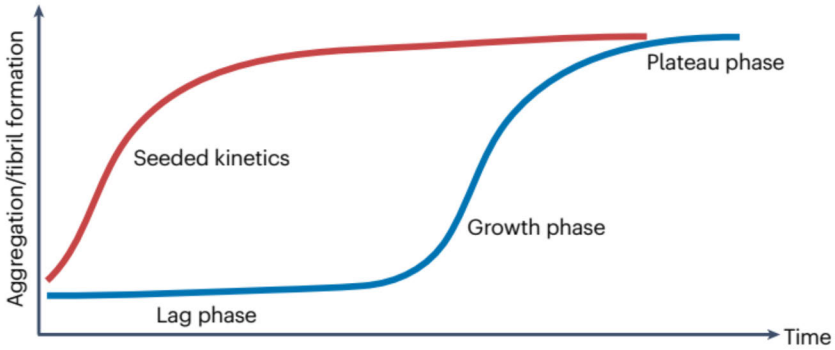

Figure 5. Kinetics of amyloid formation. When the quantity of fibrils is followed as a function of time, a lengthy lag phase is typically followed by a shorter exponential growth phase before the process reaches an equilibrium that appears as a plateau phase (blue line). Lag phase can be surpassed by seeded experiments (red line). Modified from [37].

Under physiological conditions, many amyloid proteins aggregate extremely slowly.[11,12] However, to perform aggregation experiments *in vitro* on a laboratory time scale, amyloid formation kinetics can be accelerated in several ways. The most obvious strategy is to use protein concentrations well above the monomeric protein's solubility limit.[13,193] Also, the environmental conditions can be altered. Low pH and high ionic strength accelerate the aggregation of α-synuclein by reducing the overall charge of the protein and disturbing its intramolecular interactions.[194-196] Higher temperatures accelerate the amyloid formation of Aβ by shortening the rate-limiting nucleation step.[197-199] Mechanical agitation through stirring or shaking is an efficient way to promote aggregation.[200] Also, different solvents and additives in the reaction mixture have been reported to promote fibril formation.[201,202] However, when selecting conditions for in vitro amyloid formation experiments, it is crucial to consider their relevance to *in vivo* conditions. Artificial conditions can result in an aggregation mechanism and fibril structure very different from that of *in vivo*.[203-205]

An *in vitro* assay is a much-simplified environment compared to the extracellular and intracellular milieu where proteins aggregate *in vivo*.[10] Many factors cannot be reproduced correctly, such as high molecular crowding and interaction with biological membranes. However, it has been known for decades that amyloid tissue deposits contain heparan sulfate proteoglycans.[206] Proteoglycans are polysaccharide-protein conjugates that are among the major macromolecules of the extracellular matrix.[207] Heparan sulfate belongs to the so-called glycosaminoglycan polysaccharides that are negatively charged, long, unbranched polysaccharides present in every mammalian tissue.[208] Biophysical studies have demonstrated that glycosaminoglycans, especially heparan sulfate and its highly sulfated derivative heparin, accelerate the amyloid formation of several amyloidogenic proteins *in*

vitro.[146,209-214] More thorough investigations have revealed that sulfated glycosaminoglycans facilitate fibril formation by providing a scaffold for concentrating and orienting oligomers.[214,215]

When monitoring amyloid formation *in vitro* to find an aggregation inhibitor, the reproducibility of the aggregation kinetics is essential. A key factor is the purity of the investigated protein.[13] All impurities should be minimized as they change the aggregation propensity of the protein.[216,217] As proteins involved in protein-misfolding diseases are typically highly aggregation-prone, having the protein in monomeric form at the beginning of the experiment is not self-evident. The presence of even a small number of preformed aggregates can change the kinetics significantly.[13] Disaggregation or monomerization protocols that use, for example, hexafluoroisopropanol (HFIP), trifluoroacetic acid (TFA), ammonium hydroxide, urea, or guanidine hydrochloride can be applied alone or combined with chromatographic fractionation.[216-221] Also, other experimental conditions like waiting times, surfaces, and air-water interfaces should be carefully controlled.[13] Seeding is an easy way to enhance the reproducibility of the aggregation process, but as the number of fibril ends in the seed preparation affects the efficiency of the seeds, the same batch of seeds should be used when comparing seeded experiments.

2.4 Therapeutic antibody discovery and optimization

2.4.1 Natural role of antibodies

Antibodies, also called immunoglobulins, are protective proteins of the immune system produced by B cells during the humoral immune response.[222] When a foreign substance, an antigen, binds to the B cell surface, it activates the B cell with the help of T cells in secondary lymphoid tissues. Activated B cells begin to proliferate and differentiate either into antibody-secreting plasma cells or memory B cells. Plasma cells can no longer respond to antigens, but they produce large amounts of soluble antibodies in the bloodstream and lymphatic system. Circulating antibodies recognize and bind to antigens that are identical to the one that initially triggered the immune response. After that, antigens are eliminated through multiple tightly regulated processes, including neutralization, opsonization, and complement activation.

Structurally, human immunoglobulins are large Y-shaped multi-domain proteins, which are composed of two identical light chains (LCs) and two identical heavy chains (HCs) (Figure 6).[223,224] One light chain pairs with one heavy chain, and this heterodimer associates with another identical heterodimer to form the

intact antibody. The light chain and heavy chain of a heterodimer are linked by disulfide bridges, as well as the two heavy chains of the heterotetramer. The human light chain has two domains, a constant domain (CL) and a variable domain (VL). Human heavy chains are composed of three or four constant domains (CH1-4) and a variable domain (VH). Functionally, an intact human immunoglobulin can be divided into three distinct regions: it has two antigen-binding fragments (Fabs), regions that bind antigen, a crystallizable fragment (Fc) region that interacts with immune effector molecules, and a hinge region, that links the Fab regions to the Fc region and defines conformational flexibility (Figure 6). The Fab regions are formed by the pairing of VL and CL of the light chain with the VH and CH1 of the heavy chain. The non-covalently paired variable domains (VL and VH) form the variable or antigen-binding region (Fv), which contains the antigen-binding site, also known as the paratope. Both variable domains have three specific regions called hypervariable or complementarity-determining regions (CDRs), short amino acid sequences that are capable of binding to the antigen. As both variable domains have three CDRs, altogether six CDRs (CDR-L1–3 and CDR-H1–3) form the paratope. The opposite region in the antigen, which is bound by the antibody, is called an epitope.

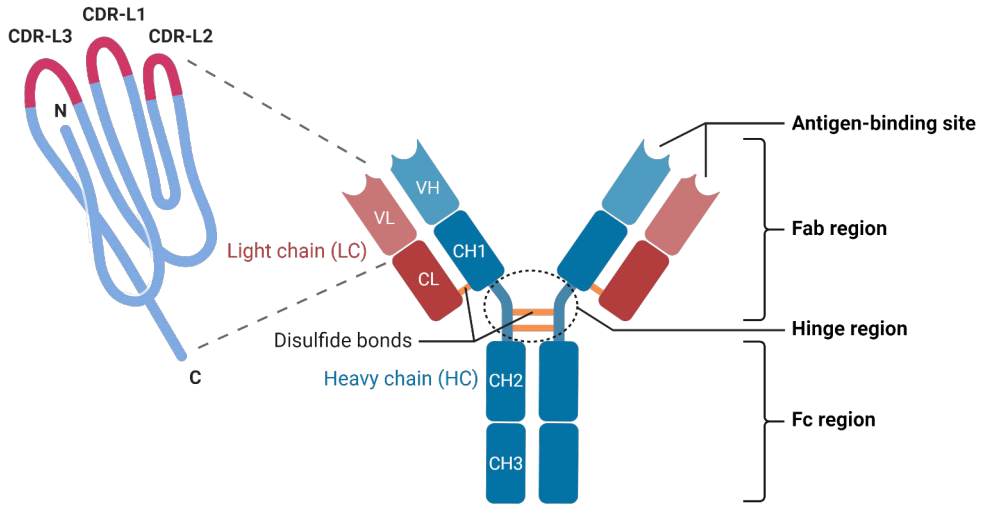

Figure 6. Schematic representation of the structure of IgG1 antibody. Two identical light chains (red) and two identical heavy chains (blue) are connected via disulfide bonds, creating a Y-shaped heterotetramer. VL, variable light domain; VH, variable heavy domain; CL, constant light domain; CH1, constant heavy domain 1; CH2, constant heavy domain 2; CH3, constant heavy domain 3; CDR, complementarity-determining region. N, amino-terminal end of variable domain; C, carboxy-terminal end of variable domain; Fab, fragment antigen-binding; Fc, fragment crystallizable. Created using Biorender.com.

Each B cell can bind only to one type of antigenic epitope with its antigen receptor (BCR) and secrete only identical soluble antibodies.[222] Still, collectively, B cells mount a diverse polyclonal B cell response against a virtually unlimited array of antigens sharing little or no similarity.[224] The vast diversity of natural antibodies depends on complex DNA rearrangement processes taking place during the B cell development in the bone marrow and later when B cells are stimulated by foreign antigens. With the random combination of inherited gene segments that code variable regions (so-called VDJ recombination), humans can make hundreds of different light chains and thousands of different heavy chains, with the most diversity in the CDR-H3 region.[225] Furthermore, the imprecise joining of gene segments greatly increases the diversity of variable regions by the loss and gain of nucleotides (so-called junctional diversification). When light chains and heavy chains pair to form the final antibody, millions of different antigen-binding sites are formed. Finally, after successful recognition of the antigen, during the proliferation, the variable region coding sequences are subject to point hypermutations that increase the affinity to the antigen (somatic hypermutation).

In addition to producing an enormous diversity of antigen-binding sites, B cells can alter the Fc region of the antibodies they produce during an immune response.[225] The changes in the Fc region can significantly affect the result of an antibody-antigen interaction as the Fc fragment mediates effector functions by binding to the Fc receptor (FcR) on effector cells or activating other immune mediators such as complement.[224] Variations in the heavy chain constant domain coding gene sequence generate five different isotypes (also known as classes): IgM, IgD, IgG, IgA, and IgE. First, all B cells make membrane-bound IgM antibodies, which serve as BCRs on the B cell surface (immature naïve B cells).[225] After the B cells leave the bone marrow but before they interact with an antigen, they start to produce membrane-bound IgD molecules (mature naïve B cells). Soluble pentameric IgM molecules dominate the primary antibody response to antigens. In the secondary immune response, many B cells switch making soluble, monomeric IgG and IgE, and monomeric and dimeric IgA antibodies, without changing the antigen-binding site (isotype or class switching). Each isotype is specialized to attack antigens in different ways and at different sites.

IgG is the most abundant immunoglobulin isotype in the body, with the longest serum half-life and the ability to cross the placenta to give passive immunity to the fetus.[224] There are four IgG subclasses in humans, named in order of their prevalence in serum: IgG1 (60%), IgG2 (32%), IgG3 (4%), and IgG4 (4%).[226] The global structures of the four subclasses are very similar (over 90% homology in amino acid sequence), but there are important differences in their hinge regions and upper CH2 domains that affect their binding to complement and IgG-Fc receptors, affecting their functionality (Figure 7).

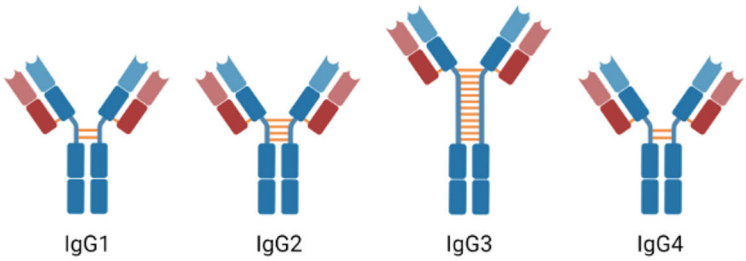

Figure 7. IgG subclasses. IgG4 is prone to form intra-chain disulfide bridges instead of inter-chain disulfide bridges, resulting in half-molecule exchange. Created using Biorender.com.

IgG1 is predominantly responsible for the immune response against protein and polypeptide antigens. It is a potent trigger of Fc-mediated effector mechanisms. In addition to direct neutralization, complement-dependent cytotoxicity (CDC), antibody-dependent cellular cytotoxicity (ADCC), and antibody-dependent cellular phagocytosis (ADCP) are key mechanisms for the elimination of antigens from the body.[227] In addition to the heavy chain structure, the glycosylation profile of antibodies affects their function.[224] In the IgG molecules, there is a conserved glycan at the Asn297 position of the heavy chains. The core structure of IgG glycan comprises N-acetylglucosamine and mannose residues, but several dozen IgG-Fc glycoforms have been found in healthy human serum.[226]

2.4.2 Therapeutic antibodies

The immune response to an antigen within the body is polyclonal. Many B cell clones react to the antigen and a heterogeneous population of antibodies with different paratopes for the different antigen epitopes are formed. Before the discovery of antibiotics, animal-derived polyclonal antibodies were used as a serum therapy to treat various bacterial infections.[228] While polyclonal antibody preparations of human or animal origin are still in use in acute conditions e.g. in antibody deficiencies, autoimmune diseases, severe intoxications and to prevent rhesus syndrome, they have limited potential due to variability in product quality and safety risks.[229]

The production of mAbs became possible after Köhler and Milstein invented the hybridoma technology in 1975.[230] After immunization, the mouse spleen B cells are fused with immortal myeloma cancer cells. The hybridoma cell lines enabled the *in vitro* production of a large number of identical antibodies, which have the same amino acid sequence and affinity, and specificity to one binding epitope.[231] The first therapeutic monoclonal antibody, a mouse anti-CD3 IgG2a muromonab, for the prevention of graft rejection after organ transplantation, was approved by the FDA in 1986.[232] However, the murine antibodies were discovered to be immunogenic to

humans, producing a high titer of anti-drug antibodies (ADA) in the patients. The development of recombinant DNA technologies enabled modification of the antibody sequence and different degrees of humanization of murine mAbs produced by hybridoma technology (Figure 8).[233,234]

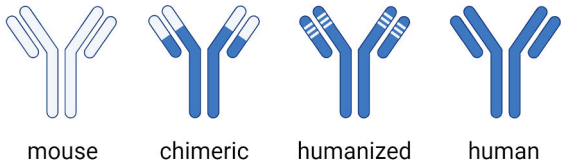

Figure 8. Different degrees of antibody humanization. White, mouse origin; blue, human origin. In chimeric antibodies, mouse (or other species) variable domains are grafted onto a human antibody. In humanized antibodies, mouse (or other species) CDRs are grafted onto a human antibody. In fully human antibodies, the whole antibody sequence is of human origin. Created using Biorender.com.

More human-likeness and less immunogenicity made the antibodies suitable for various chronic diseases like cancer and autoimmune diseases. The success of two chimeric human/murine antibodies, anti-B lymphocyte antigen CD20 IgG1 rituximab, for treatment of B cell lymphoma, approved in 1997 by FDA, and anti-tumor necrosis factor (TNF) IgG1 infliximab, for treatment of rheumatoid arthritis, approved in 1998 by FDA, was a significant turning point for the monoclonal antibody therapies.[235,236] Since then, monoclonal antibodies have emerged as a major class of therapeutic agents on the market. In 2021, the 100th monoclonal antibody product was approved by the FDA, and each year, over 100 new monoclonal antibody therapies enter clinical development.[237] Cancer and autoimmune diseases are still the largest indication groups, partly because of the success of the initial mAb treatments for these indications, but also because of the occurrence of these diseases.[238] The wide spectrum of therapeutic indications covers infections, asthma, allergy, migraine, transplantation, osteoporosis, and many others, highlighting the versatile possibilities of antibody treatments.

The success of monoclonal antibodies as therapeutic agents is due to their high specificity and affinity for both secreted and cell-surface targets.[237] The long half-life in plasma brings additional benefits.[231] Therapeutic antibodies can be used to neutralize circulating proteins and block signaling pathways (e.g. anti-TNF and anti-vascular endothelial growth factor receptor 2 (VEGF) antibodies). Many antibodies used to treat cancers induce cytotoxicity through the recruitment and activation of effector cells (e.g. anti-CD20 and anti-human epidermal receptor 2 (HER2) antibodies).[239] Immune checkpoint inhibitors (e.g. anti-programmed cell death protein/ligand 1 (PD1/PDL1) and anti-cytotoxic T lymphocyte-associated protein 4 (CTLA4) antibodies) kill cancer cells through T cell activation.[240] Most

currently approved monoclonal antibodies are monospecific symmetrical Y-shaped (canonical) IgG1 subclass antibodies, but the number of other antibody-derived modalities is slowly increasing.[237] Antibody-drug-conjugates (ADCs) combine the specificity of monoclonal antibodies with the potency of highly cytotoxic agents.[241] Bispecific antibodies (bsAbs) can bind to two different epitopes, which enables novel mechanisms of action that cannot be achieved using conventional antibodies.[242]

The high molecular weight and biological nature of antibodies bring some limitations and challenges to their use as therapeutics.[231] The target space is limited to extracellular targets because antibodies cannot cross the cell membrane. The poor permeability and proteolytic instability prevent their oral administration. Recombinant DNA technology has allowed the efficient production of monoclonal antibodies in mammalian cell expression systems, mainly in Chinese hamster ovary cells (CHO), but the production process is undeniably complex and expensive.[243] Above all, the biggest concern when developing new therapeutic antibodies is still their possible immune-related adverse events.[231] Today a range of techniques are used to identify antibodies or antibody fragments against therapeutic targets, each having its advantages and disadvantages. Two completely different discovery strategies enable the discovery of fully human antibodies, lowering the risk of possible immunogenicity, namely the human antibody-expressing transgenic mouse models and *in vitro* selection technologies, where an antibody library is screened *in vitro* against a target.[240]

2.4.3 Antibody discovery *in vivo*

The hybridoma technology is still the most popular method to obtain monoclonal antibodies as it is well-established and has a proven track record for generating antibodies for research and therapeutic use.[244,245] In hybridoma technology, animals are immunized with a target antigen, and the antibody-secreting B cells are fused with immortal myeloma cells. The resulting hybridomas are screened for antibodies of interest, and these cells are cloned to produce a monoclonal population. Confirmed antigen-specific clones are then expanded and utilized to produce large quantities of the desired monoclonal antibody. Antibodies can be derived from species that have suitable fusion partners, including mice, rats,[246] rabbits,[247] and chickens[248]. The species selection depends on the presence of homologous protein in the immunized species, the amount of antigen available for immunization, the time required to obtain an antibody response, and the purpose for which the antibody is needed.[245] Single B cell technologies, which are much newer methods to obtain monoclonal antibodies from *in vivo* sources, use fluorescence-activated cell sorting (FACS) and microfluidics to screen isolated single B cells from various immunized

animals.[249,250] The discovery process is faster and enables larger species diversity (e.g. llama) compared to hybridoma technology, but it is technically complex and requires special equipment and training.

The main advantage of *in vivo* technologies is the exploitation of natural immune selection; the antibodies preserve the native pairing of variable domains and undergo *in vivo* affinity maturation and specificity tuning.[251] The biggest disadvantage of *in vivo*-derived antibodies is that normally they require humanization before therapeutic use. Antibody humanization is a slow process done mostly on a trial-and-error basis.[252] To bypass this bottleneck, human antibody-expressing transgenic mouse models have been developed.[253-256] In these systems, the human genomic regions that include the genes responsible for the antibody repertoire, along with the associated regulatory regions for gene expression, are stably integrated into the host animal's genome. These resulting transgenic animals can then be immunized with a target antigen like wild-type animals to obtain fully human antibodies. However, transgenic animal platforms are very expensive due to the complex genetic engineering and regulatory compliance they require. A common disadvantage of all *in vivo* technologies is that antigens must be inherently immunogenic or require additional modifications to enhance their immunogenicity.

2.4.4 Antibody discovery *in vitro*

All *in vitro* selection technologies are based on G.P. Smith´s initial finding in 1985 that peptides can be fused to the *Escherichia coli (E. coli)* phage M13 envelope proteins, which allows their display on the surface of the phage, and the phenotypic *in vitro* selection of the corresponding peptide encoding gene sequence packed in the same phage particle.[257] The antibody phage display technology was developed in the 1990s after the discovery of antibody single-chain variable fragments (scFv) that could be expressed in *E. coli*.[258-260] Today, also cell surface display (yeast, bacteria, and mammalian), ribosome display, and mRNA display technologies are used for antibody generation.[240] *In vitro* selection technologies do not depend on the *in vivo* immune response and can be used to discover fully human antibodies to almost every type of antigen and a broader range of epitopes.[261]

Antibody libraries serve as a critical resource for antibody discovery through *in vitro* selection technologies.[261] They are collections of antibody genes encoding antibodies with unknown properties. Immune human libraries are constructed from B cell samples from patients who have suffered an infection or disease, or from individuals who have received vaccination. Immune libraries contain already affinity-matured antibodies because they are generated from antibody repertoires that underwent antigen-driven *in vivo* selection. For the same reason, they must be generated separately for each antigen. Universal libraries, instead, are intended for

general use, i.e., for isolation of antigen-specific antibodies against any target.[262] They can be further divided into three categories according to the source of diversity: naïve, synthetic, and semi-synthetic libraries. Naïve human libraries are constructed from B cells of non-immunized donors and contain the natural human IgM gene repertoire. During library construction, heavy and light chains are randomly combined as a combinatorial library.[263] This unnatural pairing increases the library diversity dramatically and enables the generation of antibodies against self-antigens. The structural complexity of the library is also high due to diverse framework structures (non-CDR regions in the variable domains). Fully synthetic libraries consist of only synthetic gene sequences that mimic the human antibody repertoire.[263] In synthetic libraries, the developability of the antibodies has usually been considered by the removal of sequence liability motifs and by the selection of heavy and light chain frameworks with the best biophysical properties. The designed CDR diversity usually far exceeds the natural CDR diversity. Synthetic libraries can also be designed especially for challenging targets and epitopes and for special applications. Semi-synthetic libraries are a mixture of natural and synthetic antibody sequences.

For the initial discovery of new antibodies, phage display technology is the method of choice among different *in vitro* selection technologies.[32] The main advantage of phage display is the ease of phage display library generation, comprising huge diversities exceeding 10^{11} unique clones. Also, the selection process, called panning, is fast, easily controllable, and requires no special equipment (Figure 9).[264] This enables high-affinity variants to be readily obtainable.

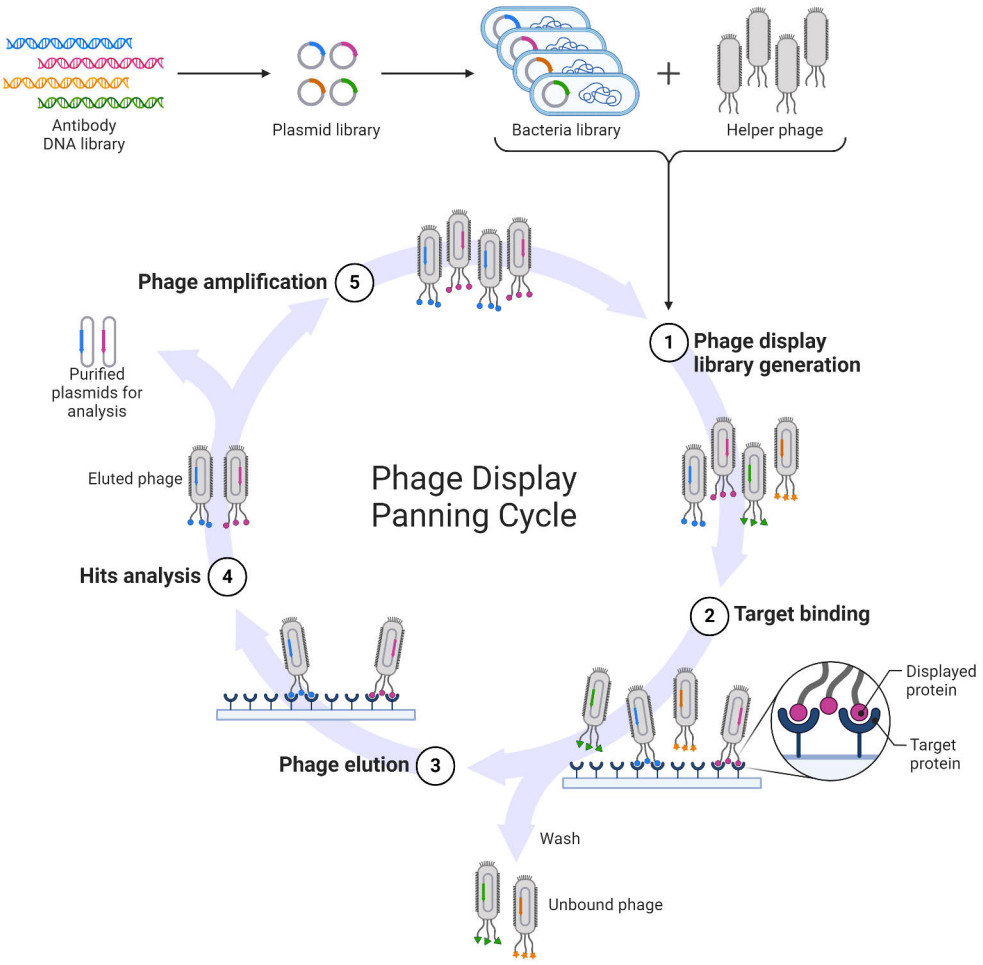

Figure 9. Phage display panning cycle. 1. The phage display library is generated by fusing the antibody DNA library with the phage surface protein pIII coding gene. The recombinant plasmid library is transformed into *E. coli*, where it is replicated, translated, and assembled into infective phages, with the antibody library displayed on the surface. A helper phage is co-transformed into the *E. coli* to produce full phages. 2. The target binding of individual antibody clones is screened by incubating the library of antibody-displaying phage with the target antigen immobilized on a microtiter plate or beads. Unbound phages are washed away. 3. The bound phages are eluted. 4. Hit analysis is performed on single phage clones parallel to panning to determine the positive hits' diversity and evaluate the binding affinity. 5. The eluted phages are reamplified by infection of *E. coli* to produce a new antibody phage sublibrary, which will be used for the next panning round. Normally, 3-5 rounds of panning are sufficient to enrich antibodies with desired properties. Created using Biorender.com.

Phage display is a versatile technology; the choice of antibody display format, antigen presentation, selection strategy, and library construction all affect the outcome of the antibody discovery campaign.[265] As *E. coli*´s secretion and folding

apparatus cannot process full-length antibodies properly, the two most commonly used antibody formats are scFv and Fab fragments. ScFvs being smaller than Fabs are a more robust format for large libraries, but the potential affinity loss during conversion to IgG format might be less of an issue for antibodies discovered in Fab format. The most popular technique to present the antigen is through indirect immobilization via strong binding between streptavidin on the surface and biotin conjugated to the antigen via a linker or tag. The antigen can also be presented on whole cells or amphiphilic structures, when there is a risk that the antigen loses its native conformation when isolated from its natural environment (e.g. membrane proteins). The phage display selection can be performed using various strategies and protocols to maximize the chance of discovering antibodies with desired properties. Deselection steps are normally included to limit the enrichment of antibodies that bind to tags, fusion partners, and support matrices. For therapeutic applications, it is often important that the antibody binds to a certain epitope in the antigen. To discover epitope-specific antibodies, only the desired parts of the antigen can be used in the selections, or so-called epitope masking with another antibody can be applied.

The first phage display-derived and fully human monoclonal antibody approved for therapeutic use was an anti-TNF IgG1, adalimumab, in 2002.[261] A murine antibody was used as a template for the guided selection of human antibody V domains to achieve binding to a similar epitope on TNF with a similar high affinity.[266] Adalimumab binds to TNF with subnanomolar affinity and very high specificity and is one of the most prescribed medicines for immune-mediated disorders.[31,267] Today, around 20 phage-derived therapeutic antibodies have been granted approvals with indications for cancer and other medical conditions, such as inflammatory, ocular, infectious, or immunological diseases, and numerous are in clinical development.[31,32,263] Although currently most of the approved therapeutic antibodies were discovered through animal immunization, the number of phage-derived therapeutic antibodies is steadily increasing due to the successful track record of the discovery platform, phage display technology maturation and patent expiration, and ethical considerations related to animal immunization.[263,268]

2.4.5 Optimization of therapeutic antibodies

Affinity to the target and effective biological function are not the only quality attributes that therapeutic antibodies must meet. To progress successfully from discovery to development, antibody molecules need to have favorable biophysical properties and chemical stability.[33,269-274] The set of such properties is often described as “developability”. Although developability problems usually arise only after the antibody is needed in high quantity and concentration in preclinical and clinical stages, they can typically be solved only by antibody sequence engineering. To avoid

costly delays and failures in clinical development, it is essential to be able to predict possible developability risks using multiple *in silico* and experimental tools and remove them by optimizing the antibody sequence already during the discovery stage. The most important physicochemical properties of therapeutic antibodies, their common screening methods in the discovery stage, and optimal values are listed in Table 2.

Table 2. The most important physicochemical properties of therapeutic antibodies, their common screening methods in discovery, and reported optimal values.

Property	Screening assay	Optimal values
Hydrophobicity	In silico analysis,[275] HIC,[276] CIC,[277] SMAC[278]	Low hydrophobicity. Low level of heterogeneity.[271,272,274]
Charge	In silico analysis,[275] cIEF[279]	Isoelectric points (pIs) between 8-8.5.[280] Low levels of charge variants.[274]
Non-specific binding	ELISA,[281] PSR,[282] BVP,[283] CIC,[277] SMAC,[278] heparin chromatography[284]	Low levels of non-specific binding.[285,286]
Colloidal stability (Self-interaction, aggregation propensity, viscosity)	In silico analysis,[275] AC-SINS,[287] CS-SINS,[288] DLS,[289] SEC,[290] SEC-MALS[291]	Low levels of self-interaction.[285,289] AC-SINS values < 14.[271] Diffusion interaction parameter in histidine buffer ($k_{D,His}$) > 20 ml/g.[289]
Solubility	In silico analysis,[275] PEG precipitation[292]	Solubility > 100 mg/ml for subcutaneous administration.[33]
Conformational stability (Thermal unfolding)	DSC,[293,294] DSF,[295] nanoDSF[269]	Fab midpoint of thermal unfolding (T_m) > 65 °C.[269]
Chemical stability/ Post-translational modifications	In silico analysis[275]	No problematic sequence attributes.[274]

HIC, hydrophobic interaction chromatography; CIC, cross-interaction chromatography; SMAC, standup monolayer chromatography; cIEF, capillary isoelectric focusing; ELISA, enzyme-linked immunosorbent assay; PSR, polyspecificity reagent assay; BVP, baculovirus particle assay, AC-SINS, affinity-capture self-interaction nanoparticle spectroscopy; CS-SINS, charge-stabilized self-interaction nanoparticle spectroscopy; DLS, dynamic light scattering; SEC, size-exclusion chromatography, SEC-MALS, size-exclusion chromatography coupled with multi-angle light scattering; DSC, differential scanning calorimetry; DSF, differential scanning fluorimetry; nanoDSF, nano-differential scanning fluorimetry.

Developability problems can occur in antibodies from any discovery platform, including immunized animals.[36,270,272] The concentrations and conditions the antibody needs to tolerate during manufacturing, storage, and transport are much more demanding than those in the body. The developability of phage display-derived antibodies has been a special concern due to the lack of *in vivo* protein quality control machinery during the selection process.[296-299] Jain et al. investigated the biophysical properties of 137 clinical-stage antibodies using a panel of twelve *in vitro* characterization assays and discovered that the number of flags for antibodies engineered at some point by phage display is significantly higher than for those derived

from mammalian sources.[272] In the subsequent analysis, especially higher self-interaction and non-specific binding profiles were observed for the phage display-derived therapeutic antibodies.[300] Replicating the precision of multistep *in vivo* affinity maturation, which enables the preservation of high specificity while achieving high affinities, has proven to be challenging using phage display.[286,301] In some cases, the developability issues can be solved by identifying problematic regions, producing individual variants, and assessing these for improved biophysical characteristics.[302,303] However, it is common to observe trade-offs between key antibody traits, where improving one key trait easily compromises another important trait.[301,304,305] As nearly all therapeutic antibodies are expressed in mammalian cells as full-length IgGs, the optimization steps must be done in a similar context, decreasing the throughput significantly and making multi-parameter optimization very challenging.[304]

Mammalian display is an *in vitro* selection technique that can be used to efficiently optimize the biophysical properties of a candidate antibody.[34] Mammalian cell surface display of antibodies is typically enabled by the genetic fusion of the C-terminus of the heavy chain constant region to a transmembrane domain, e.g., of the murine H-2Kk protein or the human platelet-derived growth factor (PDGF) receptor.[35,306,307] This allows the expression of properly folded full-length antibody molecules with human-like glycosylation patterns and other post-translational modifications on the cell surface of mammalian cells.[32] The display levels of antibody variants on the mammalian cell surface are related to their biophysical properties.[35,36] During display, antibodies are exposed to high local concentrations in the endoplasmic reticulum or cell surface, and clones with poor biophysical properties aggregate and are removed by the cell's quality control machinery. This results in low presentation levels of these clones on the cell surface. Antibody variants showing simultaneously the highest affinities and display levels on the cell surface can be selected by FACS. The prerequisite for making selections solely based on the properties of the displayed antibody is that the antibody genes are integrated into the host cell genome in an irreversible, site-specific, single-copy manner.[35,36] This can be achieved, for example, by nuclease-directed integration[36,306] or by integrating a landing pad for Bxb1 integrase-mediated integration[35]. As the construction of large libraries in mammalian cells is substantially more difficult than in yeast and bacteria, the greatest limitation of mammalian display technology is the limited library sizes. In 2019, Parthiban et al. showed that mammalian display libraries of up to 10 million clones with strictly monoclonal and site-specific display can be successfully constructed.[306] This library size is not optimal for routinely screening high-affinity antibodies from non-enriched sources, but it is enough for searching enriched populations, such as the output from phage display selection, or variant libraries created from the candidate antibody sequence, for optimized biophysical properties.

3 Aims

Gelsolin amyloidosis is an inherited systemic amyloidosis for which there is no disease-modifying treatment. The quality of life of patients is reduced due to many adverse symptoms, some of which can only be alleviated by surgical operations.

Monoclonal antibodies have achieved remarkable success as a drug modality due to their high affinity and specificity, and they are being developed for a variety of diseases, including complex protein-misfolding diseases like Alzheimer´s disease. However, no antibodies have been reported for plasma gelsolin fragment AGelD187N, although it is the only disease-causing agent in gelsolin amyloidosis and easily accessible for pharmacotherapy.

This study aimed to discover human antibodies that would bind to the AGelD187N fragment and inhibit its pathological aggregation in laboratory conditions. For this purpose, a method was needed to assess the aggregation inhibition. In addition, attention was paid to the fact that the antibodies found would have such properties that it would be possible to develop them into a subcutaneous medicinal product.

The specific aims were:

- To develop a physiologically as relevant as possible *in vitro* aggregation assay for the amyloidogenic gelsolin fragment AGelD187N to assess the potential aggregation inhibitors
- To discover human antibody fragments that bind to AGelD187N and inhibit its aggregation efficiently
- To optimize the biophysical properties of the anti-AGelD187N antibody for therapeutic purposes

4 Materials and Methods

4.1 Peptides and polypeptides

All peptides and polypeptides used in the study are listed in Table 3.

Table 3. Peptides and polypeptides used in the study.

Peptide/polypeptide	Amino acid numbers* and length	Terminal modification	Origin (supplier)	Used in
AGelD187N 173-242 (RP-HPLC purity 90%)	173-242, 70 aa	amidated C-terminus	synthetic (Caslo)	I
Ac-AGelD187N 173-243 (RP-HPLC purity 95%)	173-243, 71 aa	acetylated N-terminus, amidated C-terminus	synthetic (Caslo)	I
AGelD187N 173-242 (RP-HPLC purity 95%)	173-242,70 aa	amidated C-terminus	synthetic (Caslo)	I, II
Ag2	181-192,12 aa	biotinylation in C-terminus (epsilon-amide)	synthetic (Genscript)	II
Ag3	173-186, 14 aa	biotinylation in C-terminus (epsilon-amide)	synthetic (Genscript)	II
Ag4	227-242,16 aa	biotinylated PEG4 linker in N-terminus	synthetic (Genscript)	II
Ag7	173-242,70 aa	biotin-, avi- and hexahistidine tag in N-terminus	recombinant	II
Ag1	173-242,70 aa	biotinylation in N-terminus	synthetic (Caslo)	II, III
Ag9	173-242,70 aa	biotinylation in C-terminus	synthetic (Caslo)	II

*Amino acid numbering is based on UniProt entry P06396-1, human plasma gelsolin, without the signal peptide 1 to 27. RP-HPLC, reversed-phase high-performance liquid chromatography; aa, amino acids.

The disease-relevant mutant plasma gelsolin fragment comprising amino acids 173-242/243 is named AGelD187N as recommended by the Nomenclature Committee of the International Society of Amyloidosis (ISA). The amino acid sequence of AGelD187N is presented in Figure 2. Biotinylated panning and

screening antigens are named Ag1–9 to separate them from the disease-relevant fragment, despite Ag1, Ag7, and Ag9 having the same amino acid sequence as AGelD187N. All peptides and polypeptides used in the study except for Ag7 are synthetic and custom-made by commercial vendors Caslo Asp and GenScript Biotech. Ag7 was produced by recombinant bacterial expression and BirA enzyme-mediated *in vivo* biotinylation in the Department of Life Technologies, University of Turku.

4.2 AGelD187N

4.2.1 Monomerization

Lyophilized AGelD187N polypeptides were dissolved in 6 M guanidine hydrochloride (Sigma-Aldrich) in phosphate-buffered saline (PBS) and sonicated in a water bath sonicator for 30 minutes to disrupt any aggregates or oligomers. The solution was then centrifuged at 20,000 rpm for 15 minutes and loaded onto a Superdex 75 Increase 10/300 GL gel filtration column (GE Healthcare) pre-equilibrated with PBS for buffer exchange and removal of aggregated species. The main fractions from the monomer peak, yielding 10-30% of the original material, were collected on ice, and the polypeptide concentration was determined using a DS-11 UV-Vis spectrophotometer (Denovix) with an extinction coefficient of 15,780 $M^{-1}cm^{-1}$. The monomerized polypeptide was diluted to 30 µM with PBS and used immediately in aggregation studies.

4.2.2 Thioflavin T assay

Stock solutions of 500 µM ThT (Sigma-Aldrich) and 150 µM heparin with a molecular weight of 17-19 kDa (Sigma-Aldrich) were prepared by dissolving the dry powders in PBS and filtering through sterile 0.22 µm pore size polyethersulfone (PES) membrane filters (Corning) or sterile 0.2 µm pore size Supor PES syringe filters (Acrodisc, Pall), respectively. All freshly monomerized and diluted AGelD187N batches were further diluted with PBS, followed by sequential addition of heparin and ThT, with thorough mixing by pipetting up and down several times after each addition. The final concentrations in the reaction mixtures were 5-25 µM AGelD187N, 10 µM heparin, and 50 µM ThT. The mixtures were dispensed into 96-well plates (Greiner Bio-One) in 3-4 replicates of 200 µl each, and later into non-protein binding half-area 96-well plates (Corning) in 3-4 replicates of 100 µl each. Seeding was performed by adding 0.3-0.6 µl of freeze-thawed reaction solution from experiments with sigmoidal aggregation curves to each well, or by dipping a copolyamide monofilament thread (0.46 mm, BASF) into the preformed fibrils and

then into each well. Plates were sealed promptly with LightCycler sealing film (Roche) after seeding. Kinetic measurements were conducted at 37°C using an Envision 2105 multimode plate reader (PerkinElmer) by measuring ThT fluorescence at 485 nm (20 nm bandwidth) upon excitation at 440 nm (20 nm bandwidth) every 10 minutes for 16-62 hours. Orbital shaking at 200 rpm (3 mm diameter) for 15 seconds was performed before each measurement.

Data analyses were performed using GraphPad Prism software (v. 9.0). Maximum fluorescence intensities/signals represent usually the means of three replicate reactions. The signal-to-background ratio (S/B) was determined by dividing the mean maximum fluorescence intensity of the protein sample by the fluorescence intensity of the ThT control at the end of the experiment. The time to reach 50% of the maximum signal (t_{50}) was calculated by fitting the kinetic data with a non-linear regression (five-parameter) model up to the point where the signal began to decline.

4.2.3 Transmission electron microscopy

The aggregation assay samples were analyzed with transmission electron microscopy (TEM). After the ThT assay, the sealing foil was removed from the plate and the three replicates were pooled. Carbon-coated copper grids (Formvar/carbon 200 mesh, Ted Pella) were treated with glow discharge for 20 seconds. Four microliters of each pooled, well-mixed sample were then placed onto separate grids and allowed to stand for 2 minutes. The excess solution was removed using blotting paper. Each grid was washed twice with 4 µl of deionized water, and subsequently negatively stained for 1 minute with 4 µl of 2% uranyl acetate in water. Excess uranyl acetate was removed with blotting paper, and the samples were air-dried for at least 5 minutes under a petri dish cover. Transmission electron images were captured using a JEM-1400 Plus transmission electron microscope operating at an acceleration voltage of 120 kV.

4.2.4 Size exclusion chromatography

The monomerized AGelD187N polypeptide and the aggregation assay supernatants were analyzed using analytical size exclusion chromatography (SEC). An Advance Bio SEC column having dimensions of 4.6 mm x 300 mm, particle size of 2.7 µm and pore size of 300 Å (Agilent) along with a guard column having dimensions of 4.6 mm x 50 mm, particle size of 2.7 µm and pore size of 300 Å (Agilent) was used. Isocratic elution was performed with a mobile phase of 150 mM sodium phosphate buffer (pH 7.0) at a flow rate of 0.35 ml/min. The column was connected to a 1200 Infinity HPLC system (Agilent) sequentially with a diode array detector (DAD) 1200 Infinity (Agilent).

The monomerized AGelD187N polypeptide and the aggregation assay supernatants were analyzed also using analytical size exclusion chromatography coupled with multiangle light scattering (SEC-MALS). An Advance Bio SEC column having dimensions of 4.6 mm x 300 mm, particle size of 2.7 µm and pore size of either 130 Å or 300 Å (Agilent) along with a guard column having dimensions of 4.6 mm x 50 mm, particle size of 2.7 µm and pore size of either 130 Å or 300 Å (Agilent) was used. Isocratic elution was performed with a mobile phase of 150 mM sodium phosphate buffer (pH 7.0) at a flow rate of 0.35 ml/min. The column was connected to a bioinert 1260 Infinity II HPLC system (Agilent) in sequence with a diode array detector (DAD) 1260 Infinity II (Agilent), a MiniDawn MALS detector (Wyatt), and an Optilab refractive index (RI) detector (Wyatt). The MALS detector utilized a laser source at 659 nm with three detectors positioned at different angles, while the RI detector operated at 658 nm. Data from the DAD, MALS, and RI detectors were processed using ASTRA software (Wyatt). Bovine serum albumin (BSA) was used as an independent molecular weight control standard (Wyatt).

4.2.5 Tricine-polyacrylamide gel electrophoresis

The monomerized AGelD187N was analyzed using tricine-sodium dodecyl sulphate-polyacrylamide gel electrophoresis (tricine-SDS-PAGE). A precast tris-SDS-PAGE gel with a gel concentration of 10-20% (Mini-Protean, Bio-Rad) was used. The peptide analysis buffer was prepared by diluting a 10x stock solution (Bio-Rad). Five microliters of the sample were mixed with 5 µl of tricine sample buffer (Bio-Rad), and a total of 10 µl was loaded into the gel wells. A Precision Plus Protein Dual Xtra Standard (Bio-Rad), consisting of 12 recombinant proteins ranging from 2 to 250 kDa, was used as a molecular weight marker. Electrophoresis was carried out in a Mini-Protean Tetra cell with an initial voltage of 50 V for 100 minutes, followed by 75 V for 60 minutes, and finally 100 V for an additional 60 minutes. After electrophoresis, the bands were fixed by incubating the gel in a fixation solution containing 40% methanol and 10% acetic acid for 30 minutes. The gel was then stained using Imperial protein stain (Thermo Fisher Scientific) and imaged with a GelDoc EZ System (Bio-Rad).

4.2.6 Mass spectrometry

The monomerized AGelD187N was analyzed using reversed-phase-high performance liquid chromatography (RP-HPLC) coupled with mass spectrometry (MS). The analysis was conducted on a Vanquish LC system (Thermo Fisher Scientific) equipped with a 2.1 mm BioZen XB-C8 intact 3.6 µM column (Phenomenex) maintained at 60 °C. The mobile phase consisted of 0.1% formic acid

in acetonitrile as phase B and 0.1% formic acid in water as phase A. The gradient program was as follows: 0 min at 5% B, 2 min at 5% B, 25 min at 65% B, 30 min at 90% B, 34 min at 90% B, 35 min at 5% B, and 45 min at 5% B, with a flow rate of 0.25 ml/min. Samples were prepared at a concentration of 5 μM in 20 mM phosphate buffer with 1 M NaCl (pH 7) and injected in 10 μL volumes using the microliter pickup method.

The samples were analyzed on a Q Exactive (QE) mass spectrometer (Thermo Fisher Scientific) equipped with a HESI II Ion Max source (Thermo Fisher Scientific). Mass spectra were acquired at a resolution of 35,000, with a scan range from m/z 500 to 2,000. The MS settings included a spray voltage of 3.5 kV, a sheath gas flow rate of 45, an auxiliary gas flow rate of 10, an in-source collision-induced dissociation energy of 0 eV, and a capillary temperature of 275 °C. The ion transfer optics were optimized during annual maintenance and remained unchanged.

Mass spectra were viewed and analyzed using Thermo Xcalibur Qual Browser software (Thermo Fisher Scientific), and data processing was performed using the Intact Protein Analysis module in BioPharma Finder 3.0. The initial deconvolution was carried out with the default settings of the ReSpect algorithm, followed by adjustments to the targeted mass and charge state ranges. A deconvolution mass tolerance of 50 ppm was applied to identify individual charge states and their distribution.

4.3 Anti-AGelD187N Fabs

4.3.1 Phage display

Anti-AGelD187N scFvs and Fabs were discovered using phage display technology. In the solid phase panning protocol, biotinylated peptide antigens Ag2, Ag3, Ag4, and Ag7 listed in Table 3 were loaded to saturation on streptavidin beads (Invitrogen) or epoxy beads (Invitrogen) coated with neutravidin. The beads were incubated with the primary scFv library (10^{12} cfu) or a phage pool of scFv or Fabs ($5 \cdot 10^{10}$ cfu) from a previous panning round, in selection buffer (PBS containing 0.1 % BSA and 0.05 % Tween-20) at room temperature for 30–60 minutes. Using the solution phase protocol, the antigens (0.1 nM or 1 nM) and phage pools were preincubated at room temperature for 30–60 minutes and subsequently mixed with streptavidin beads for 5 minutes. The bead-bound antigen–phage complexes were collected from the selection buffer using a bar magnet (Invitrogen). Beads were washed three times with selection buffer and once with PBS. Phages were eluted with trypsin and rescued by infecting mid-log *E. coli* XL1-Blue cultures for phage propagation. Phage stocks were prepared the following day with PEG-NaCl precipitation, and the selection was repeated for four rounds with scFv phage libraries and a further three

rounds with Fab libraries. The progress of panning was monitored by dilution plating of infected cells from phage outputs and by phage immunoassays.

4.3.2 Production of soluble Fabs

The VL and VH domains of selected scFvs and Fabs were cloned into Fab expression vector[308]. All plasmids were sequenced to confirm the sequence of the variable domains as well as the correctness of cloning. Plasmids were transfected into 30 ml cultures of ExpiCHO cells (Thermo Fisher Scientific) according to the manufacturer´s instructions. ExpiFectamine CHO Enhancer (Thermo Fisher Scientific) and ExpiCHO Feed (Thermo Fisher Scientific) were added 19 h after transfection, and the cultures were incubated at 32°C, 5% CO_2 at 120 rpm for 11 days. The cultures were harvested by centrifugation. The secreted Fabs were purified using CaptureSelect CH1-XL affinity chromatography column (ThermoFisher) and Superdex 200 Increase 10 300 GL size exclusion chromatography column (Cytiva) on an ÄKTA Pure 25 instrument (Cytiva).

4.3.3 Glycine-polyacrylamide gel electrophoresis

The expression levels and correct molecular weights of anti-AGelD187N Fabs were assessed using glycine-sodium dodecyl sulphate-polyacrylamide gel electrophoresis (glycine-SDS-PAGE). A precast glycine-SDS-PAGE gel with a gel concentration of 4-15% was used (Mini-Protean TGX, Bio-Rad). The samples were mixed with 4× Laemmli buffer (Bio-Rad) with or without 10% β-mercaptoethanol, boiled at 95°C for 5 minutes, and loaded on the gel wells. A Precision Plus Protein Dual Color Standard (Bio-Rad) consisting of 10 recombinant proteins ranging from 10 to 250 kDa was used as a molecular weight marker. Electrophoresis was carried out in a Mini-Protean Tetra cell with an initial voltage of 100 V, followed by 150 V until the sample front was just over the lower edge of the gel. The gel was then stained using Instant blue stain (Sigma-Aldrich) and imaged with a GelDoc EZ System (Bio-Rad).

4.3.4 Biolayer interferometry

The binding kinetics of anti-AGelD187N Fabs were evaluated using biolayer interferometry (BLI) on an Octet RED384 instrument (Sartorius, formerly ForteBio). Streptavidin biosensors were loaded with biotinylated antigens Ag1 and Ag9 and Fabs were added as analytes. The single-concentration equilibrium dissociation constant (K_D) values were determined at 300 nM concentration. Curves were fitted and kinetic parameters were calculated using Octet analysis software (Sartorius,

formerly ForteBio). Multiple concentration kinetics of selected Fabs were determined using the kinetic titration series method at six concentrations ranging from 31 nM to 1 µM. Curves were fitted, and the kinetic parameters were calculated using TraceDrawer software (Ridgeview Instruments).

4.3.5 Aggregation inhibition

Aggregation inhibition experiments were performed similarly to the previously described ThT assay, except that the freshly monomerized and diluted AGelD187N polypeptide was mixed with selected anti-AGelD187N Fabs before the start of the experiments. Anti-poly(GA) Fab was used as a negative control. The mixtures were incubated for 20 minutes at room temperature before adding heparin and ThT and starting the measurement. The final concentrations in the reaction mixtures were 10 µM of AGelD187N, 2.5 µM, 5 µM or 10 µM of anti-AGelD187N Fabs, 10 µM of heparin and 50 µM ThT. In addition to examining the kinetic aggregation curves, the functional activity was evaluated using two different parameters: the effect of Fabs on the AGelD187N aggregation rate and the maximum ThT fluorescence intensities. The aggregation rates were determined by fitting a straight line to the linear range of 0–110 minutes of each aggregation curve by nonlinear regression. Maximum ThT fluorescence intensities were used to evaluate the number of amyloids formed. After the aggregation inhibition experiments, TEM for the pooled samples and SEC-MALS for the pooled sample supernatants were performed as previously described.

4.4 Anti-AGelD187N antibodies

4.4.1 Mammalian display

Error-prone PCR was used to create VL and VH libraries from parental antibody for mammalian display. VL and VH sequences were randomly mutagenized using GeneMorph II Random Mutagenesis Kit (Agilent) according to the manufacturer's instructions. The VL or VH fragments were cloned into the Bxb1-TV[35] vector backbone using the NEBuilder HiFi DNA Assembly Cloning Kit (New England Biolabs) according to the manufacturer's instructions. After assembling the final plasmid constructs, the antibody libraries were electroporated into NEB 10-beta electrocompetent *E. coli* cells (New England Biolabs) using Gene Pulser Xcell (Bio-Rad) and the transformation mixtures were plated on agar plates (Miller´s Luria-Bertani (LB) broth with agar, Sigma-Aldrich) containing 100 µg/ml of ampicillin (Sigma-Aldrich). The next day, the transformants were scraped into Miller´s LB broth containing ampicillin and incubated for 3 hours at 37°C at 250 rpm. Plasmid

DNA for both libraries was extracted from liquid cultures using the Plasmid Plus Midi Kit (Qiagen) with high-copy plasmid protocol according to the manufacturer´s instructions.

A previously established suspension-adapted landing pad cell line (CHO-LP) was used for mammalian display.[35] The cell line was cultured in FectoCHO CD Medium (Polyplus), supplemented with 2 mM GlutaMAX (Gibco) at 37°C, 5% CO_2 at 120 rpm. The antibody libraries were transfected into CHO-LP cells using FectoPro transfection reagent (PolyPlus) according to the manufacturer´s instructions. Two days post-transfection, the antibiotic selection was started with 10 µg/ml puromycin (InvivoGen) and maintained. Eighteen days post-transfection, the libraries were first sorted based on antibody surface display level using anti-phycoerythrin (PE) microbeads (Miltenyi Biotec) according to the manufacturer´s instructions. Six days after the magnetic-activated cell sorting, the libraries were first stained for Ag1 (Caslo) at 37 nM followed by a second staining with Alexa Fluor 647-conjugated mouse anti-biotin antibody (Jackson ImmunoResearch Labs) and PE anti-human Ig light κ chain (BioLegend) according to the manufacturer's instructions. Cells were sorted using the parental antibody as a control, selecting cells exhibiting higher display levels and binding to Ag1 than the parental antibody using the BD FACSMelody Cell Sorter (BD Biosciences).

After FACS, the genomic DNA was extracted from frozen cell pellets using the Monarch Genomic DNA Purification Kit (New England Biolabs). DNA Library Prep Kit (Illumina) was used for the next-generation sequencing (NGS) library preparation following the general workflow for 16S metagenomic library prep (Illumina). Libraries were sequenced on the Illumina MiSeq platform using the MiSeq Reagent Kit v2 (2×250 cycles, paired-end). The sequences were annotated, and the variants were clustered with 100% identity in the whole VH or VL domain using the PipeBio online software. The normalized count for each cluster in each sample was determined by dividing the number of reads in the cluster by the total number of reads in the sample. To assess enrichment after sorting, the normalized count of a cluster was divided by the normalized count of that same cluster in the pre-selection sample. Only variants with more than 1000 reads in the pre-selection sample with more than two-fold enrichment were included.

4.4.2 Production of soluble antibodies

The genes expressing the antibody light and heavy chains were synthesized and cloned into pTwist CMV vector by Twist Biosciences. Plasmids were transfected into 10 ml cultures of ExpiCHO cells (Thermo Fisher Scientific) according to the manufacturer´s instructions. ExpiCHO Feed (Thermo Fisher Scientific) was added 19 h after transfection, and the cultures were incubated at 32°C, 5% CO_2 at 200 rpm

for 11 days. The cultures were harvested by centrifugation. The secreted antibody variants were purified using two-step purification (peak-to-loop method) with HiTrap MabSelect PrismA affinity chromatography column (Cytiva) combined with Superdex 200 Increase 10 300 GL size exclusion chromatography column (Cytiva) on an ÄKTA Pure 25 instrument (Cytiva). The samples were injected using an ALIAS autosampler (Cytiva).

4.4.3 Chip capillary gel electrophoresis

The purity of the anti-AGelD187N antibodies was analyzed in reduced and non-reduced conditions using chip-based capillary gel electrophoresis (chip CE-SDS) on a LabChip GXII Touch instrument (PerkinElmer). Two µl of each sample at ≤ 1 mg/ml concentration was mixed in a 96-well plate with 14 µl of loading buffer (HT Protein Express Sample Buffer) and 2 µl of each sample was mixed with denaturing solution containing 50 mM dithiothreitol. The plate was incubated at 95°C for 5 minutes and 28 µl of water was added to each well. Each sample was analyzed using an HT Protein Express Chip (PerkinElmer). Electropherograms were collected by measuring the sample's fluorescence over time and processed using LabChip® GX Reviewer software (PerkinElmer).

4.4.4 Dynamic light scattering and nano-differential scanning fluorimetry

The hydrodynamic radius and polydispersity of the anti-AGelD187N antibodies were measured using dynamic light scattering (DLS) on a Prometheus Panta instrument (Nanotemper). Ten µl of samples at ≤ 1 mg/ml concentration were loaded by capillarity into high-sensitivity nano-differential scanning fluorimetry (nano-DSF) capillaries (Nanotemper) and placed on the instrument sample tray. Measurements were carried out at 25°C using the high-sensitivity mode in the size analysis function of the Panta Control software. Autocorrelation functions were fitted using both the size distribution analysis and the cumulant analysis method.

The thermal stability of anti-AGelD187N antibodies was measured using nanoDSF method on the same sample capillaries on the same instrument. Samples were subjected to a temperature ramping of 1°C per minute from 20°C to 94.8°C. Tryptophan and tyrosine fluorescence at the emission wavelengths of 330 nm and 350 nm were monitored and the ratio of fluorescence intensities (350nm/330nm) was plotted vs. temperature as an unfolding curve. The inflection point of the unfolding curve corresponds to the thermal unfolding transition midpoint (T_m) and was determined via the curve's derivative.

4.4.5 Affinity-capture self-interaction nanoparticle spectroscopy

Self-interaction of anti-AGelD187N antibodies was assessed using affinity capture self-interaction nanoparticle spectroscopy (AC-SINS). Gold nanoparticles (20 nm, Ted Pella) were washed and diluted by centrifuging for 6 minutes at 21,130 x *g*, after which 95% of the supernatant was removed, and the remaining volume was resuspended to 1.5 times the original volume in ultrapure water (Milli-Q). The washed nanoparticles were conjugated overnight at room temperature with 160 µg/ml of goat anti-human Fc capture antibody (Jackson ImmunoResearch Laboratories, product no. 109-001-008), which had been buffer-exchanged twice into 20 mM potassium acetate (pH 4.3) using Zeba Spin desalting columns with 40 kDa molecular weight cut-off (Thermo Fisher Scientific). Unbound anti-Fc antibody was removed by centrifugation, removing 95% of the supernatant, and resuspending to 18.5% of the original volume in 2 mM potassium acetate pH 4.3.

Antibody variants were diluted to 10 µg/ml using PBS with 100 µg/ml goat non-specific antibody (Jackson ImmunoResearch Laboratories, product no. 005-000-003) added to minimize non-specific binding. Eight microliters of the prepared capture conjugates were then pipetted into the clear-bottomed 384-well plate (Thermo Fisher Scientific) wells, followed by the addition of 72 µl of the prepared antibody sample. After 2 hours of incubation, absorbance spectra were recorded using an Envision 2105 multimode plate reader (PerkinElmer) over a range of 500-600 nm with 1 nm increments. A macro was used to fit a second-order polynomial function to the data to identify the wavelength with the maximum absorbance (plasmon wavelength). The plasmon wavelength of a blank sample with PBS was subtracted from the values of the antibody samples to determine the AC-SINS score. All measurements were conducted in triplicate.

4.4.6 Surface plasmon resonance

The binding kinetics of anti-AGelD187N antibodies were evaluated using surface plasmon resonance (SPR) on a Biacore 8K+ instrument (Cytiva). A capture assay was employed for affinity measurements to reduce avidity effects from the bivalent nature of antibodies. The assay buffer was PBS-P containing 1 g/l BSA. A human antibody capture kit (Cytiva) was used to immobilize anti-human IgG (Fc) antibody onto a CM5 sensor chip (Cytiva) via amine coupling at approximately 7000 RU on flow cells 1 and 2 of each of the 8 channels. The sample antibodies were captured at a concentration of 0.5 µg/ml for 60 seconds at a flow rate of 10 µl/min on flow cell 2 of each channel, achieving capture levels between 60 and 120 RU. A 4-fold dilution series of AGelD187N, with concentrations ranging from 200 nM to 49 pM, was flowed over the captured IgG surface for 300 seconds at a flow rate of 40 µl/min,

followed by a dissociation phase of 600 seconds. Flow cell 1 of each channel was treated similarly but without antibody capture and was used for double referencing. The surface was regenerated between measurement cycles using 3M $MgCl_2$. Association and dissociation rates were determined using Biacore Insight Evaluation software with the Langmuir 1:1 global fitting model, Rmax fit local, and RI set to constant 0. All samples were run in duplicate, and the blank injection in each concentration series was used for double referencing.

5 Results

5.1 AGelD187N aggregation assay development (I)

5.1.1 Assay setup

Lyophilized AGelD187N polypeptides were dissolved in 6 M guanidine hydrochloride, sonicated, and monomerized by gel filtration chromatography to dispose of any residual aggregates. After dilution, their aggregation process was monitored using ThT fluorescence. Ten µM of heparin was added to imitate the chemical environment of the extracellular matrix, where AGelD187N deposits are found in patients. Also, the ThT concentration was kept at 50 µM, which was reported to give the highest fluorescence intensity for three other amyloidogenic proteins.[172] Several other assay parameters were modified to achieve a sigmoidal aggregation curve in a convenient time scale and the highest possible S/B. Different assay setups with used polypeptides, concentrations, well volumes, possible seeding, and achieved S/B ratios are listed in Table 4.

Table 4. Summary of different assay setups and achieved S/B ratios.

Polypeptide	Concentration	Well volume	Seeding	S/B ratio
Ac-AGelD187N 173-243 (95%)[1]	25 µM	200 µl	No	4
AGelD187N 173-242 (90%)[1]	25 µM	200 µl	No	7
AGelD187N 173-242 (95%)[2]	25 µM	200 µl	No	37
AGelD187N 173-242 (95%)[2]	10 µM	200 µl	No	65
AGelD187N 173-242 (95%)[2]	10 µM	200 µl	Yes	85
AGelD187N 173-242 (95%)[2]	**10 µM**	**100 µl**	**Yes**	**127**
AGelD187N 173-242 (95%)[2]	5 µM	100 µl	Yes	70

*__Assay setup in the bold font__ was selected for the aggregation inhibition experiments. S/B, signal-to-background; Ac, acetylated. The percentage in parentheses refers to the RP-HPLC purity of the polypeptide. [1]SEC-HPLC purity after monomerization <90%; [2]SEC-HPLC purity after monomerization >95%

First, AGelD187N polypeptides with different purities and terminal modifications were tested. The best results (S/B ratio 37) were obtained with >95% pure non-acetylated polypeptide (AGelD187N 173-242 (95%)), which was selected for all further experiments. Although TEM revealed long and curvy fibril-like structures, the aggregation curves were hyperbolic, and the maximum intensities were moderate. Next, a lower concentration of AGelD187N 173-242 (95%) polypeptide was tested to achieve better *in vivo* relevancy and save material. Surprisingly, the dilution of AGelD187N from 25 µM to 10 µM led to a sigmoidal aggregation curve, lower initial and higher maximum intensity (S/B ratio 65) (Figure 10). SEC analysis from the assay supernatants revealed a high extent of soluble aggregates in the 25 µM reaction and much less in the 10 µM reaction. The results indicated that some reversible aggregates existed at the beginning of 25 µM reactions, leading to off-pathway aggregation not proceeding into fibrils. Dilution to 10 µM dissociated the reversible aggregates into monomers, triggering proper nucleation and on-pathway aggregation.

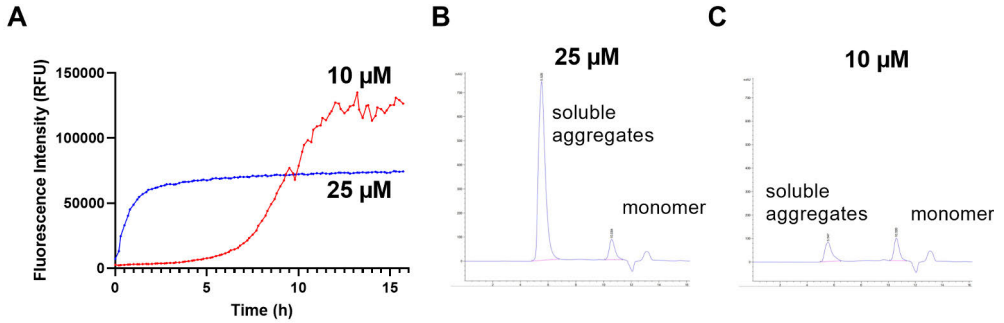

Figure 10. (**A**) Amyloid formation kinetics of AGelD187N 173-242 (95%) at 25 µM (blue curve) and 10 µM (red curve) monitored continuously in ThT assay. Analytical SEC chromatograms after the aggregation assay from (**B**) the assay supernatant of 25 µM reaction and (**C**) from the assay supernatant of 10 µM reaction.

Seeding with preformed fibrils from earlier sigmoidal reactions was tested to improve the exponential phase's reproducibility. Seeding practically eliminated the lag phase observed in spontaneous reactions and increased the maximum signal further (S/B ratio 85). Lastly, the seeded aggregation reaction was transferred to half-area plates to decrease the polypeptide consumption. This further improved the S/B ratio to 127 as the relative ratio of seeds to monomers was higher. As the reproducibility of the assay was maintained despite downscaling, this assay setup was selected for the aggregation inhibition experiments. To further decrease the polypeptide consumption, also AGelD187N concentration of 5 µM was attempted, but this led to lower sensitivity (S/B ratio 70). Also, seeding with a thin copolyamide

thread was tested instead of the pipette. As expected, the lower quantity of transferred seeds led to the reappearance of the lag phase. Still, it also led to a decrease in assay reproducibility due to the manual nature of the technique.

5.1.2 Quality of the polypeptide

The quality of monomerized AGelD187N 173-242 (95%) polypeptide selected for the aggregation inhibition studies was confirmed with tris-SDS-PAGE, SEC-MALS, and LC-MS (Figure 11). In SDS-PAGE analysis with Tri-tricine gel a clear band was visible at the correct location of 8 kDa. LC-MS analysis provided a measured monoisotopic mass of 7857.8 Da, which corresponded fully to the calculated monoisotopic mass of the polypeptide. SEC-MALS analysis also showed the correct molecular weight of 8 kDa for the polypeptide peak, and most importantly, it proved that the monomerized material did not contain aggregates.

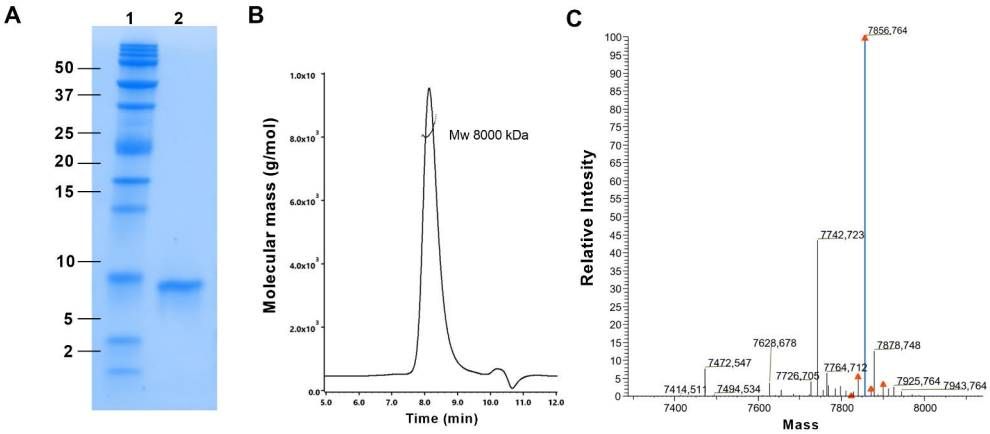

Figure 11. The purity assessment of monomerized AGelD187N 173-242 batch by (**A**) tricine-SDS-PAGE including molecular weight marker (Lane 1) and AGelD187N (Lane 2), (**B**) SEC-MALS, and (**C**) LC-MS (deconvoluted spectrum).

5.2 Discovery of anti-AGelD187N Fabs (II)

5.2.1 Generation of anti-AGelD187N antibody fragments

In addition to full-length AGelD187N (Ag7), three short stretches of AGelD187N (Ag2-4) were used as selection antigens in scFv phage display to discover scFv clones that bind to distinct epitopes in AGelD187N. The initial scFv phage pool consisted of an equal mixture of two closely related synthetic scFv phage libraries, scFvP[309] and scFvM[310]. Both were constructed within the same human framework. The first two or three panning rounds were carried out using a solid-phase protocol, where avidin-coated magnetic beads were loaded with an excess of biotinylated antigens before incubation with phage. A solution-phase protocol was used for the third and fourth rounds, or only the final fourth round. In this approach, avidin-coated beads were employed to capture phage-antigen complexes that had formed during preincubation. Three concentrations of antigens (1 nM, 0.1 nM, or 0.01 nM) were used during the preincubation to optimize the capture of high-affinity binders. The specificities of the scFv phage pools were evaluated after each round using phage immunoassays. After three or four panning rounds, signal-to-background ratios ranging from 140 to 1611 were achieved. In total, 744 single scFv clones were expressed in a soluble screening format in *E. coli*. Of them, 482 clones showed higher than cut-off binding to respective panning antigens in an immunoassay. After a confirmatory secondary screening of 32 purified clones,18 clones were directly converted to Fabs, expressed in CHO cells, purified, and characterized.

In addition to the above-described scFv phage display campaign, Fab libraries were generated from enriched anti-AGelD187N scFv outputs by randomly shuffling VL and VH domains between the clones. This was to convert the antibodies from scFv format to a more stable Fab format before phage display and identify novel VL-VH combinations with higher affinity. The VL/VH shuffled Fab libraries were panned for three rounds against the same antigens as scFvs, and the enrichment was monitored by phage immunoassays. Screening of individual Fab clones resulted in identifying active binders for all selection antigens. Five of the VL/VH-shuffled Fabs were expressed in CHO cells, purified, and characterized.

Overall, 23 clones with unique amino acid sequences of the complementarity-determining regions were expressed as Fabs 1–23 in CHO cells. Their generation method, selection antigen in phage display, and binding affinities against the full-length AGelD187N (N-terminally biotinylated Ag1 and C-terminally biotinylated Ag9) using two different BLI methods (kinetic screening method and kinetic titration series method) are presented in Table 5. Based on binding affinity and antigen specificity, Fabs 4, 14, 19, and 21 were chosen for aggregation inhibition studies.

Table 5. Generation method, selection antigen in phage display, and binding affinities of selected anti-AGelD187N Fabs.

Fab clone	Generation method	Selection antigen in phage display	Affinity, K_D (nM)			
			Kinetic screening[1]		Kinetic titration series[2]	
			Ag1	Ag9	Ag1	Ag9
Fab 19	**VL/VH shuffling**	**Ag3**	**-**	**120**	**-**	**145**
Fab 16	direct conversion	Ag3	-	4770	n.d.	n.d.
Fab 18	direct conversion	Ag3	-	2650	n.d.	n.d.
Fab 17	direct conversion	Ag3	-	3900	n.d.	n.d.
Fab 21	**VL/VH shuffling**	**Ag2**	**125**	**127**	**251**	**324**
Fab 1	direct conversion	Ag2	1580	2500	n.d.	n.d.
Fab 9	direct conversion	Ag2	-	-	n.d.	n.d.
Fab 8	direct conversion	Ag2	-	-	n.d.	n.d.
Fab 10	direct conversion	Ag2	-	-	n.d.	n.d.
Fab 5	direct conversion	Ag2	-	344	n.d.	n.d.
Fab 4	**direct conversion**	**Ag4**	**33**	**46**	**66**	**105**
Fab 20	VL/VH shuffling	Ag4	37	54	34	71
Fab 23	VL/VH shuffling	Ag4	41	57		
Fab 13	direct conversion	Ag4	54	83	79	132
Fab 15	direct conversion	Ag4	97	94	123	129
Fab 3	direct conversion	Ag4	101	120	147	175
Fab 14	**direct conversion**	**Ag7**	**76**	**92**	**67**	**113**
Fab 22	VL/VH shuffling	Ag7	63	87	71	116
Fab 7	direct conversion	Ag7	868	770	2199	1808
Fab 6	direct conversion	Ag7	-	-	n.d.	n.d.
Fab 12	direct conversion	Ag7	-	-	n.d.	n.d.
Fab 2	direct conversion	Ag7	-	-	n.d.	n.d.
Fab 11	direct conversion	Ag7	-	-	n.d.	n.d.

*The clones are grouped according to the selection antigens used in the phage display. **Fabs in bold font** were selected for the aggregation inhibition experiments. [1] 300 nM concentration; [2] Six concentrations ranging from 31 nM to 1 μM; -, not detected; n.d., not determined

Fab 4 was discovered using selection antigen Ag4, which represents the C-terminal region of AGelD187N, Fab 19 using selection antigen Ag3, which represents the N-terminal region of AGelD187N, and Fab 21 using selection antigen Ag2, which represents the proposed fibril-forming region of AGelD187N. Fab 14 was found using the full-length AGelD187N as a selection antigen, and therefore, its binding region in AGelD187N is unknown.

5.2.2 AGelD187N aggregation inhibition

Selected anti-AGelD187N Fabs 4, 14, 19, and 21 were tested in the developed AGelD187N aggregation assay to determine their functional effect on amyloid formation. Ten µM of freshly monomerized AGelD187N was mixed with 2.5 µM, 5 µM, and 10 µM of Fabs and incubated briefly. Each well was seeded with preformed fibrils before the start of the measurement. All Fabs inhibited the amyloid formation at 10 µM concentration (Figure 12). Fabs 4, 19, and 21 showed a concentration-dependent inhibition. Surprisingly, Fab 14 seemed to induce amyloid formation at two lower concentrations. The observation that Fabs 4 and 19 blocked the amyloid formation fully at a 1:1 stoichiometric ratio to AGelD187N was supported by TEM images, taken of all 10 µM samples after the aggregation assay (Figure 13). While in samples without any Fab or with negative control Fab, there were a lot of long fibrils (> 2 mm) present, in samples with Fab 4 and Fab 19, there were only a few short (<0.5 mm) fibrils detected. Fab 14 caused decreased fluorescence intensity by over 30% at 10 µM concentration, and Fab 21 by over 50%. This was supported by the TEM images, where a lower fibril quantity was observed.

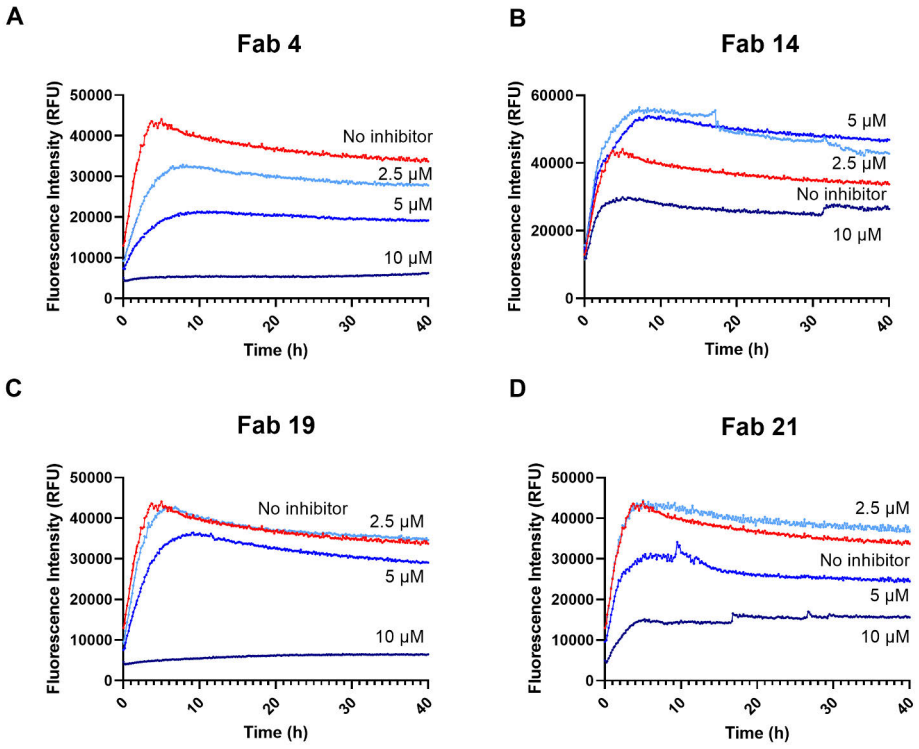

Figure 12. Inhibition of AGelD187N amyloid formation by (**A**) Fab 4, (**B**) Fab 14, (**C**) Fab 19, and (**D**) Fab 21 at 2.5 µM, 5 µM, and 10 µM concentration monitored continuously for 40 h in ThT assay. The mean curve of three replicate measurements is shown.

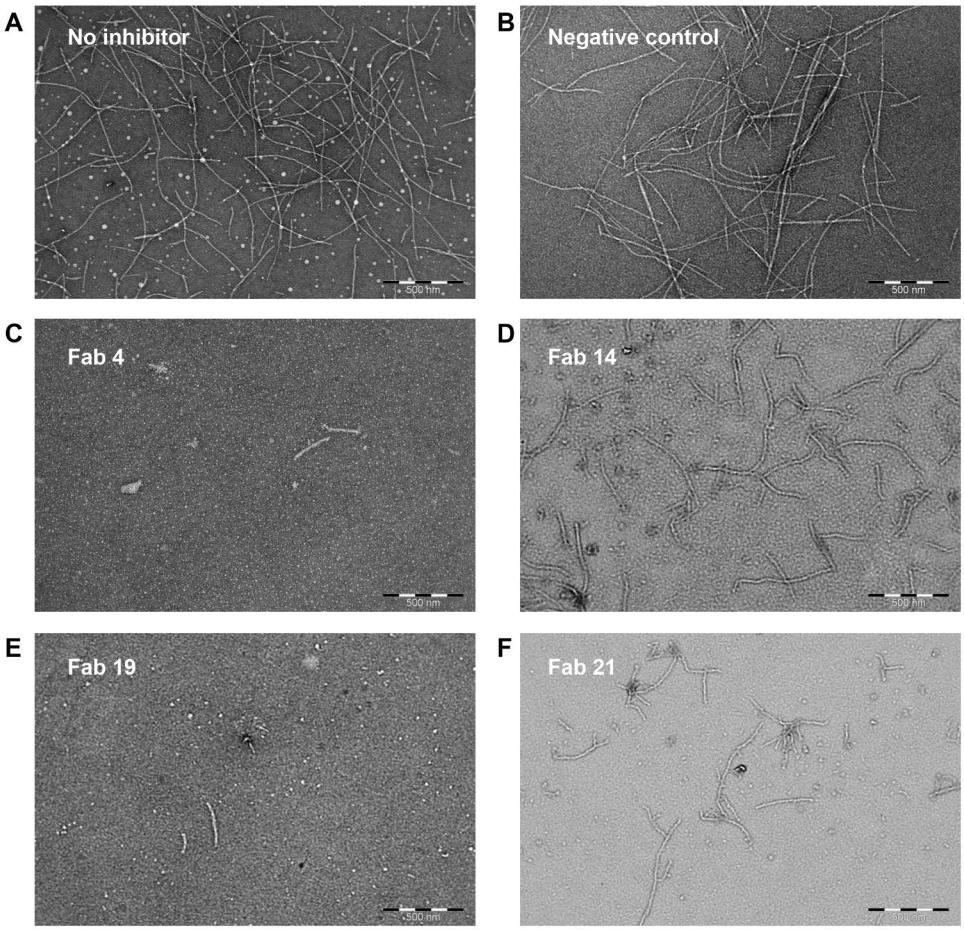

Figure 13. Representative electron micrograph after aggregation assay performed (**A**) in the absence of Fabs, and in the presence of 10 μM (**B**) negative control, (**C**) Fab 4, (**D**) Fab 14, (**E**) Fab 19, and (**F**) Fab 21. The scale bar represents 500 nm.

In addition to examining the kinetic aggregation curves and the TEM images, the functional effect of Fabs on amyloid formation was evaluated using two parameters: the effect of Fabs on the AGelD187N aggregation rate and the maximum ThT fluorescence intensities. The aggregation rates were calculated by fitting a straight line to the linear range of 0 to 110 minutes of each aggregation curve by nonlinear regression. Fab 4 was the most potent aggregation inhibitor as it had a significant effect on both parameters, even at the lowest concentration (Figure 14). Fab 19 was the second potent aggregation inhibitor, as it had more significant effects on the aggregation rate and maximum signal than Fab 21 (Figures 15 and 16).

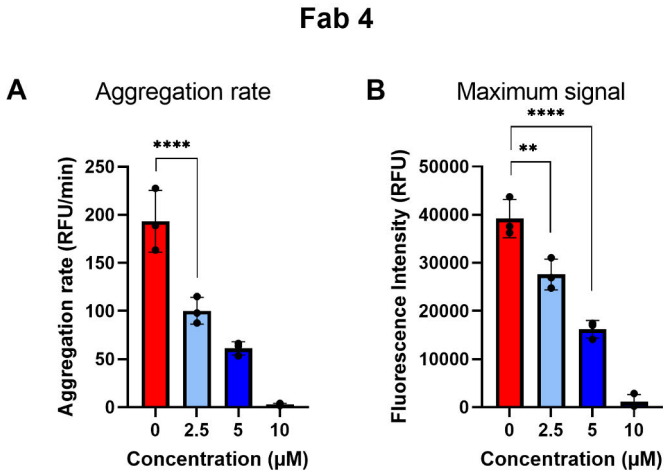

Figure 14. Effect of Fab 4 on (**A**) aggregation rate and (**B**) maximum fluorescence intensity at 2.5 μM, 5 μM, and 10 μM concentration in ThT assay. The data is presented as the mean ± SD. The maximum fluorescence intensities have been baseline-corrected. ****, $p < 0.0001$; **, $p < 0.01$ (one-way ANOVA test, followed by Dunnett´s multiple comparisons test).

Fab 14 was not evaluated further as its functional effects were not concentration-dependent. The emergence of soluble non-ThT binding aggregates due to Fab interference was investigated by SEC-MALS analysis on the assay supernatant of the 10 μM Fab 4 sample. In the control sample, only low levels of soluble monomers and aggregates were present in the assay supernatant, indicating complete amyloid formation. In the Fab 4 sample supernatant, there were no free monomers and even fewer soluble aggregates than in the control. This demonstrated that Fab 4 molecules had bound tightly to all monomers and that the aggregation reaction was blocked without forming off-pathway species. The completeness of the control reaction also confirmed that Fab 14 could not have induced more amyloid formation. Most likely, Fab 14 interfered with the

aggregation process at lower concentrations in a manner that altered fibril morphology, which affected ThT binding and fluorescence.

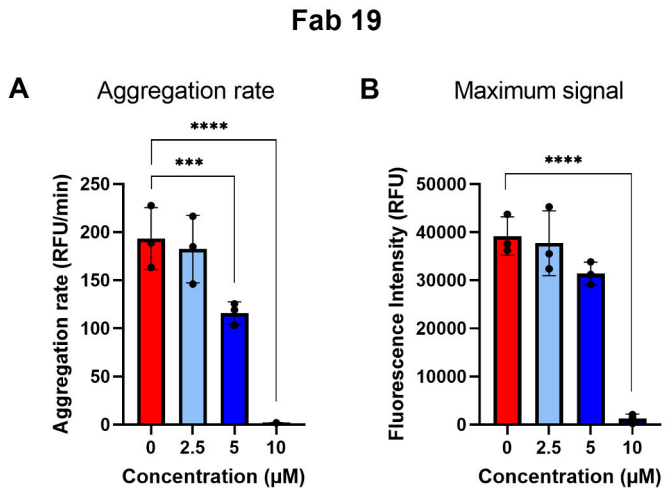

Figure 15. Effect of Fab 19 on (**A**) aggregation rate and (**B**) maximum fluorescence intensity at 2.5 μM, 5 μM, and 10 μM concentration in ThT assay. The data is presented as the mean ± SD. The maximum fluorescence intensities have been baseline-corrected. ****, $p < 0.0001$; ***, $p < 0.001$ (one-way ANOVA test, followed by Dunnett´s multiple comparisons test).

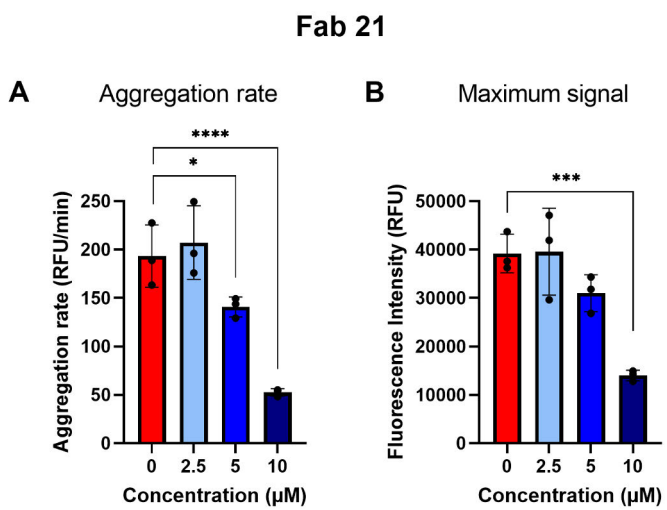

Figure 16. Effect of Fab 21 on (**A**) aggregation rate and (**B**) maximum fluorescence intensity at 2.5 μM, 5 μM, and 10 μM concentration in ThT assay. The data is presented as the mean ± SD. The maximum fluorescence intensities have been baseline-corrected. ****, $p < 0.0001$; ***, $p < 0.001$; *, $p < 0.05$ (one-way ANOVA test, followed by Dunnett´s multiple comparisons test).

5.3 Optimization of anti-AGelD187N antibody (III)

5.3.1 Properties of parental anti-AGelD187N antibody

As monoclonal antibodies are the predominant class of biopharmaceuticals, the conversion of the best anti-AGelD187N Fab to IgG format was pursued. Fab 20 was selected as it had a higher affinity in the BLI kinetic titration series assay (K_D 34 nM vs. 66 nM) and the same CDR regions as Fab 4. The only amino acid difference was in light chain framework position 78 (according to the Kabat numbering scheme), where Fab 4 had leucine and Fab 20 proline. After IgG conversion, the antibody was expressed in CHO cells, purified, buffer exchanged to 50 mM histidine-acetate buffer pH 6.0, and characterized. The total purity of the resulting antibody was 100% (with reduced chip CE-SDS), the aggregate level was 1.4% (with SEC), and the cumulant polydispersity index was 0.05 (with DLS). These analyses confirmed that the sample was a homogeneous monomeric solution free of fragments and aggregates.

After purity analyses, the intrinsic biophysical properties of the antibody were evaluated. The affinity of the full-length antibody to AGelD187N was investigated. BLI kinetic measurements, where the assay setup was similar to Fabs (antibody as the analyte and AGelD187N immobilized on the sensor), were not successful as the results could not be fitted reliably. An SPR capture assay was employed in which the sample antibody was captured on the sensor chip by an anti-human Fc antibody to reduce avidity effects. The affinity of anti-AGelD187N antibody to AGelD187N was measured to be 370 pM at 1:1 binding mode (Figure 17).

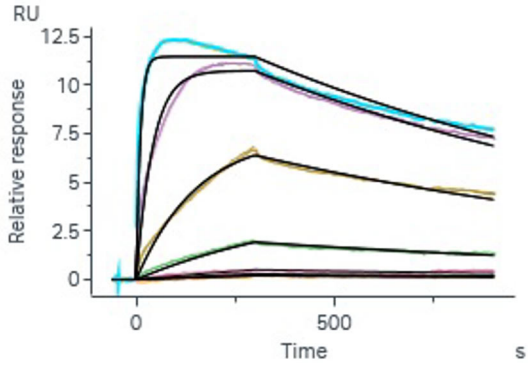

Figure 17. Representative SPR sensorgram of AGelD187N binding to captured anti-AGelD187N antibody. Increasing concentrations (0.049, 0.195, 0.78, 3.125, 12.5, and 50 nM) of AGelD187N were passed over a surface containing anti-AGelD187N IgG. Dissociation constant K_D = 3.70E-10 nM, association rate constant k_a = 2.04E+06 1/Ms, dissociation rate constant k_d = 7.53E-04 1/s. The values are an average of five separate measurements.

Next, the thermal stability was investigated with nanoDSF by gradually heating the sample and monitoring the unfolding process by exploiting the autofluorescence of the antibody´s tryptophan and tyrosine residues. The unfolding midpoint (T_m) of the antibody Fab region was discovered to be very high, 72.9°C, indicating high conformational stability.

Last, the colloidal stability of the antibody was investigated by measuring the self-interaction by AC-SINS. Gold nanoparticles were coated with polyclonal, anti-human antibodies that bind to the anti-AGelD187N antibody. This enabled the detection of potential self-association of antibody molecules based on clustering of the nanoparticle conjugates, which leads to a redshift in their absorption. Jain et al. have determined thresholds for developability warning flags by examining the biophysical properties of 137 clinical-stage antibodies.[272] According to the updated 90% developability threshold (cutoff of 10% worst values), a redshift value of more than 13.8 nm in the AC-SINS assay was determined as a red flag.[271] An average redshift of 27.3 nm was observed for the anti-AGelD187N antibody, indicating poor colloidal stability.

5.3.2 Generation of anti-AGelD187N antibody variants

The high self-interaction propensity of the anti-AGelD187N antibody indicated potential developability problems at higher concentrations. To enable the development of a desired subcutaneous drug product, an optimization campaign to improve the poor colloidal stability of the antibody was initiated. Random mutagenesis by error-prone PCR was performed to create VL and VH libraries from the parental anti-AGelD187N sequence for mammalian display. The VL and VH libraries were stably integrated into the CHO-LP cells, and mutant libraries containing 3 - 4 × 10^5 variants were obtained. After enriching antibody-expressing cells by magnetic-activated cell sorting, libraries were sorted by FACS. The cells were sorted using the parental antibody as a control, selecting cells exhibiting higher display levels and binding to AGelD187N than the parental antibody. Next-generation sequencing was used to analyze the enrichment of variants. The enrichment factor was calculated by dividing the normalized count of variants after sorting by the normalized count of the variants before sorting. The four most enriched VL variants (VL1-VL4) and the seven most enriched VH variants (VH1-VH7) were selected (Figure 18).

Enriched mutations were located in both the CDRs and the framework regions. VL1 and VL2 mutations were in the CDR-L1 region, VH1 and VH3 mutations in the CDR-H3 region, and VH4 and VH6 mutations in the CDR-H2 region. The remaining mutations were in framework regions. Four mutations were subtle changes to amino acids that were similar to the original amino acids. Polar serine (S) was changed to polar asparagine (N) in VL1, and hydrophobic amino acids phenylalanine (F) and alanine (A) to hydrophobic valine (V) and leucine (L) in VL3,

VH1, and VH7. Five mutations increased the polarity or positive charge. Polar asparagine was changed to positive lysine (K) in VL2, hydrophobic isoleucine (I) to polar serine in VL4, hydrophobic tryptophan (W) to positive arginine (R) in VH2, hydrophobic alanine to polar threonine (T) in VH3 and finally a full charge reversal of negative glutamic acid (E) to positive lysine in VH6. The remaining two mutations increased hydrophobicity. A glutamic acid was changed to valine in VH4, and an arginine was changed to tryptophan in VH5.

Each mutated variable domain was combined with the corresponding parental variable domain to investigate each mutation's impact on the antibody's biophysical properties. Moreover, each mutated variable light domain was combined with each mutated heavy domain to investigate the synergy of the two mutations. All variants were expressed as full-length IgGs in 10 ml CHO cell cultures, purified, and buffer exchanged to 50 mM histidine-acetate buffer pH 6.0. The yield of the parental anti-AGelD187N antibody was 360 µg, and the yields of 36 variants were 20-460 µg. Yields of all VL4 variants were less than 50 µg. No material was recovered for three variants, VL4-VH1, VL4-VH2, and VL4-VH7.

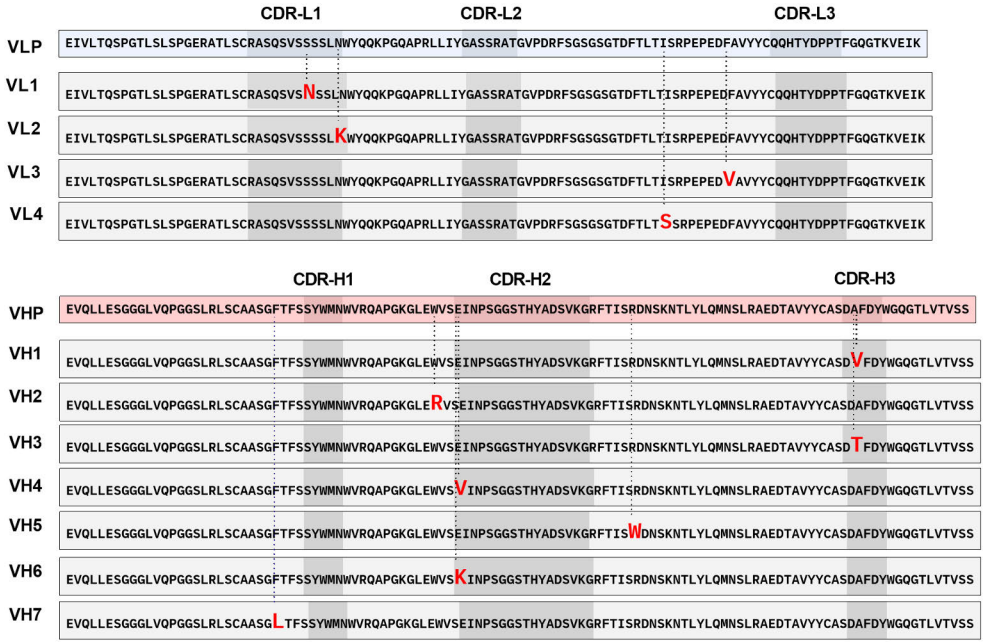

Figure 18. Sequence alignment of parental VL (VLP) and selected variant VLs (VL1-VL4) and parental VH (VHP) and selected variant VHs (VH1-VH7) of anti-AGelD187N antibody. Mutated amino acids are enlarged and red. The dotted vertical line indicates the parental amino acid in the same position. The CDR regions follow the Kabat numbering scheme.

5.3.3 Characterization of anti-AGelD187N antibody variants

Like the parental anti-AGelD187N antibody, the obtained 36 anti-AGelD187N antibody variants were first analyzed for purity using SEC, chip CE-SDS, and DLS. All other samples were homogenous monomeric solutions free of fragments and aggregates, except the VL2-VH2, the VL3-VH4, and the parental VL-VH2 variants, which contained 39.6%, 12.3%, and 12.5% aggregates, respectively, according to SEC analyses.

After purity analyses, the colloidal and thermal stability and target binding of the variants were investigated. Initially, the 11 variants with one mutated variable domain and one parental variable domain were examined. Ten variants exhibited reduced self-interaction, and for six of them, the self-interaction decreased below the developability threshold established by Jain et al. (Figure 19A). We accepted a tenfold deterioration in affinity up to 3.7 nM based on the abundance of plasma gelsolin in the body[136] and the target binding affinities of approved Aβ antibodies[311]. Three variants retained the parental antibody target binding, and, for one variant, the decline of affinity was within set limits (Figure 19B). The VL1 variant was the only variant that had improved colloidal stability without a decrease in binding. Also, the thermal stability of the VL1 variant remained high and well above the Bailly et al. developability threshold of Fab T_m of 65 °C (Table 6).[269] Thus, it was considered to meet the requirements for a drug-like antibody.

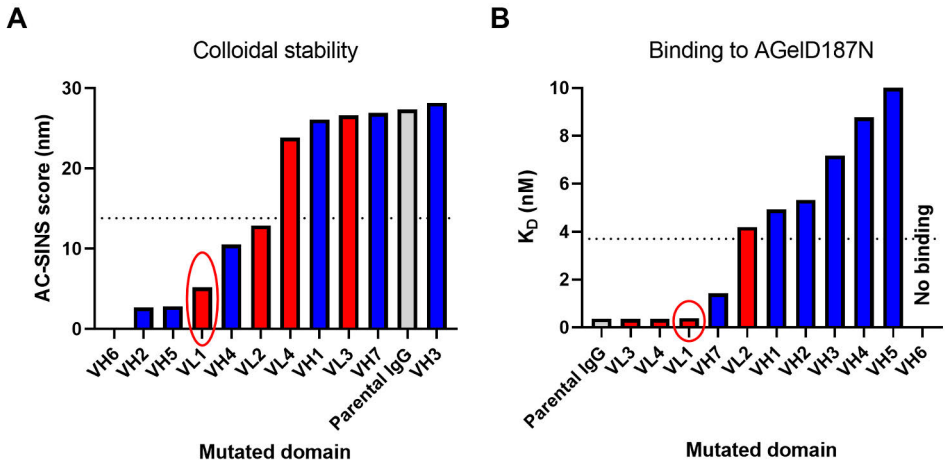

Figure 19. Effect of one mutated variable domain on (**A**) colloidal stability and (**B**) binding of anti-AGelD187N antibody variants. Variants with VL mutation are in red, variants with VH mutation are in blue, and the parental antibody is in gray. The dotted horizontal lines indicate the defined threshold values for the AC-SINS score (13.8 nm) and target binding (3.7 nM). Circled in red is the VL1 variant, the colloidal stability of which improved without loss of affinity.

Table 6. Investigated biophysical properties of anti-AGelD187N antibody variants with one mutated variable domain

Variant	Colloidal stability	Thermal stability	Binding affinity to Ag1
	AC-SINS score	Fab T_m (°C)	K_D (nM)
Parental antibody	27.3	72.9	0.37
VL1 + PARENTAL VH	**5.2**	**71.5**	**0.39**
VL2 + PARENTAL VH	12.9	71.4	4.19
VL3 + PARENTAL VH	26.6	76.9	0.36
VL4 + PARENTAL VH	23.8	63.9	0.36
PARENTAL VL + VH1	26.1	72.0	4.92
PARENTAL VL + VH2[1]	2.7	66.1	5.33
PARENTAL VL + VH3	28.2	72.8	7.18
PARENTAL VL + VH4	10.5	73.6	8.77
PARENTAL VL + VH5	2.8	70.4	10.00
PARENTAL VL + VH6	0.2	78.1	-
PARENTAL VL + VH7	26.9	72.8	1.43

*__Variant boxed and in bold font__ is identified as drug-like. [1] >10% aggregates; -, not detected

The effects of two combinatorial mutations coincided well with the effects of individual mutations. All VL1 variants, regardless of the VH pair, exhibited a low self-interaction score (Table 7). However, the added heavy chain mutations decreased the binding affinity of the variants to the nanomolar level, like when they were paired with the parental VL. Only the VL1-VH7 variant met the requirements of a drug-like antibody as its K_D remained below the cut-off value of 3.7 nM. When the VL2 domain was combined with any of the VH variants, the binding was fully lost. An unexpected synergy was observed when the VL3 variant was paired with the VH2 variant, resulting in a higher affinity than that of the VH2 domain combined with the parental VL. The VL3-VH2 variant met the requirements of a drug-like antibody, as also its colloidal and thermal stability were within acceptable ranges. Another unexpected synergy emerged when VL4 was combined with VH3, leading to a marginally acceptable colloidal stability. However, the variant's affinity and thermal stability were not high enough. Overall, two of the 25 combinatorial variants, the VL1-VH7 and the VL3-VH2 variants, were considered to meet the requirements for a drug-like antibody. Including the VL1 variant paired with the parental VH, a total of three drug-like anti-AGelD187N antibody variants were identified in this study.

Table 7. Investigated biophysical properties of anti-AGeID187N antibody variants with two mutated variable domains.

Variant	Colloidal stability	Thermal stability	Binding affinity to Ag1
	AC-SINS score	Fab T_m (°C)	K_D (nM)
Parental antibody	27.3	72.9	0.37
VL1+ VH1	1.0	70.5	5.77
VL1+ VH2	0.2	64.6	8.37
VL1 + VH3	1.5	71.2	7.96
VL1 + VH4	0.5	71.8	9.26
VL1 + VH5	0.0	68.9	9.52
VL1 + VH6	-0.3	76.1	-
VL1 + VH7	**0.9**	**71.4**	**1.76**
VL2 + VH1	8.7	70.0	-
VL2 + VH2[1]	0.4	64.9	-
VL2 + VH3	10.6	70.8	-
VL2 + VH4	6.6	71.2	-
VL2 + VH5	0.4	68.9	-
VL2 + VH6	0.1	74.9	-
VL2 + VH7	4.7	71.0	18.9
VL3 + VH1	25.4	75.5	4.27
VL3 + VH2	**3.7**	**68.7**	**2.66**
VL3 + VH3	28.7	76.4	7.39
VL3 + VH4[1]	8.1	76.8	8.07
VL3 + VH5	2.8	74.2	11.9
VL3 + VH6	0.5	81.0	-
VL3 + VH7	23.9	76.1	1.1
VL4 + VH3	13.5	63.8	8.28
VL4 + VH4	9.9	65.3	9.23
VL4 + VH5	1.9	58.7	12.6
VL4 + VH6	0.3	67.9	-

*__Variants boxed and in bold font__ are identified as drug-like. [1] >10% aggregates; -, not detected

6 Discussion

6.1 AGelD187N aggregation assay development (I)

In study I, we described the development of an *in vitro* aggregation assay for the 70-residue polypeptide AGelD187N 173-242, the main amyloidogenic fragment in gelsolin amyloidosis. Our results show that reproducible aggregation kinetics were attainable for the synthetic full-length AGelD187N when it was correctly handled. The ability to reliably monitor the aggregation process of AGelD187N 173-242 enables the evaluation of the functional impact of potential aggregation inhibitors. To our knowledge, this is the first time that this long amyloidogenic polypeptide made by solid-phase chemical synthesis has been successfully used for aggregation studies.

We aimed to use the full-length AGelD187N fragment containing amino acid residues 173-242 in our studies because we did not consider the aggregation studies performed with short synthetic segments of AGelD187N[17-19] *in vivo*-relevant. However, the biotechnological production of amyloidogenic proteins on a sufficient scale for drug screening presents numerous challenges due to their inherent hydrophobic nature.[312] We chose to use synthetic material, but special efforts were also needed here to overcome the barriers that existed in the use of such a long synthetic polypeptide in sensitive aggregation studies. The first step was to find a supplier willing to try to produce the exceptionally long polypeptide with chemical synthesis. In the course of the investigation, it also became clear that the ordinary quality of commercial peptides was not sufficient, but the purity requirement had to be set very high (RP-HPLC >95%). Typically, N- and C-terminal modifications are routinely added to synthetic peptides to mimic the native proteins more closely. During the study I we learned that N-terminal acetylation had to be excluded from AGelD187N 173-242 as it had a significant negative effect on its aggregation tendency. This was surprising, as N-terminal acetylation neutralizes the positive charge and increases the hydrophobicity of the N-terminus.[313] However, most likely also the disease-relevant AGelD187N 173-242 does not have N-terminal acetylation, as it has formed as a result of aberrant cleavage.

Given that proteins associated with misfolding diseases are typically highly prone to aggregation, obtaining the protein in monomeric form at the start of the experiment is not a straightforward task. To eliminate the possible residual aggregates after dissolution of the lyophilized product, we added a monomerization step and control analysis to our workflow. Yet, a typical sigmoidal aggregation curve and a background-level initial fluorescence signal for AGelD187N 173-242 were achieved only after adding an extra dilution step to the workflow. The dilution shifted the equilibrium of the reaction more to the direction of stable monomers, which led to the dissociation of most likely existing but not detectable, reversible associated species.[314] These transient off-pathway species were not detectable by control SEC analysis but led to the growth of aggregates that did not proceed to form fibrils.[315] Since the growth of an aggregate occurs at a higher rate with a lower free energy barrier than nucleation, the ´correct´ amyloid formation could occur only after the starting material was a fully homogeneous monomer solution.[314]

As always, *in vitro* assays are much simplified compared to the *in vivo* situation. A biological system is a highly dynamic environment with high molecular crowding and a variable single protein concentration.[10] Additionally, interactions may occur with various biological membranes instead of the water-air interface and laboratory material surfaces present *in vitro*. Fully monomeric starting material results in a clean mass balance *in vitro*, meaning that most material will convert into fibrils, but the highly different conditions *in vitro* and *in vivo* still most likely affect the aggregation process and the fibril morphology.[37,60] However, when investigating the aggregation inhibition of a monomer, the most relevant aspect is that the monomer is disease-relevant and aggregation-competent. The aggregation process must also be reproducible to be able to evaluate and compare the functional effects of potential aggregation inhibitors. Primary nucleation is inherently a slow process, characterized by a high free energy barrier.[314] This results in high sensitivity to any variations in the sample or environment, leading to inevitable fluctuations in the timescale of the aggregation process. Study I demonstrated that by introducing AGelD187N 173-242 fibrils from previous experiments into the monomer solution at the start of the experiment, primary nucleation could be bypassed and simultaneous on-pathway aggregation across all wells achieved. We confirmed that the reproducibility of the seeded assay was maintained despite assay downscaling, which allows for a greater number of potential inhibitors to be screened using the same quantity of assay components.

As a note from study II, despite assay downscaling, when many candidates are screened with several concentrations, the amount of needed protein becomes large, and as a result, many details in the experiment will change (monomerization process, surfaces, waiting times, etc.). As protein aggregation studies are particularly vulnerable to any changes in the assay setup, the aggregation assay reproducibility

should be ensured on the same scale as the actual inhibition experiment, even if it means losing a large amount of precious material. The automation of the procedures should be an effective means to decrease sample volumes and increase reproducibility further.

6.2 Discovery of anti-AGelD187N Fabs (II)

In study II, we described the discovery of epitope-specific antibody fragments that blocked the aggregation of AGelD187N in the aggregation assay described in study I. Antibody fragments were discovered using different regions of AGelD187N as selection antigens, however, all inhibited its aggregation *in vitro*. To our knowledge, this is the first time that specific binding to AGelD187N has been achieved, and it has been demonstrated that all regions of the full-length AGelD187N are important in modulating its assembly into fibrils.

Many anti-amyloid antibodies have high selectivity for the aggregated forms over the protein monomers.[106,107,316-319] Their main mechanism of action is the removal of amyloid plaques by antibody-mediated activation of phagocytic immune cells. One major reason for targeting aggregates is the amyloid cascade hypothesis in the Alzheimer´s disease field, suggesting that Aβ deposits in the brain are the initiating event in the disease pathogenesis.[320] Another justification for targeting aggregates is to avoid interfering with the monomer´s physiological function.[116] However, although effective removal of amyloids has been demonstrated, this mechanism of action has severe safety concerns. Amyloid-related imaging abnormalities (ARIA) have been reported during Alzheimer´s disease immunotherapy.[112-115] Anti-serum amyloid P antibody, which activates the complement and triggers clearance of all amyloid deposits by macrophage-derived multinucleated giant cells, was recently discontinued because of a suboptimal safety profile.[321,322] In addition to the safety problems, the clinical benefit of amyloid removal has been modest in Alzheimer´s disease. This might be explained by the theory that the neuronal damage is caused more by the transient soluble oligomers present during the aggregation process.[191,323] Unlike most other misfolding monomers, the extracellular AGelD187N monomer does not naturally occur in the body. Therefore, it is a logical target to be neutralized. Targeting the monomer can avoid the safety problems related to amyloid removal and the formation of toxic oligomers. Additionally, if artificially produced amyloid fibrils were used as antigens in antibody discovery, there could be a significant risk that the developed antibodies would not bind to amyloid deposits in patients' tissues. *In vitro*-prepared amyloid fibrils are many times structurally different from patient-derived fibrils.[37,60] This is because the same protein sequence can adopt a variety of different fibrillar polymorphs depending on conditions.

We aimed to find antibody fragments that would bind to the AGelD187N monomers before the initiation of nucleation and inhibit the aggregation process completely by steric hindrance. To effectively inhibit monomer aggregation, it may or may not be essential to target the amyloidogenic core of the protein.[324-328] An amyloidogenic region of AGelD187N comprising amino acids 182-192 of the original plasma gelsolin was proposed 30 years ago based on aggregation studies on short peptides derived from the full-length fragment.[144] To investigate the importance of this region as a target compared to other regions of AGelD187N, we needed antibody fragments binding to different regions of AGelD187N. One of the advantages of phage display is that it is possible to target distinct antigen epitopes without the need for them to be immunogenic. Three short stretches of AGelD187N were used as selection antigens to generate antibody fragments that bind to different epitopes: the proposed fibril-forming region comprising amino acids 181-192 (Ag2), the N-terminal region comprising amino acids 173-186 (Ag3), and the C-terminal region comprising amino acids 227-242 (Ag4) of AGelD187N. The results of study II demonstrated that the earlier proposed fibril-forming region of AGelD187N is not an essential target for aggregation inhibition; conversely, some other regions might be more beneficial. The best inhibitor, Fab 4, could fully block both the amyloid formation and soluble aggregate formation, although its binding region in AGelD187N was at the other end of the fragment from the proposed fibril-forming region. The aggregation inhibition may have been caused either by the stabilization of the AGelD187N by binding to an important flanking region or by inducing a conformational change of AGelD187N, which was the mechanism of action of β-wrapin AS69 that binds to β-strands β1 and β2 of α-synuclein monomer and not the central NAC region comprising strands β3 to β5.[329,330] It is also possible that the proposed fibril-forming region does not have such a central role in the aggregation of full-length AGelD187N as suggested, as full-length material was not used in those studies.[144] The anti-AGelD187N Fabs discovered in study II can now be used to study the fibril structure of disease-relevant AGelD187N fibrils. If a Fab binds only to monomeric AGelD187N and not to patient-derived AGel fibrils, it binds to a region of AGelD187N that becomes buried inside the AGel fibril core.[325] This information would help to shed light on the structure of AGelD187N fibrils, although it would not replace atomic resolution analyses. Nevertheless, based on study II, all regions of the full-length AGelD187N are important in the modulation of its assembly into fibrils. The results of study II also strengthened our vision that only the full-length AGelD187N containing amino acid residues 173–242 should be used in the aggregation experiments.

The results of study II demonstrated that one tightly bound Fab fragment could neutralize one AGelD187N polypeptide *in vitro*. To confirm the target engagement and neutralization efficiency in a biological context, next, an *in vivo* experiment

should be performed. A transgenic mouse model has been developed in which a muscle creatine kinase promoter controls the expression of human D187N plasma gelsolin.[154] The heterozygous mice develop amyloid deposits restricted in cardiac and striated muscles starting at three months and display signs of muscle weakness at 12-14 months. Overbeke et al. have reported a statistically significant efficacy in the model after treating the mice weekly for 12 weeks with a bispecific nanobody FAF Nb2-MSA21, which targets AGelD187N precursor C68 fragment.[30] We aimed to convert the best anti-AGelD187N Fab from study II to a full-length antibody since monoclonal antibodies are established biotherapeutics. For the antibody to be effective in the AGel model, it should meet several conditions related to its bioavailability and specificity. In addition to remaining stable in plasma for several days, it should enter the muscle tissue where the AGelD187N fragments are formed and aggregated. The antibody´s affinity toward the antigen can impact the tissue distribution, but a typical antibody concentration in the muscle interstitial space is 4% of the plasma concentration.[331] Furthermore, the antibody should specifically bind the AGelD187N fragment. Non-specific binding and binding to full-length plasma gelsolin should be excluded to avoid the dilution of the therapeutic effect. Also, the antibody should preferably be specific only for the monomeric form of AGelD187N, as AGel fibril binding would change the antibody from anti-aggregational to anti-amyloid antibody with a completely different mechanism of action and safety profile. After binding, the antibody-antigen complexes should exit from the aggregation site with the tissue fluid flow, and their elimination should follow the linear nonspecific clearance of the antibody.[332,333] Affinity maturation of the antibody or accelerated clearance of the formed AGelD187N-antibody complexes might be needed for sufficient efficacy, as plasma gelsolin is produced in abundance in the body. Accelerated clearance can be accomplished by engineering the antibody for efficient effector functions and pH-dependent antigen binding.[227,334-336] For instance, in a “sweeping antibody”, the constant and variable regions of the antibody are engineered for pH-dependency to enhance the neonatal Fc receptor (FcRn)-mediated uptake and recycling of the antibody-antigen complex, allowing the antibody to be recirculated while the antigen undergoes lysosomal degradation.[337]

Assuming that the efficacy of an anti-AGelD187N antibody can be demonstrated in AGel mice, preclinical and clinical safety must be ensured before entering into clinical studies with gelsolin amyloidosis patients. Since healthy animals and humans do not generate AGelD187N fragments, the AGel mouse model is also needed to study the on-target toxicity.[338,339] A successful example of a similar approach is the human-cynomolgus monkey chimeric antibody keliximab, for which the preclinical safety assessment was conducted mainly using humanized transgenic mice expressing human CD4.[340] The transgenic animal model can also be used for

the development of a translatable pharmacodynamic biomarker for clinical studies. Verhelle et al. have tested three AGelD187N binding nanobodies, FAF Nb1-3, as ^{99m}Tc-based SPECT/CT imaging agents in AGel mice. [341] The clinical application of these nanobodies as non-invasive imaging agents should not pose a problem, as nanobodies can also be linked with PET-compatible radiopharmaceuticals. Anti-AGelD187N Fabs from study II could also be used as similar imaging agents if their plasma stability, tissue accessibility, and specificity are adequate.

The anti-AGelD187N antibody would probably be dosed via the intravenous route in the first preclinical and clinical studies, like most of the therapeutic mAbs. However, subcutaneous administration would alleviate the healthcare burden, enhance the quality of life for patients, and minimize costs and resource strain on infusion centers.[342] This is especially important when treating chronic diseases like gelsolin amyloidosis. Local administration of anti-AGelD187N therapy in the eye could be a viable option either as an independent treatment or in addition to systemic therapy, as corneal amyloidosis is the earliest clinical manifestation of gelsolin amyloidosis. Several reports have demonstrated the clinical efficacy of topical anti-vascular endothelial growth factor (VEGF) antibody bevacizumab in reducing corneal neovascularization.[343-346] Also, ranibizumab, a Fab fragment derived from the same antibody as bevacizumab, has been studied as a topical treatment for corneal neovascularization in a small pilot study.[347] Kessel et al. have trained and validated deep-learning algorithms to quantify relative amyloid deposition in corneal sections from gelsolin amyloidosis patients and assess its relationship with visual acuity.[348] A non-invasive approach was reported by Gu et al., where the algorithm was trained using ocular surface images.[349] Latter would be an elegant way to evaluate the efficacy of either systemic or local anti-AGelD187N antibody or Fab treatment.

It is likely to be expected that the maximum effect of anti-AGelD187N therapy is reached when the treatment is started early in the course of the disease, when the number of AGelD187N fragments to be neutralized is still small. Timely recruitment of patients to a clinical study should be possible as gelsolin amyloidosis is an autosomal dominant disease with complete penetrance, meaning patients can be identified before explicit clinical signs appear.[350] The bigger question is the clinical study duration; as gelsolin amyloidosis is a slowly progressing disease, a long treatment period with anti-AGelD187N antibody is likely needed to demonstrate the efficacy of the treatment. Another challenge for conducting clinical studies is the rarity of gelsolin amyloidosis. Traditional clinical trial designs, validation, and evaluation methodologies used for non-orphan drugs are often unsuitable due to small patient populations.[351] For these reasons, close collaboration between stakeholders, including researchers, clinicians, regulators, patient advocacy groups, and industry, is needed for success.

6.3 Optimization of anti-AGelD187N antibody (III)

In study III, we described the optimization of anti-AGelD187N antibody, which exhibited problematic self-interaction tendency, for subcutaneous use. The colloidal stability of the parental antibody was improved using mammalian display to select improved VL and VH variants from libraries created by error-prone PCR. Three variants with significantly lower self-interaction and retained target binding and thermal stability were identified. To our knowledge, this is the first time that mammalian display has been successfully used to improve the biophysical properties of an antibody in combination with error-prone PCR.

A very high self-interaction score for the anti-AGelD187N antibody was measured, indicating low colloidal stability. Poor colloidal stability affects the bulk solution rheology and can lead to high viscosity, low solubility, and phase separation at high concentrations.[289,299,352] Poor colloidal stability has also been found to be connected to undesired non-specificity, which means the antibody´s general stickiness and ability to interact with a variety of binding partners.[286,302] In our case, poor colloidal stability was a particular challenge because it was known that high antibody concentrations would be needed. Gelsolin amyloidosis is a chronic disease so it should be possible to administer the treatment at home via subcutaneous injection. Many previous studies have shown that there is a trade-off between affinity and colloidal stability[300,302,305,353,354] and that suboptimal developability properties have been particularly observed in antibodies derived from phage display, which lacks the quality control machinery of higher eukaryotic cells.[272,300,305] Therefore, we exploited another, more suitable *in vitro* selection technology to solve the developability problem. In mammalian display, millions of full-length antibody variants are presented on the surface of mammalian cells. They can be screened for desired affinity and developability properties simultaneously, although the library sizes remain smaller than in phage display.[34-36]

Information on the three-dimensional structure of an antibody-antigen complex would help understand the antibody-antigen interactions at the atomic level and design a targeted optimization library.[35] Giorgino et al. have obtained the crystal structure of the isolated G2 domain of the human D187N plasma gelsolin in a complex with nanobody Nb11.[138] A high-resolution structural analysis of the AGelD187N fragment and anti-AGelD187N Fab based on X-ray crystallography is not applicable, as the AGelD187N fragment is intrinsically disordered and lacks a stable 3D structure. Although recent artificial intelligence (AI) approaches combined with experimental techniques like nuclear magnetic resonance (NMR) spectroscopy can increase our understanding of the conformational properties of IDPs and their complexes, their structural prediction remains challenging.[355] On the other hand, comprehensively mutagenized libraries would have been too large for the mammalian display platform. Therefore, error-prone PCR was selected as a suitable

method to generate small fully random libraries without the need for any knowledge of the antibody-antigen interactions. [356]

Based on the results of study III, the strong interactions between the anti-AGelD187N antibody and the target were mainly governed by the whole VH domain and CDR-L1 of the antibody. The target binding could no longer be improved, which was expected for a picomolar binder. All VH mutations, whether in the CDRs or framework regions, decreased the target binding. Mutations in CDR-H2 and its surroundings were the most harmful. The VH6 mutation on the border of the CDR-H2 fully eliminated the binding, although at the same time, it significantly improved both thermal and colloidal stability. Similar to the VH6 mutation, the VL2 mutation in CDR-L1 decreased the affinity while increasing the colloidal stability. Unlike these, both CDR-H3 mutations reduced the affinity, but they did not affect thermal or colloidal stability simultaneously. These results imply that the antibody´s self-interaction propensity was mainly governed by CDR-H2 and L1 but not by H3.

The most important result of study III was the identification of the VL1 mutation in CDR-L1 that reduced the self-interaction of the variant antibody without disturbing the target binding interactions. The replacement of one small, flexible, and highly interactive serine in the middle of a four-serine-repeat motif with a larger and less interactive asparagine, although also polar, probably added enough rigidity to the paratope to reduce self-interaction without changing the conformation of the paratope too much. In addition to the beneficial VL1 mutation, two drug-like combinatorial variants were identified. The VH7 mutation in the FR1 region resulted in the smallest reduction in affinity among all VH mutations, causing only a four-fold decrease. However, the VH7 did not significantly improve colloidal stability on its own. Interestingly, this level of reduced interaction in the VH domain was sufficient to minimize self-interaction when combined with the VL1 mutation. This finding underscores that, like antibody affinity, an antibody's overall self-interaction propensity is influenced by multiple distinct interactions, which can be fine-tuned. In contrast, the affinity reduction caused by the VH2 mutation was too substantial to be considered acceptable on its own. Surprisingly, when the VH2 mutation was combined with the VL3 mutation, the decrease in affinity was significantly less severe than expected. While the VL3 mutation alone did not enhance colloidal stability or affect affinity, it improved the antibody's conformational stability by four degrees. Conversely, the VH2 mutation reduced conformational stability by nearly seven degrees. Notably, the VH3 mutation contributed to the conformational stability of the combinatorial variant, mitigating the negative effect of the VH2 mutation on affinity while preserving its beneficial impact on colloidal stability.

The results of study III demonstrate how subtle and difficult-to-design changes were needed to eliminate unwanted interactions without losing the binding affinity. A successful case example of rational optimization is the optimization of mAb2

made by Van der Kant et al. where they were able to computationally predict a single amino acid exchange (S52R) in the CDR2 of LC that diminished an APR triggering the aggregation of mAb2.[303] In practice, rational optimization has proven to be difficult, especially in the case of the self-interaction propensity. Mieczkowski et al. evaluated 22 *in silico*-optimized variants, and only one of them maintained subnanomolar target antigen affinity, although many had lower self-interaction.[353] Compared to rational optimization, which is based on a thorough computational analysis of the antibody sequence, our approach did not require any prior antibody sequence analysis. Error-prone PCR in combination with mammalian display mimics the natural process of antibody affinity maturation during B-cell development. First, mutations are randomly generated over the length of the selected amino acid sequence, and then the best variants are selected based on both affinity and non-affinity interactions, simultaneously. This fully empirical strategy is rapid, economical, and effective. By adding more selection rounds to our study, the affinity-impaired mutations would likely have been eliminated. Moreover, larger mutant libraries could have led to the discovery of more improved variants. Small library sizes are the most significant challenge for mammalian display technology currently. To address this issue, Huhtinen et al. have conducted studies to improve the stable integration efficiency of genes into our mammalian display platform.[357] An important future direction for rational antibody optimization is using machine learning-based models. Recently, Makowski et al. showed that interpretable machine learning classifiers trained on experimental data for a panel of 80 clinical-stage monoclonal antibodies can identify variable chain mutations that optimize non-affinity interactions, maintaining the high-affinity antigen binding interactions.[305] The developed models were also successful when the antibody paratopes were defined only using sequence-based prediction methods without any information about the antigen.[358] However, before a machine learning model can be used for predictions, significant investments are needed in its development; a sufficient amount of representative data needs to be collected and preprocessed, the right model has to be selected and trained, and the model performance needs to be evaluated and optimized before deploying the model.

Bauer et al. compared the difficult-to-develop parental mAb2 to the *in silico*-optimized antibody variant in bioprocess development and discovered a threefold increased product titer for the optimized variant after stable expression in CHO cells, lower levels of aggregates after downstream process purification, and significantly lower opalescence of the formulated drug product.[359] The results of study III should be validated similarly by comparing the solution behavior of the parental anti-AGelD187N antibody and the improved variants at high concentrations.

7 Conclusions

Gelsolin amyloidosis is an inherited systemic amyloidosis for which, like other protein-misfolding diseases, no disease-modifying treatment is available. Unlike most protein-misfolding diseases, gelsolin amyloidosis has a simple and well-known pathophysiology. Another feature differentiating gelsolin amyloidosis from other protein-misfolding diseases is that the causative agent for the disease, the aberrant extracellular fragment of plasma gelsolin, AGelD187N, does not play an innate role in the body. This makes it an excellent therapeutic target to be neutralized. In this study, we sought to find human antibodies that would inhibit the pathological aggregation of AGelD187N and that would have such biophysical properties that they could be used as a therapeutic substance.

The complexity and sensitivity of protein aggregation were well illustrated in the study. AGelD187N is a 70 amino acid-long intrinsically disordered polypeptide. Lengthy assay development was needed to be able to reliably monitor the aggregation process of AGelD187N *in vitro* on a scale that allowed the evaluation of the functional impact of potential aggregation inhibitors. This was achieved using a synthetic polypeptide made by solid-phase chemical synthesis and carefully controlling the quality and all handling procedures.

The power of antibodies and the combination of two *in vitro* display techniques, the phage display and mammalian display, was well demonstrated in the study. Using phage display technology and the scFv libraries of the University of Turku, it was possible to find antibody fragments binding to different regions of AGelD187N with high affinity. All investigated Fabs prevented the aggregation of AGelD187N efficiently and gave new insights into the assembly process of AGelD187N fibrils. When the most promising Fab was converted into a full-length antibody, a high level of self-interaction was observed, indicating poor colloidal stability. The antibody´s biophysical properties were optimized using mammalian display technology and small random libraries based on the parental antibody sequence. Three antibody variants with lower self-interaction and acceptable target binding and thermal stability were discovered, mitigating a significant developability risk.

The fully human and drug-like anti-AGelD187N antibodies presented in this thesis can be used in fundamental research on gelsolin amyloidosis as well as

diagnostic tools for the disease. Most importantly, they provide an excellent starting point for developing a currently lacking disease-modifying treatment for gelsolin amyloidosis. Such treatment could inhibit the pathological processes of gelsolin amyloidosis, which can be life-threatening and cannot be surgically or otherwise alleviated. For drug development, a transgenic mouse model of the disease exists, along with several options to develop a translatable pharmacodynamic biomarker. The rarity of gelsolin amyloidosis likely presents challenges for funding the necessary preclinical and clinical studies and for the execution of clinical trials. However, successful anti-aggregational immunotherapy for a relatively simple protein-misfolding disease like gelsolin amyloidosis could be a significant breakthrough and a signpost for more complex protein-misfolding diseases, such as Alzheimer's and Parkinson's diseases, where the effectiveness of anti-amyloid immunotherapy remains debated. If effective anti-aggregational immunotherapy were found for these common neurodegenerative conditions or any other prevalent protein-misfolding disease, its economic and social implications would be tremendous.

Acknowledgements

This study was initiated in 2019 as the first Industrial PhD project at the University of Turku. It was conducted as a collaboration between Orion Pharma, R&D, Turku, and the Institute of Biomedicine, Pharmacology, Drug Development and Therapeutics, and the Department of Life Technologies, Biotechnology, at the University of Turku, and was financially supported by Orion Pharma.

I am deeply grateful to my supervisors, Professor Antti Haapalinna and Professor Ullamari Pesonen. This work would not have been possible without Professor Haapalinna's belief in me and my ability to grow and develop in new directions. I have continuously worked to be worthy of that trust. Professor Pesonen played a key role in establishing the Industrial PhD programme — an initiative that has already produced several successful doctoral graduates. During my studies, Professor Pesonen guided me in the academic world and created trust in the process with her ever-positive way. Both supervisors continuously encouraged me and pushed the work forward, even when there was no clear path and my full-time work at Orion slowed things down. I am also profoundly thankful to Professor Urpo Lamminmäki, whom I consider my unofficial third supervisor. Your expertise and advice have been invaluable throughout this journey, as well as your genuine interest in the project.

My heartfelt thanks go to my reviewers, Professor Jan Gettemans and Associate Professor Sari Atula, for their careful and constructive review of my dissertation. Your professional comments helped me broaden my perspective and, in particular, improve the discussion section of the thesis manuscript. I also thank Professor Timo Myöhänen for kindly accepting the important role of the opponent.

I want to express my sincere thanks to my other co-authors, Patrik Holm, Dr. Olli Huhtinen, Oskar Haavisto, Dr. Victor Nesati, Dr. Rune Salbo, Dr. Anna Gąciarz, Dr. Stuart Prince, Dr. Tuomas Huovinen, Elisa Lankinen, Dr. Antti Kulmala, Anja Vilkman, and Dr. Bryce Nelson. I greatly enjoyed working with such talented people from diverse scientific backgrounds, and I learned a lot from you. I would like to especially acknowledge Patrik, Olli, and Anja, whose attitude toward science, others, and life I truly admire and appreciate. Warm thanks to Dr. Terhi Oja, Satu Kaskinoro, Mirkka Papinkivi, Mirka Lång, and Mona Niiranen for your superb expertise in antibody expression, purification, and characterization, and for always keeping the spirits high in the lab.

Thank you to the recent PhDs, Dr. Krista Ojala, Dr. Olli Huhtinen, and Dr. Veera Nikoskelainen, for your invaluable peer support and friendship. I am grateful for your example, guidance, and the tips you shared with me, and I am extremely proud of all three of you. I would also like to acknowledge the Drug Research Doctoral Programme and all my fellow students for an encouraging and joyful atmosphere.

As my postgraduate studies progressed, Orion R&D was simultaneously building its capabilities in biologics in Turku, Finland. I had the privilege of being part of that work. I would like to express my sincere thanks to my supervisors at Orion, Dr. Jyrki Lehtimäki, Dr. Rune Salbo, and Dr. Leena Otsomaa, for entrusting me with responsibility while still allowing me to pursue my studies. My heartfelt thanks to everyone involved in building the units, and especially to the members of the Protein and Antibody Engineering and Characterization teams. We accomplished an incredible amount together through team spirit and dedication. I hope that each of you finds a place where you can truly thrive and feel appreciated.

This past spring has been a difficult one, and it has made clear what matters most in life—and it is not work or science. I want to thank all my dear friends for the many memorable moments we've shared, both outdoors and indoors—in forests, fields, and bushes, during summer holidays with our families, at cultural and not-so-cultural events, and over coffee and lunch breaks at Orion. Thank you for helping me stay grounded and joyful. You have supported me more than you know.

My deepest gratitude belongs to my family. To my parents, Eva and Ismo, you taught me the courage to follow my dreams, to trust in life, and to work hard. Your love and belief in me have shaped who I am. To my parents-in-law, Tuula and Pekka, your interest and heartfelt support in my studies made it unthinkable to ever consider leaving this project unfinished. To my siblings, Petteri and Paula, and Paula´s family—thank you for being there. You know me better than anyone, and your company and grounded humour have always helped put things in perspective.

Finally, to my dear children, Olli and Inkeri, and my dear husband, Tapani—thank you for being my heart. Olli and Inkeri, you have grown from little ones into big ones during this project. I am endlessly proud of you and grateful to have you in my life. You bring light and laughter to my days and have supported this work in your own special way, while always reminding me that life is about so much more. And Tapani—thank you for everything. I don't know why we always choose the harder road, but somehow, we always make it through. Together. You are my rock.

Naantali, May 2025

Laura Leimu

References

1 Chiti, F. & Dobson, C. M. Protein Misfolding, Amyloid Formation, and Human Disease: A Summary of Progress Over the Last Decade. *Annu Rev Biochem* **86**, 27-68 (2017).

2 Pearson, E. R. Type 2 diabetes: a multifaceted disease. *Diabetologia* **62**, 1107-1112 (2019).

3 Samanta, S., Ramesh, M. & Govindaraju, T. in *Alzheimer's Disease: Recent Findings in Pathophysiology, Diagnostic and Therapeutic Modalities* (ed Thimmaiah Govindaraju) (The Royal Society of Chemistry, 2022).

4 Solomon, J. P., Page, L. J., Balch, W. E. & Kelly, J. W. Gelsolin amyloidosis: genetics, biochemistry, pathology and possible strategies for therapeutic intervention. *Crit Rev Biochem Mol Biol* **47**, 282-296 (2012).

5 Kiuru, S., Salonen, O. & Haltia, M. Gelsolin-related spinal and cerebral amyloid angiopathy. *Ann Neurol* **45**, 305-311 (1999).

6 Kiuru-Enari, S., Somer, H., Seppäläinen, A.-M., Notkola, I.-L. & Haltia, M. Neuromuscular Pathology in Hereditary Gelsolin Amyloidosis. *Journal of Neuropathology & Experimental Neurology* **61**, 565-571 (2002).

7 Koskelainen, S., Zhao, F., Kalimo, H., Baumann, M. & Kiuru-Enari, S. Severe elastolysis in hereditary gelsolin (AGel) amyloidosis. *Amyloid* **27**, 81-88 (2020).

8 Koskelainen, S. *et al.* Gelsolin amyloid angiopathy causes severe disruption of the arterial wall. *APMIS* **124**, 639-648 (2016).

9 Schmidt, E.-K., Kiuru-Enari, S., Kivelä, T. & Atula, S. Finnish gelsolin amyloidosis causes significant disease burden but does not affect survival: FIN-GAR phase II study. *Orphanet Journal of Rare Diseases* **15** (2020).

10 Villar-Pique, A. *et al.* Molecular and Clinical Aspects of Protein Aggregation Assays in Neurodegenerative Diseases. *Mol Neurobiol* **55**, 7588-7605 (2018).

11 Linse, S. Mechanism of amyloid protein aggregation and the role of inhibitors. *Pure and Applied Chemistry* **91**, 211-229 (2019).

12 Vácha, R., Linse, S. & Lund, M. Surface Effects on Aggregation Kinetics of Amyloidogenic Peptides. *Journal of the American Chemical Society* **136**, 11776-11782 (2014).

13 Meisl, G. *et al.* Molecular mechanisms of protein aggregation from global fitting of kinetic models. *Nat Protoc* **11**, 252-272 (2016).

14 Corradin, G., Kajava, A. V. & Verdini, A. Long Synthetic Peptides for the Production of Vaccines and Drugs: A Technological Platform Coming of Age. *Science Translational Medicine* **2**, 50rv53 (2010).

15 Fauvet, B., Butterfield, S. M., Fuks, J., Brik, A. & Lashuel, H. A. One-pot total chemical synthesis of human α-synuclein. **49**, 9254-9256-9254-9256.

16 Hartrampf, N. *et al.* Synthesis of proteins by automated flow chemistry. *Science* **368**, 980-987 (2020).

17 Ahmad, M., Esposto, J., Golec, C., Wu, C. & Martic-Milne, S. Aggregation of gelsolin wild-type and G167K/R, N184K, and D187N/Y mutant peptides and inhibition. *Mol Cell Biochem* (2021).

18 Arya, P. *et al.* Selective interception of gelsolin amyloidogenic stretch results in conformationally distinct aggregates with reduced toxicity. *ACS Chem Neurosci* **5**, 982-992 (2014).

19 Bollati, M. *et al.* Rational Design of a Peptidomimetic Inhibitor of Gelsolin Amyloid Aggregation. *International Journal of Molecular Sciences* **23**, 13973 (2022).

20 Srivastava, A. *et al.* Gelsolin Amyloidogenesis Is Effectively Modulated by Curcumin and Emetine Conjugated PLGA Nanoparticles. *PLoS One* **10**, e0127011 (2015).

21 Linse, S. *et al.* Kinetic fingerprints differentiate the mechanisms of action of anti-Aβ antibodies. *Nat Struct Mol Biol* **27**, 1125-1133 (2020).

22 Ashraf, A. *et al.* Efficacy and Safety of Anti-Amyloid Antibodies in Patients with AL Amyloidosis: A Systematic Review of Literature. *Blood* **140**, 12591-12592 (2022).

23 Griffin, J. M. *et al.* ATTR Amyloidosis: Current and Emerging Management Strategies: JACC: CardioOncology State-of-the-Art Review. *JACC CardioOncol* **3**, 488-505 (2021).

24 Plotkin, S. S. & Cashman, N. R. Passive immunotherapies targeting Aβ and tau in Alzheimer's disease. *Neurobiol Dis* **144**, 105010 (2020).

25 Vijayakumar, D. & Jankovic, J. Slowing Parkinson's Disease Progression with Vaccination and Other Immunotherapies. *CNS Drugs* **36**, 327-343 (2022).

26 Desai, A. A. *et al.* Rational affinity maturation of anti-amyloid antibodies with high conformational and sequence specificity. *Journal of Biological Chemistry* **296** (2021).

27 Julian, M. C. *et al.* Nature-inspired design and evolution of anti-amyloid antibodies. *Journal of Biological Chemistry* **294**, 8438-8451 (2019).

28 Hitt, B. D. *et al.* Anti-tau antibodies targeting a conformation-dependent epitope selectively bind seeds. *Journal of Biological Chemistry* **299** (2023).

29 De Genst, E., Messer, A. & Dobson, C. M. Antibodies and protein misfolding: From structural research tools to therapeutic strategies. *Biochimica et Biophysica Acta (BBA) - Proteins and Proteomics* **1844**, 1907-1919 (2014).

30 Van Overbeke, W. *et al.* Chaperone nanobodies protect gelsolin against MT1-MMP degradation and alleviate amyloid burden in the gelsolin amyloidosis mouse model. *Mol Ther* **22**, 1768-1778 (2014).

31 Alfaleh, M. A. *et al.* Phage Display Derived Monoclonal Antibodies: From Bench to Bedside. *Front Immunol* **11**, 1986 (2020).

32 Valldorf, B. *et al.* Antibody display technologies: selecting the cream of the crop. *Biological Chemistry* **403**, 455-477 (2022).

33 Zhang, W. *et al.* Developability assessment at early-stage discovery to enable development of antibody-derived therapeutics. *Antib Ther* **6**, 13-29 (2023).

34 Slavny, P. *et al.* Advancements in mammalian display technology for therapeutic antibody development and beyond: current landscape, challenges, and future prospects. *Frontiers in Immunology* **15** (2024).

35 Huhtinen, O., Salbo, R., Lamminmäki, U. & Prince, S. Selection of biophysically favorable antibody variants using a modified Flp-In CHO mammalian display platform. *Front Bioeng Biotechnol* **11**, 1170081 (2023).

36 Dyson, M. R. *et al.* Beyond affinity: selection of antibody variants with optimal biophysical properties and reduced immunogenicity from mammalian display libraries. *MAbs* **12**, 1829335 (2020).

37 Louros, N., Schymkowitz, J. & Rousseau, F. Mechanisms and pathology of protein misfolding and aggregation. *Nature Reviews Molecular Cell Biology* **24**, 912-933 (2023).

38 Anfinsen, C. B. Principles that govern the folding of protein chains. *Science* **181**, 223-230 (1973).

39 Hipp, M. S., Kasturi, P. & Hartl, F. U. The proteostasis network and its decline in ageing. *Nature Reviews Molecular Cell Biology* **20**, 421-435 (2019).

40 Balchin, D., Hayer-Hartl, M. & Hartl, F. U. Recent advances in understanding catalysis of protein folding by molecular chaperones. *FEBS Lett* **594**, 2770-2781 (2020).

41 Holehouse, A. S. & Kragelund, B. B. The molecular basis for cellular function of intrinsically disordered protein regions. *Nature Reviews Molecular Cell Biology* **25**, 187-211 (2024).

42 Lermyte, F. Roles, Characteristics, and Analysis of Intrinsically Disordered Proteins: A Minireview. *Life (Basel)* **10** (2020).

43 Houben, B., Rousseau, F. & Schymkowitz, J. Protein structure and aggregation: a marriage of necessity ruled by aggregation gatekeepers. *Trends in Biochemical Sciences* **47**, 194-205 (2022).

44 Ulamec, S. M., Brockwell, D. J. & Radford, S. E. Looking Beyond the Core: The Role of Flanking Regions in the Aggregation of Amyloidogenic Peptides and Proteins. *Frontiers in Neuroscience* **14** (2020).

45 Ciryam, P. *et al.* A metastable subproteome underlies inclusion formation in muscle proteinopathies. *Acta Neuropathologica Communications* **7**, 197 (2019).

46 Ciryam, P., Kundra, R., Morimoto, R. I., Dobson, C. M. & Vendruscolo, M. Supersaturation is a major driving force for protein aggregation in neurodegenerative diseases. *Trends Pharmacol Sci* **36**, 72-77 (2015).

47 Powers, E. T., Morimoto, R. I., Dillin, A., Kelly, J. W. & Balch, W. E. Biological and chemical approaches to diseases of proteostasis deficiency. *Annu Rev Biochem* **78**, 959-991 (2009).

48 Sonninen, T. M., Goldsteins, G., Laham-Karam, N., Koistinaho, J. & Lehtonen, Š. Proteostasis Disturbances and Inflammation in Neurodegenerative Diseases. *Cells* **9** (2020).

49 Flagmeier, P. *et al.* Mutations associated with familial Parkinson's disease alter the initiation and amplification steps of α-synuclein aggregation. *Proc Natl Acad Sci U S A* **113**, 10328-10333 (2016).

50 Spillantini, M. G. & Goedert, M. Tau pathology and neurodegeneration. *Lancet Neurol* **12**, 609-622 (2013).

51 Raimondi, S. *et al.* Effects of the known pathogenic mutations on the aggregation pathway of the amyloidogenic peptide of apolipoprotein A-I. *J Mol Biol* **407**, 465-476 (2011).

52 Ahn, M. *et al.* The Significance of the Location of Mutations for the Native-State Dynamics of Human Lysozyme. *Biophys J* **111**, 2358-2367 (2016).

53 Sekijima, Y. *et al.* The biological and chemical basis for tissue-selective amyloid disease. *Cell* **121**, 73-85 (2005).

54 Singleton, A. B. *et al.* alpha-Synuclein locus triplication causes Parkinson's disease. *Science* **302**, 841 (2003).

55 Rovelet-Lecrux, A. *et al.* APP locus duplication causes autosomal dominant early-onset Alzheimer disease with cerebral amyloid angiopathy. *Nat Genet* **38**, 24-26 (2006).

56 Caubet, C. *et al.* A new amyloidosis caused by fibrillar aggregates of mutated corneodesmosin. *Faseb j* **24**, 3416-3426 (2010).

57 Vidal, R. *et al.* A decamer duplication in the 3' region of the BRI gene originates an amyloid peptide that is associated with dementia in a Danish kindred. *Proc Natl Acad Sci U S A* **97**, 4920-4925 (2000).

58 Fan, H. C. *et al.* Polyglutamine (PolyQ) diseases: genetics to treatments. *Cell Transplant* **23**, 441-458 (2014).

59 Chiti, F. & Dobson, C. M. Protein misfolding, functional amyloid, and human disease. *Annu Rev Biochem* **75**, 333-366 (2006).

60 Iadanza, M. G., Jackson, M. P., Hewitt, E. W., Ranson, N. A. & Radford, S. E. A new era for understanding amyloid structures and disease. *Nature Reviews Molecular Cell Biology* **19**, 755-773 (2018).

61 Scheres, S. H., Zhang, W., Falcon, B. & Goedert, M. Cryo-EM structures of tau filaments. *Curr Opin Struct Biol* **64**, 17-25 (2020).

62 Suzuki, G. *et al.* α-synuclein strains that cause distinct pathologies differentially inhibit proteasome. *Elife* **9** (2020).

63 Peng, C. *et al.* Cellular milieu imparts distinct pathological α-synuclein strains in α-synucleinopathies. *Nature* **557**, 558-563 (2018).

64 Campioni, S. *et al.* A causative link between the structure of aberrant protein oligomers and their toxicity. *Nat Chem Biol* **6**, 140-147 (2010).

65 He, Y. *et al.* Amyloid β oligomers suppress excitatory transmitter release via presynaptic depletion of phosphatidylinositol-4,5-bisphosphate. *Nature Communications* **10**, 1193 (2019).

66 Lasagna-Reeves, C. A. *et al.* Tau oligomers impair memory and induce synaptic and mitochondrial dysfunction in wild-type mice. *Mol Neurodegener* **6**, 39 (2011).

67 Olzscha, H. *et al.* Amyloid-like aggregates sequester numerous metastable proteins with essential cellular functions. *Cell* **144**, 67-78 (2011).

68 Milanesi, L. *et al.* Direct three-dimensional visualization of membrane disruption by amyloid fibrils. *Proc Natl Acad Sci U S A* **109**, 20455-20460 (2012).

69 Griffin, J. M., Rosenblum, H. & Maurer, M. S. Pathophysiology and Therapeutic Approaches to Cardiac Amyloidosis. *Circulation Research* **128**, 1554-1575 (2021).

70 Picken, Maria M. The Pathology of Amyloidosis in Classification: A Review. *Acta Haematologica* **143**, 322-334 (2020).

71 Buxbaum, J. N. *et al.* Amyloid nomenclature 2022: update, novel proteins, and recommendations by the International Society of Amyloidosis (ISA) Nomenclature Committee. *Amyloid* **29**, 213-219 (2022).

72 Wechalekar, A. D., Gillmore, J. D. & Hawkins, P. N. Systemic amyloidosis. *The Lancet* **387**, 2641-2654 (2016).

73 Wechalekar, A. D. The Evolving Epidemiology of Amyloidosis. *JACC CardioOncol* **3**, 534-536 (2021).

74 Benson, M. D. in *Emery and Rimoin's Principles and Practice of Medical Genetics and Genomics (Seventh Edition)* (eds Reed E. Pyeritz, Bruce R. Korf, & Wayne W. Grody) 213-235 (Academic Press, 2023).

75 Westermark, P. in *Amyloid and Related Disorders: Surgical Pathology and Clinical Correlations* (eds PhD Fasn Maria M. Picken Md, M. D. Ph D. Ahmet Dogan, & M. D. Guillermo A. Herrera) 81-103 (Humana Press, 2012).

76 Akter, R. *et al.* Islet Amyloid Polypeptide: Structure, Function, and Pathophysiology. *J Diabetes Res* **2016**, 2798269 (2016).

77 Scarpioni, R. *et al.* Dialysis-related amyloidosis: challenges and solutions. *Int J Nephrol Renovasc Dis* **9**, 319-328 (2016).

78 Samlaska, C., Reber, S. & Murry, T. Insulin-derived amyloidosis: The insulin ball, amyloidoma. *JAAD Case Rep* **6**, 351-353 (2020).

79 Collinge, J. & Clarke, A. R. A general model of prion strains and their pathogenicity. *Science* **318**, 930-936 (2007).

80 Mirian, A., Aljohani, Z., Grushka, D. & Florendo-Cumbermack, A. Diagnosis and management of patients with polyneuropathy. *Cmaj* **195**, E227-e233 (2023).

81 Armstrong, M. J. & Okun, M. S. Diagnosis and Treatment of Parkinson Disease: A Review. *JAMA : the journal of the American Medical Association* **323**, 548-560 (2020).

82 DeMarsilis, A. *et al.* Pharmacotherapy of type 2 diabetes: An update and future directions. *Metabolism* **137**, 155332 (2022).

83 Bomasang-Layno, E. & Bronsther, R. Diagnosis and Treatment of Alzheimer's Disease:: An Update. *Dela J Public Health* **7**, 74-85 (2021).

84 Tschöpe, C. & Elsanhoury, A. Treatment of Transthyretin Amyloid Cardiomyopathy: The Current Options, the Future, and the Challenges. *J Clin Med* **11** (2022).

85 Theodorakakou, F., Fotiou, D., Dimopoulos, Meletios A. & Kastritis, E. Solid Organ Transplantation in Amyloidosis. *Acta Haematologica* **143**, 352-364 (2020).

86 Ericzon, B. G. *et al.* Liver Transplantation for Hereditary Transthyretin Amyloidosis: After 20 Years Still the Best Therapeutic Alternative? *Transplantation* **99**, 1847-1854 (2015).

87 Wechalekar, A. D. & Sanchorawala, V. Daratumumab in AL amyloidosis. *Blood* **140**, 2317-2322 (2022).

88 Aimo, A. *et al.* RNA-targeting and gene editing therapies for transthyretin amyloidosis. *Nat Rev Cardiol* **19**, 655-667 (2022).

89 Said, G., Grippon, S. & Kirkpatrick, P. Tafamidis. *Nature Reviews Drug Discovery* **11**, 185-186 (2012).
90 Tsoi, M. R., Lin, J. H. & Patel, A. R. Emerging Therapies for Transthyretin Amyloidosis. *Current Oncology Reports* **25**, 549-558 (2023).
91 Hoy, S. M. Patisiran: First Global Approval. *Drugs* **78**, 1625-1631 (2018).
92 Gales, L. Tegsedi (Inotersen): An Antisense Oligonucleotide Approved for the Treatment of Adult Patients with Hereditary Transthyretin Amyloidosis. *Pharmaceuticals (Basel)* **12** (2019).
93 Keam, S. J. Inotersen: First Global Approval. *Drugs* **78**, 1371-1376 (2018).
94 Keam, S. J. Vutrisiran: First Approval. *Drugs* **82**, 1419-1425 (2022).
95 Nie, T. Eplontersen: First Approval. *Drugs* **84**, 473-478 (2024).
96 Dhillon, S. Aducanumab: First Approval. *Drugs* **81**, 1437-1443 (2021).
97 Hoy, S. M. Lecanemab: First Approval. *Drugs* **83**, 359-365 (2023).
98 Mullard, A. FDA approves third anti-amyloid antibody for Alzheimer disease. *Nat Rev Drug Discov* (2024).
99 Bulawa, C. E. *et al.* Tafamidis, a potent and selective transthyretin kinetic stabilizer that inhibits the amyloid cascade. *Proc Natl Acad Sci U S A* **109**, 9629-9634 (2012).
100 Coelho, T. *et al.* Safety and efficacy of RNAi therapy for transthyretin amyloidosis. *N Engl J Med* **369**, 819-829 (2013).
101 Jayaraman, M. *et al.* Maximizing the Potency of siRNA Lipid Nanoparticles for Hepatic Gene Silencing In Vivo. *Angewandte Chemie International Edition* **51**, 8529-8533 (2012).
102 Benson, M. D., Dasgupta, N. R. & Monia, B. P. Inotersen (transthyretin-specific antisense oligonucleotide) for treatment of transthyretin amyloidosis. *Neurodegener Dis Manag* **9**, 25-30 (2019).
103 Al Hamed, R. *et al.* Comprehensive Review of AL amyloidosis: some practical recommendations. *Blood Cancer Journal* **11**, 97 (2021).
104 de Weers, M. *et al.* Daratumumab, a novel therapeutic human CD38 monoclonal antibody, induces killing of multiple myeloma and other hematological tumors. *J Immunol* **186**, 1840-1848 (2011).
105 Plascencia-Villa, G. & Perry, G. Lessons from antiamyloid-β immunotherapies in Alzheimer's disease. *Handb Clin Neurol* **193**, 267-292 (2023).
106 Arndt, J. W. *et al.* Structural and kinetic basis for the selectivity of aducanumab for aggregated forms of amyloid-β. *Scientific Reports* **8**, 6412 (2018).
107 DeMattos, Ronald B. *et al.* A Plaque-Specific Antibody Clears Existing β-amyloid Plaques in Alzheimer's Disease Mice. *Neuron* **76**, 908-920 (2012).
108 Bard, F. *et al.* Peripherally administered antibodies against amyloid beta-peptide enter the central nervous system and reduce pathology in a mouse model of Alzheimer disease. *Nat Med* **6**, 916-919 (2000).
109 Sevigny, J. *et al.* The antibody aducanumab reduces Aβ plaques in Alzheimer's disease. *Nature* **537**, 50-56 (2016).
110 Tucker, S. *et al.* The murine version of BAN2401 (mAb158) selectively reduces amyloid-β protofibrils in brain and cerebrospinal fluid of tg-ArcSwe mice. *J Alzheimers Dis* **43**, 575-588 (2015).
111 Nilsberth, C. *et al.* The 'Arctic' APP mutation (E693G) causes Alzheimer's disease by enhanced Aβ protofibril formation. *Nature Neuroscience* **4**, 887-893 (2001).
112 Dyck, C. H. v. *et al.* Lecanemab in Early Alzheimer's Disease. *New England Journal of Medicine* **388**, 9-21 (2023).
113 Salloway, S. *et al.* Amyloid-Related Imaging Abnormalities in 2 Phase 3 Studies Evaluating Aducanumab in Patients With Early Alzheimer Disease. *JAMA Neurol* **79**, 13-21 (2022).
114 Budd Haeberlein, S. *et al.* Two Randomized Phase 3 Studies of Aducanumab in Early Alzheimer's Disease. *J Prev Alzheimers Dis* **9**, 197-210 (2022).

115 Sims, J. R. *et al.* Donanemab in Early Symptomatic Alzheimer Disease: The TRAILBLAZER-ALZ 2 Randomized Clinical Trial. *JAMA* **330**, 512-527 (2023).
116 Zhang, Y., Chen, H., Li, R., Sterling, K. & Song, W. Amyloid β-based therapy for Alzheimer's disease: challenges, successes and future. *Signal Transduction and Targeted Therapy* **8**, 248 (2023).
117 Gertz, M. A. *et al.* Birtamimab plus standard of care in light-chain amyloidosis: the phase 3 randomized placebo-controlled VITAL trial. *Blood* **142**, 1208-1218 (2023).
118 Hughes, M. S. *et al.* Updated OS of patients with AL amyloidosis after CAEL-101. *Journal of Clinical Oncology* **41**, 8026-8026 (2023).
119 Garcia-Pavia, P. *et al.* Phase 1 Trial of Antibody NI006 for Depletion of Cardiac Transthyretin Amyloid. *New England Journal of Medicine* **389**, 239-250 (2023).
120 Fontana, M. *et al.* NNC6019–0001, a humanized monoclonal antibody, in patients with transthyretin amyloid cardiomyopathy (ATTR-CM): rationale and study design of a phase 2, randomized, placebo-controlled trial. *European Heart Journal* **43** (2022).
121 Kotit, S. Lessons from the first-in-human in vivo CRISPR/Cas9 editing of the TTR gene by NTLA-2001 trial in patients with transthyretin amyloidosis with cardiomyopathy. *Glob Cardiol Sci Pract* **2023**, e202304 (2023).
122 Meretoja, J. Familial systemic paramyloidosis with lattice dystrophy of the cornea, progressive cranial neuropathy, skin changes and various internal symptoms. A previously unrecognized heritable syndrome. *Ann Clin Res* **1**, 314-324 (1969).
123 Meretoja, J. Genetic aspects of familial amyloidosis with corneal lattice dystrophy and cranial neuropathy. *Clin Genet* **4**, 173-185 (1973).
124 Kiuru-Enari, S. & Haltia, M. Hereditary gelsolin amyloidosis. *Handb Clin Neurol* **115**, 659-681 (2013).
125 Haltia, M. *et al.* Amyloid protein in familial amyloidosis (Finnish type) is homologous to gelsolin, an actin-binding protein. *Biochemical and Biophysical Research Communications* **167**, 927-932 (1990).
126 Maury, C. P. J., Alii, K. & Baumann, M. Finnish hereditary amyloidosis. *FEBS Letters* **260**, 85-87 (1990).
127 Levy, E. *et al.* Mutation in gelsolin gene in Finnish hereditary amyloidosis. *Journal of Experimental Medicine* **172**, 1865-1867 (1990).
128 Maury, C. P. J., Kere, J., Tolvanen, R. & de la Chapelle, A. Finnish hereditary amyloidosis is caused by a single nucleotide substitution in the gelsolin gene. *FEBS Letters* **276**, 75-77 (1990).
129 Chapelle, A. d. l. *et al.* Gelsolin–derived familial amyloidosis caused by asparagine or tyrosine substitution for aspartic acid at residue 187. *Nature Genetics* **2**, 157-160 (1992).
130 Maury, C. P. *et al.* Danish type gelsolin related amyloidosis: 654G-T mutation is associated with a disease pathogenetically and clinically similar to that caused by the 654G-A mutation (familial amyloidosis of the Finnish type). *J Clin Pathol* **53**, 95-99 (2000).
131 Kiuru, S. Gelsolin-related familial amyloidosis, Finnish type (FAF), and its variants found worldwide. *Amyloid* **5**, 55-66 (1998).
132 Inês Antunes, C., Brás, A., Silva, F. & Matos, A. Familial amyloidosis of the Finnish type: clinical and neurophysiological features of two index cases. *BMJ Case Reports* **15** (2022).
133 Nikoskinen, T., Schmidt, E.-K., Strbian, D., Kiuru-Enari, S. & Atula, S. Natural course of Finnish gelsolin amyloidosis. *Annals of Medicine* **47**, 506-511 (2015).
134 Kwiatkowski, D. J. Functions of gelsolin: motility, signaling, apoptosis, cancer. *Curr Opin Cell Biol* **11**, 103-108 (1999).
135 Nag, S., Larsson, M., Robinson, R. C. & Burtnick, L. D. Gelsolin: The tail of a molecular gymnast. *Cytoskeleton* **70**, 360-384 (2013).
136 Kwiatkowski, D. J., Mehl, R., Izumo, S., Nadal-Ginard, B. & Yin, H. L. Muscle is the major source of plasma gelsolin. *Journal of Biological Chemistry* **263**, 8239-8243 (1988).

137 Chen, C. D. *et al.* Furin initiates gelsolin familial amyloidosis in the Golgi through a defect in Ca(2+) stabilization. *Embo j* **20**, 6277-6287 (2001).

138 Giorgino, T. *et al.* Nanobody interaction unveils structure, dynamics and proteotoxicity of the Finnish-type amyloidogenic gelsolin variant. *Biochim Biophys Acta Mol Basis Dis* **1865**, 648-660 (2019).

139 Kangas, H., Paunio, T., Kalkkinen, N., Jalanko, A. & Peltonen, L. In vitro expression analysis shows that the secretory form of gelsolin is the sole source of amyloid in gelsolin-related amyloidosis. *Hum Mol Genet* **5**, 1237-1243 (1996).

140 Kangas, H. *et al.* Functional consequences of amyloidosis mutation for gelsolin polypeptide — analysis of gelsolin-actin interaction and gelsolin processing in gelsolin knock-out fibroblasts. *FEBS Letters* **454**, 233-239 (1999).

141 Nag, S. *et al.* Ca2+ binding by domain 2 plays a critical role in the activation and stabilization of gelsolin. *Proc Natl Acad Sci U S A* **106**, 13713-13718 (2009).

142 Page, L. J. *et al.* Metalloendoprotease cleavage triggers gelsolin amyloidogenesis. *The EMBO Journal* **24**, 4124-4132 (2005).

143 Maury, C. P. Gelsolin-related amyloidosis. Identification of the amyloid protein in Finnish hereditary amyloidosis as a fragment of variant gelsolin. *The Journal of Clinical Investigation* **87**, 1195-1199 (1991).

144 Maury, C. P., Nurmiaho-Lassila, E. L. & Rossi, H. Amyloid fibril formation in gelsolin-derived amyloidosis. Definition of the amyloidogenic region and evidence of accelerated amyloid formation of mutant Asn-187 and Tyr-187 gelsolin peptides. *Lab Invest* **70**, 558-564 (1994).

145 Ratnaswamy, G., Koepf, E., Bekele, H., Yin, H. & Kelly, J. W. The amyloidogenicity of gelsolin is controlled by proteolysis and pH. *Chem Biol* **6**, 293-304 (1999).

146 Suk, J. Y., Zhang, F., Balch, W. E., Linhardt, R. J. & Kelly, J. W. Heparin accelerates gelsolin amyloidogenesis. *Biochemistry* **45**, 2234-2242 (2006).

147 Ardalan, M. R., Shoja, M. M. & Kiuru-Enari, S. Amyloidosis-related nephrotic syndrome due to a G654A gelsolin mutation: the first report from the Middle East. *Nephrology Dialysis Transplantation* **22**, 272-275 (2006).

148 Fernández, A. L., Herreros, J. M., Monzonis, A. M. & Panizo, A. Heart transplantation for Finnish type familial systemic amyloidosis. *Scand Cardiovasc J* **31**, 357-359 (1997).

149 Maury, C. P., Kere, J., Tolvanen, R. & de la Chapelle, A. Homozygosity for the Asn187 gelsolin mutation in Finnish-type familial amyloidosis is associated with severe renal disease. *Genomics* **13**, 902-903 (1992).

150 Solomon, J. P. *et al.* The 8 and 5 kDa fragments of plasma gelsolin form amyloid fibrils by a nucleated polymerization mechanism, while the 68 kDa fragment is not amyloidogenic. *Biochemistry* **48**, 11370-11380 (2009).

151 Van Overbeke, W. *et al.* An ER-directed gelsolin nanobody targets the first step in amyloid formation in a gelsolin amyloidosis mouse model. *Hum Mol Genet* **24**, 2492-2507 (2015).

152 Verhelle, A. *et al.* AAV9 delivered bispecific nanobody attenuates amyloid burden in the gelsolin amyloidosis mouse model. *Hum Mol Genet* **26**, 1353-1364 (2017).

153 Hamers-Casterman, C. *et al.* Naturally occurring antibodies devoid of light chains. *Nature* **363**, 446-448 (1993).

154 Page, L. J. *et al.* Secretion of amyloidogenic gelsolin progressively compromises protein homeostasis leading to the intracellular aggregation of proteins. *Proc Natl Acad Sci U S A* **106**, 11125-11130 (2009).

155 Adriaan, V. & Jan, G. in *Exploring New Findings on Amyloidosis* (ed Fernandez-Escamilla Ana-Maria) Ch. 13 (IntechOpen, 2016).

156 Ahmed, R. *et al.* Molecular Mechanism for the (−)-Epigallocatechin Gallate-Induced Toxic to Nontoxic Remodeling of Aβ Oligomers. *Journal of the American Chemical Society* **139**, 13720-13734 (2017).

157 Crowe, A. *et al.* Aminothienopyridazines and Methylene Blue Affect Tau Fibrillization via Cysteine Oxidation. *Journal of Biological Chemistry* **288**, 11024-11037 (2013).
158 Liu, H., Yu, L., Dong, X. & Sun, Y. Synergistic effects of negatively charged hydrophobic nanoparticles and (−)-epigallocatechin-3-gallate on inhibiting amyloid β-protein aggregation. *Journal of Colloid and Interface Science* **491**, 305-312 (2017).
159 Necula, M. *et al.* Methylene Blue Inhibits Amyloid Aβ Oligomerization by Promoting Fibrillization. *Biochemistry* **46**, 8850-8860 (2007).
160 Pellegrino, S. *et al.* β-Hairpin mimics containing a piperidine–pyrrolidine scaffold modulate the β-amyloid aggregation process preserving the monomer species. *Chemical Science* **8**, 1295-1302 (2017).
161 Tonali, N. *et al.* Structure-activity relationships of β-hairpin mimics as modulators of amyloid β-peptide aggregation. *European Journal of Medicinal Chemistry* **154**, 280-293 (2018).
162 Greenwald, J. & Riek, R. Biology of Amyloid: Structure, Function, and Regulation. *Structure* **18**, 1244-1260 (2010).
163 Taylor, A. & Staniforth, R. General Principles Underpinning Amyloid Structure. *Frontiers in Neuroscience* **16**, 878869 (2022).
164 LeVine, H., 3rd. Thioflavine T interaction with synthetic Alzheimer's disease beta-amyloid peptides: detection of amyloid aggregation in solution. *Protein Sci* **2**, 404-410 (1993).
165 Naiki, H., Higuchi, K., Hosokawa, M. & Takeda, T. Fluorometric determination of amyloid fibrils in vitro using the fluorescent dye, thioflavin T1. *Anal Biochem* **177**, 244-249 (1989).
166 Krebs, M. R. H., Bromley, E. H. C. & Donald, A. M. The binding of thioflavin-T to amyloid fibrils: localisation and implications. *Journal of Structural Biology* **149**, 30-37 (2005).
167 Stsiapura, V. I., Maskevich, A. A., Kuzmitsky, V. A., Turoverov, K. K. & Kuznetsova, I. M. Computational study of thioflavin T torsional relaxation in the excited state. *J Phys Chem A* **111**, 4829-4835 (2007).
168 Wu, C., Biancalana, M., Koide, S. & Shea, J.-E. Binding Modes of Thioflavin-T to the Single-Layer β-Sheet of the Peptide Self-Assembly Mimics. *Journal of Molecular Biology* **394**, 627-633 (2009).
169 Wu, C. *et al.* The Binding of Thioflavin T and Its Neutral Analog BTA-1 to Protofibrils of the Alzheimer's Disease Aβ16–22 Peptide Probed by Molecular Dynamics Simulations. *Journal of Molecular Biology* **384**, 718-729 (2008).
170 Biancalana, M. & Koide, S. Molecular mechanism of Thioflavin-T binding to amyloid fibrils. *Biochimica et Biophysica Acta (BBA) - Proteins and Proteomics* **1804**, 1405-1412 (2010).
171 Nielsen, L. *et al.* Effect of environmental factors on the kinetics of insulin fibril formation: elucidation of the molecular mechanism. *Biochemistry* **40**, 6036-6046 (2001).
172 Xue, C., Lin, T. Y., Chang, D. & Guo, Z. Thioflavin T as an amyloid dye: fibril quantification, optimal concentration and effect on aggregation. *R Soc Open Sci* **4**, 160696 (2017).
173 Xue, W.-F., Homans, S. W. & Radford, S. E. Systematic analysis of nucleation-dependent polymerization reveals new insights into the mechanism of amyloid self-assembly. *Proceedings of the National Academy of Sciences* **105**, 8926-8931 (2008).
174 LeVine, H. Thioflavine T interaction with amyloid β-sheet structures. *Amyloid* **2**, 1-6 (1995).
175 Lövestam, S. *et al.* Disease-specific tau filaments assemble via polymorphic intermediates. *Nature* **625**, 119-125 (2024).
176 Sidhu, A., Vaneyck, J., Blum, C., Segers-Nolten, I. & Subramaniam, V. Polymorph-specific distribution of binding sites determines thioflavin-T fluorescence intensity in α-synuclein fibrils. *Amyloid* **25**, 189-196 (2018).
177 Biancalana, M., Makabe, K., Koide, A. & Koide, S. Molecular Mechanism of Thioflavin-T Binding to the Surface of β-Rich Peptide Self-Assemblies. *Journal of Molecular Biology* **385**, 1052-1063 (2009).
178 Groenning, M. Binding mode of Thioflavin T and other molecular probes in the context of amyloid fibrils—current status. *Journal of Chemical Biology* **3**, 1-18 (2010).

179 Hackl, E. V., Darkwah, J., Smith, G. & Ermolina, I. Effect of acidic and basic pH on Thioflavin T absorbance and fluorescence. *Eur Biophys J* **44**, 249-261 (2015).

180 Sabaté, R., Lascu, I. & Saupe, S. J. On the binding of Thioflavin-T to HET-s amyloid fibrils assembled at pH 2. *J Struct Biol* **162**, 387-396 (2008).

181 Hudson, S. A., Ecroyd, H., Kee, T. W. & Carver, J. A. The thioflavin T fluorescence assay for amyloid fibril detection can be biased by the presence of exogenous compounds. *The FEBS Journal* **276**, 5960-5972 (2009).

182 Meng, F., Marek, P., Potter, K. J., Verchere, C. B. & Raleigh, D. P. Rifampicin does not prevent amyloid fibril formation by human islet amyloid polypeptide but does inhibit fibril thioflavin-T interactions: implications for mechanistic studies of beta-cell death. *Biochemistry* **47**, 6016-6024 (2008).

183 Harel, M., Sonoda, L. K., Silman, I., Sussman, J. L. & Rosenberry, T. L. Crystal structure of thioflavin T bound to the peripheral site of Torpedo californica acetylcholinesterase reveals how thioflavin T acts as a sensitive fluorescent reporter of ligand binding to the acylation site. *J Am Chem Soc* **130**, 7856-7861 (2008).

184 Groenning, M. *et al.* Study on the binding of Thioflavin T to β-sheet-rich and non-β-sheet cavities. *Journal of Structural Biology* **158**, 358-369 (2007).

185 Sen, P., Fatima, S., Ahmad, B. & Khan, R. H. Interactions of thioflavin T with serum albumins: spectroscopic analyses. *Spectrochim Acta A Mol Biomol Spectrosc* **74**, 94-99 (2009).

186 Rovnyagina, N. R. *et al.* Binding of thioflavin T by albumins: An underestimated role of protein oligomeric heterogeneity. *International Journal of Biological Macromolecules* **108**, 284-290 (2018).

187 Gras, S. L., Waddington, L. J. & Goldie, K. N. in *Protein Folding, Misfolding, and Disease: Methods and Protocols* (eds Andrew F. Hill, Kevin J. Barnham, Stephen P. Bottomley, & Roberto Cappai) 197-214 (Humana Press, 2011).

188 Adamcik, J. *et al.* Understanding amyloid aggregation by statistical analysis of atomic force microscopy images. *Nature Nanotechnology* **5**, 423-428 (2010).

189 Adamcik, J. & Mezzenga, R. Study of amyloid fibrils via atomic force microscopy. *Current Opinion in Colloid & Interface Science* **17**, 369-376 (2012).

190 Kundel, F. *et al.* Shedding light on aberrant interactions - a review of modern tools for studying protein aggregates. *Febs j* **285**, 3604-3630 (2018).

191 Benilova, I., Karran, E. & De Strooper, B. The toxic Aβ oligomer and Alzheimer's disease: an emperor in need of clothes. *Nat Neurosci* **15**, 349-357 (2012).

192 Nichols, M. R. *et al.* Biophysical comparison of soluble amyloid-β(1-42) protofibrils, oligomers, and protofilaments. *Biochemistry* **54**, 2193-2204 (2015).

193 Jan, A., Hartley, D. M. & Lashuel, H. A. Preparation and characterization of toxic Aβ aggregates for structural and functional studies in Alzheimer's disease research. *Nature Protocols* **5**, 1186-1209 (2010).

194 Uversky, V. N. *et al.* Biophysical Properties of the Synucleins and Their Propensities to Fibrillate: Inhibition of α-synuclein Assembly by β- and γ-synucleins. *Journal of Biological Chemistry* **277**, 11970-11978 (2002).

195 Stephens, A. D., Zacharopoulou, M. & Kaminski Schierle, G. S. The Cellular Environment Affects Monomeric α-Synuclein Structure. *Trends in Biochemical Sciences* **44**, 453-466 (2019).

196 Hoyer, W. *et al.* Dependence of α-Synuclein Aggregate Morphology on Solution Conditions. *Journal of Molecular Biology* **322**, 383-393 (2002).

197 Lin, M. S. *et al.* Investigation of the mechanism of beta-amyloid fibril formation by kinetic and thermodynamic analyses. *Langmuir* **24**, 5802-5808 (2008).

198 Johansson, A.-S. *et al.* Physiochemical characterization of the Alzheimer's disease-related peptides Aβ1–42Arctic and Aβ1–42wt. *The FEBS Journal* **273**, 2618-2630 (2006).

199 Tiiman, A., Krishtal, J., Palumaa, P. & Tõugu, V. In vitro fibrillization of Alzheimer's amyloid-β peptide (1-42). *AIP Advances* **5** (2015).

200 Tiiman, A. *et al.* Effect of agitation on the peptide fibrillization: Alzheimer's amyloid-β peptide 1-42 but not amylin and insulin fibrils can grow under quiescent conditions. *Journal of Peptide Science* **19**, 386-391 (2013).
201 Narkiewicz, J., Giachin, G. & Legname, G. In vitro aggregation assays for the characterization of α-synuclein prion-like properties. *Prion* **8**, 19-32 (2014).
202 Munishkina, L. A., Phelan, C., Uversky, V. N. & Fink, A. L. Conformational Behavior and Aggregation of α-Synuclein in Organic Solvents: Modeling the Effects of Membranes. *Biochemistry* **42**, 2720-2730 (2003).
203 Schweighauser, M. *et al.* Structures of α-synuclein filaments from multiple system atrophy. *Nature* **585**, 464-469 (2020).
204 Falcon, B. *et al.* Novel tau filament fold in chronic traumatic encephalopathy encloses hydrophobic molecules. *Nature* **568**, 420-423 (2019).
205 Strohäker, T. *et al.* Structural heterogeneity of α-synuclein fibrils amplified from patient brain extracts. *Nature Communications* **10**, 5535 (2019).
206 Ancsin, J. B. Amyloidogenesis: Historical and modern observations point tO heparan sulfate proteoglycans as a major culprit. *Amyloid* **10**, 67-79 (2003).
207 Merry, C. L. R., Lindahl, U., Couchman, J. & Esko, J. D. in *Essentials of Glycobiology* (eds A. Varki *et al.*) 217-232 (Cold Spring Harbor Laboratory Press Copyright © 2022 The Consortium of Glycobiology Editors, La Jolla, California; published by Cold Spring Harbor Laboratory Press; All rights reserved., 2022).
208 Casale, J. & Crane, J. S. in *StatPearls* (StatPearls Publishing Copyright © 2024, StatPearls Publishing LLC., 2024).
209 Meng, F., Abedini, A., Song, B. & Raleigh, D. P. Amyloid formation by pro-islet amyloid polypeptide processing intermediates: examination of the role of protein heparan sulfate interactions and implications for islet amyloid formation in type 2 diabetes. *Biochemistry* **46**, 12091-12099 (2007).
210 Relini, A. *et al.* Heparin Strongly Enhances the Formation of β_2-Microglobulin Amyloid Fibrils in the Presence of Type I Collagen. *Journal of Biological Chemistry* **283**, 4912-4920 (2008).
211 Cohlberg, J. A., Li, J., Uversky, V. N. & Fink, A. L. Heparin and Other Glycosaminoglycans Stimulate the Formation of Amyloid Fibrils from α-Synuclein in Vitro. *Biochemistry* **41**, 1502-1511 (2002).
212 McLaurin, J., Franklin, T., Zhang, X., Deng, J. & Fraser, P. E. Interactions of Alzheimer amyloid-beta peptides with glycosaminoglycans effects on fibril nucleation and growth. *Eur J Biochem* **266**, 1101-1110 (1999).
213 Mclaughlin, R. W., De Stigter, J. K., Sikkink, L. A., Baden, E. M. & Ramirez-Alvarado, M. The effects of sodium sulfate, glycosaminoglycans, and Congo red on the structure, stability, and amyloid formation of an immunoglobulin light-chain protein. *Protein Science* **15**, 1710-1722 (2006).
214 Bourgault, S., Solomon, J. P., Reixach, N. & Kelly, J. W. Sulfated glycosaminoglycans accelerate transthyretin amyloidogenesis by quaternary structural conversion. *Biochemistry* **50**, 1001-1015 (2011).
215 Solomon, J. P., Bourgault, S., Powers, E. T. & Kelly, J. W. Heparin binds 8 kDa gelsolin cross-β-sheet oligomers and accelerates amyloidogenesis by hastening fibril extension. *Biochemistry* **50**, 2486-2498 (2011).
216 Teplow, D. B. Preparation of amyloid beta-protein for structural and functional studies. *Methods Enzymol* **413**, 20-33 (2006).
217 Zagorski, M. G. *et al.* Methodological and chemical factors affecting amyloid beta peptide amyloidogenicity. *Methods Enzymol* **309**, 189-204 (1999).
218 Walsh, D. M. *et al.* A facile method for expression and purification of the Alzheimer's disease-associated amyloid β-peptide. *The FEBS Journal* **276**, 1266-1281 (2009).

219 O'Malley, T. T., Linse, S. & Walsh, D. M. Production and Use of Recombinant Aβ for Aggregation Studies. *Methods Mol Biol* **1777**, 307-320 (2018).
220 Ryan, T. M. *et al.* Ammonium hydroxide treatment of Aβ produces an aggregate free solution suitable for biophysical and cell culture characterization. *PeerJ* **1**, e73-e73 (2013).
221 Stephens, A. D., Lu, M., Fernandez-Villegas, A. & Kaminski Schierle, G. S. Fast Purification of Recombinant Monomeric Amyloid-β from E. coli and Amyloid-β-mCherry Aggregates from Mammalian Cells. *ACS Chemical Neuroscience* **11**, 3204-3213 (2020).
222 Murphy, K. & Weaver, C. *Janeway's immunobiology*. 9th edition. edn, (Garland Science/Taylor & Francis Group, LLC, 2017).
223 Chiu, M. L., Goulet, D. R., Teplyakov, A. & Gilliland, G. L. Antibody Structure and Function: The Basis for Engineering Therapeutics. *Antibodies (Basel)* **8** (2019).
224 Schroeder, H. W., Jr. & Cavacini, L. Structure and function of immunoglobulins. *Journal of Allergy and Clinical Immunology* **125**, S41-S52 (2010).
225 Alberts, B. *et al. Molecular biology of the cell*. 6th ed. edn, (Garland Science, 2015).
226 Vidarsson, G., Dekkers, G. & Rispens, T. IgG subclasses and allotypes: from structure to effector functions. *Front Immunol* **5**, 520 (2014).
227 Oostindie, S. C., Lazar, G. A., Schuurman, J. & Parren, P. W. H. I. Avidity in antibody effector functions and biotherapeutic drug design. *Nature Reviews Drug Discovery* **21**, 715-735 (2022).
228 Newcombe, C. & Newcombe, A. R. Antibody production: polyclonal-derived biotherapeutics. *J Chromatogr B Analyt Technol Biomed Life Sci* **848**, 2-7 (2007).
229 Pelletier, J. P. R. & Mukhtar, F. Passive Monoclonal and Polyclonal Antibody Therapies.
230 KÖHler, G. & Milstein, C. Continuous cultures of fused cells secreting antibody of predefined specificity. *Nature* **256**, 495-497 (1975).
231 Posner, J., Barrington, P., Brier, T. & Datta-Mannan, A. in *Concepts and Principles of Pharmacology: 100 Years of the Handbook of Experimental Pharmacology* (eds James E. Barrett, Clive P. Page, & Martin C. Michel) 81-141 (Springer International Publishing, 2019).
232 Smith, S. L. Ten years of Orthoclone OKT3 (muromonab-CD3): a review. *J Transpl Coord* **6**, 109-119; quiz 120-101 (1996).
233 Güssow, D. & Seemann, G. Humanization of monoclonal antibodies. *Methods Enzymol* **203**, 99-121 (1991).
234 Morrison, S. L., Johnson, M. J., Herzenberg, L. A. & Oi, V. T. Chimeric human antibody molecules: mouse antigen-binding domains with human constant region domains. *Proc Natl Acad Sci U S A* **81**, 6851-6855 (1984).
235 Casan, J. M. L., Wong, J., Northcott, M. J. & Opat, S. Anti-CD20 monoclonal antibodies: reviewing a revolution. *Hum Vaccin Immunother* **14**, 2820-2841 (2018).
236 Shealy, D. J. & Visvanathan, S. Anti-TNF antibodies: lessons from the past, roadmap for the future. *Handb Exp Pharmacol*, 101-129 (2008).
237 Mullard, A. FDA approves 100th monoclonal antibody product. *Nat Rev Drug Discov* **20**, 491-495 (2021).
238 Houen, G. in *Therapeutic Antibodies: Methods and Protocols* (ed Gunnar Houen) 1-25 (Springer US, 2022).
239 Tsao, L.-C., Force, J. & Hartman, Z. C. Mechanisms of Therapeutic Antitumor Monoclonal Antibodies. *Cancer Research* **81**, 4641-4651 (2021).
240 Paul, S. *et al.* Cancer therapy with antibodies. *Nature Reviews Cancer* **24**, 399-426 (2024).
241 Dumontet, C., Reichert, J. M., Senter, P. D., Lambert, J. M. & Beck, A. Antibody–drug conjugates come of age in oncology. *Nature Reviews Drug Discovery* **22**, 641-661 (2023).
242 Klein, C., Brinkmann, U., Reichert, J. M. & Kontermann, R. E. The present and future of bispecific antibodies for cancer therapy. *Nature Reviews Drug Discovery* **23**, 301-319 (2024).
243 Wurm, F. M. Production of recombinant protein therapeutics in cultivated mammalian cells. *Nature Biotechnology* **22**, 1393-1398 (2004).

244 Moraes, J. Z. *et al.* Hybridoma technology: is it still useful? *Current Research in Immunology* **2**, 32-40 (2021).
245 Parray, H. A. *et al.* Hybridoma technology a versatile method for isolation of monoclonal antibodies, its applicability across species, limitations, advancement and future perspectives. *International Immunopharmacology* **85**, 106639 (2020).
246 Fang, J. C., Bodeus, M. & Burtonboy, G. Study on rat-rat hybridoma technique and production of rat monoclonal antibodies against HIV and HBsAg. *Chin J Biotechnol* **7**, 73-81 (1991).
247 Mei-Chang, K., Soon, J. A., Max, E. E. & Kindt, T. J. Rabbit-mouse hybridomas secreting intact rabbit immunoglobulin. *Molecular Immunology* **22**, 351-359 (1985).
248 Nishinaka, S., Suzuki, T., Matsuda, H. & Murata, M. A new cell line for the production of chicken monoclonal antibody by hybridoma technology. *Journal of Immunological Methods* **139**, 217-222 (1991).
249 Broketa, M. & Bruhns, P. Single-Cell Technologies for the Study of Antibody-Secreting Cells. *Frontiers in Immunology* **12** (2022).
250 Pedrioli, A. & Oxenius, A. Single B cell technologies for monoclonal antibody discovery. *Trends in Immunology* **42**, 1143-1158 (2021).
251 Ma, B. & Osborn, M. in *Introduction to Antibody Engineering* (eds Florian Rüker & Gordana Wozniak-Knopp) 97-127 (Springer International Publishing, 2021).
252 Clavero-Álvarez, A., Di Mambro, T., Perez-Gaviro, S., Magnani, M. & Bruscolini, P. Humanization of Antibodies using a Statistical Inference Approach. *Scientific Reports* **8**, 14820 (2018).
253 Green, L. L. *et al.* Antigen–specific human monoclonal antibodies from mice engineered with human Ig heavy and light chain YACs. *Nature Genetics* **7**, 13-21 (1994).
254 Mendez, M. J. *et al.* Functional transplant of megabase human immunoglobulin loci recapitulates human antibody response in mice. *Nat Genet* **15**, 146-156 (1997).
255 Fishwild, D. M. *et al.* High-avidity human IgG kappa monoclonal antibodies from a novel strain of minilocus transgenic mice. *Nat Biotechnol* **14**, 845-851 (1996).
256 Lonberg, N. *et al.* Antigen-specific human antibodies from mice comprising four distinct genetic modifications. *Nature* **368**, 856-859 (1994).
257 Smith, G. P. Filamentous fusion phage: novel expression vectors that display cloned antigens on the virion surface. *Science* **228**, 1315-1317 (1985).
258 Bird, R. E. *et al.* Single-chain antigen-binding proteins. *Science* **242**, 423-426 (1988).
259 Skerra, A. & Plückthun, A. Assembly of a functional immunoglobulin Fv fragment in Escherichia coli. *Science* **240**, 1038-1041 (1988).
260 McCafferty, J., Griffiths, A. D., Winter, G. & Chiswell, D. J. Phage antibodies: filamentous phage displaying antibody variable domains. *Nature* **348**, 552-554 (1990).
261 Frenzel, A., Schirrmann, T. & Hust, M. Phage display-derived human antibodies in clinical development and therapy. *mAbs* **8**, 1177-1194 (2016).
262 Almagro, J. C., Pedraza-Escalona, M., Arrieta, H. I. & Pérez-Tapia, S. M. Phage Display Libraries for Antibody Therapeutic Discovery and Development. *Antibodies* **8**, 44 (2019).
263 Zhang, Y. Evolution of phage display libraries for therapeutic antibody discovery. *MAbs* **15**, 2213793 (2023).
264 Hutchings, C. J. & Sato, A. K. Phage display technology and its impact in the discovery of novel protein-based drugs. *Expert Opinion on Drug Discovery*, 1-29
265 Ledsgaard, L. *et al.* Advances in antibody phage display technology. *Drug Discovery Today* **27**, 2151-2169 (2022).
266 Osbourn, J., Groves, M. & Vaughan, T. From rodent reagents to human therapeutics using antibody guided selection. *Methods* **36**, 61-68 (2005).
267 Kaymakcalan, Z. *et al.* Comparisons of affinities, avidities, and complement activation of adalimumab, infliximab, and etanercept in binding to soluble and membrane tumor necrosis factor. *Clin Immunol* **131**, 308-316 (2009).

268 Lu, R.-M. *et al.* Development of therapeutic antibodies for the treatment of diseases. *Journal of Biomedical Science* **27**, 1 (2020).

269 Bailly, M. *et al.* Predicting Antibody Developability Profiles Through Early Stage Discovery Screening. *MAbs* **12**, 1743053 (2020).

270 Fernández-Quintero, M. L. *et al.* Assessing developability early in the discovery process for novel biologics. *mAbs* **15**, 2171248 (2023).

271 Jain, T., Boland, T. & Vásquez, M. Identifying developability risks for clinical progression of antibodies using high-throughput in vitro and in silico approaches. *mAbs* **15**, 2200540 (2023).

272 Jain, T. *et al.* Biophysical properties of the clinical-stage antibody landscape. *Proceedings of the National Academy of Sciences* **114**, 944-949 (2017).

273 Mieczkowski, C. *et al.* Blueprint for antibody biologics developability. *mAbs* **15**, 2185924 (2023).

274 Xu, Y. *et al.* Structure, heterogeneity and developability assessment of therapeutic antibodies. *MAbs* **11**, 239-264 (2019).

275 Khetan, R. *et al.* Current advances in biopharmaceutical informatics: guidelines, impact and challenges in the computational developability assessment of antibody therapeutics. *mAbs* **14**, 2020082 (2022).

276 Haverick, M., Mengisen, S., Shameem, M. & Ambrogelly, A. Separation of mAbs molecular variants by analytical hydrophobic interaction chromatography HPLC: overview and applications. *MAbs* **6**, 852-858 (2014).

277 Tessier, P. M., Sandler, S. I. & Lenhoff, A. M. Direct measurement of protein osmotic second virial cross coefficients by cross-interaction chromatography. *Protein Sci* **13**, 1379-1390 (2004).

278 Kohli, N. *et al.* A novel screening method to assess developability of antibody-like molecules. *MAbs* **7**, 752-758 (2015).

279 Goyon, A. *et al.* Determination of isoelectric points and relative charge variants of 23 therapeutic monoclonal antibodies. *J Chromatogr B Analyt Technol Biomed Life Sci* **1065-1066**, 119-128 (2017).

280 Gupta, P. *et al.* Antibodies with Weakly Basic Isoelectric Points Minimize Trade-offs between Formulation and Physiological Colloidal Properties. *Molecular Pharmaceutics* **19**, 775-787 (2022).

281 Wardemann, H. *et al.* Predominant autoantibody production by early human B cell precursors. *Science* **301**, 1374-1377 (2003).

282 Xu, Y. *et al.* Addressing polyspecificity of antibodies selected from an in vitro yeast presentation system: a FACS-based, high-throughput selection and analytical tool. *Protein Eng Des Sel* **26**, 663-670 (2013).

283 Hötzel, I. *et al.* A strategy for risk mitigation of antibodies with fast clearance. *MAbs* **4**, 753-760 (2012).

284 Kraft, T. E. *et al.* Heparin chromatography as an in vitro predictor for antibody clearance rate through pinocytosis. *MAbs* **12**, 1683432 (2020).

285 Starr, C. G. & Tessier, P. M. Selecting and engineering monoclonal antibodies with drug-like specificity. *Current Opinion in Biotechnology* **60**, 119-127 (2019).

286 Ausserwöger, H. *et al.* Non-specificity as the sticky problem in therapeutic antibody development. *Nature Reviews Chemistry* **6**, 844-861 (2022).

287 Liu, Y. *et al.* High-throughput screening for developability during early-stage antibody discovery using self-interaction nanoparticle spectroscopy. *MAbs* **6**, 483-492 (2014).

288 Starr, C. G. *et al.* Ultradilute Measurements of Self-Association for the Identification of Antibodies with Favorable High-Concentration Solution Properties. *Mol Pharm* **18**, 2744-2753 (2021).

289 Kingsbury, J. S. *et al.* A single molecular descriptor to predict solution behavior of therapeutic antibodies. *Sci Adv* **6**, eabb0372 (2020).

290 Hong, P., Koza, S. & Bouvier, E. S. Size-Exclusion Chromatography for the Analysis of Protein Biotherapeutics and their Aggregates. *J Liq Chromatogr Relat Technol* **35**, 2923-2950 (2012).
291 Some, D., Amartely, H., Tsadok, A. & Lebendiker, M. Characterization of Proteins by Size-Exclusion Chromatography Coupled to Multi-Angle Light Scattering (SEC-MALS). *J Vis Exp* (2019).
292 Oeller, M., Sormanni, P. & Vendruscolo, M. An open-source automated PEG precipitation assay to measure the relative solubility of proteins with low material requirement. *Scientific Reports* **11**, 21932 (2021).
293 Brader, M. L. *et al.* Examination of thermal unfolding and aggregation profiles of a series of developable therapeutic monoclonal antibodies. *Mol Pharm* **12**, 1005-1017 (2015).
294 Bowers, K. & Markova, N. in *Microcalorimetry of Biological Molecules: Methods and Protocols* (ed Eric Ennifar) 33-44 (Springer New York, 2019).
295 He, F., Hogan, S., Latypov, R. F., Narhi, L. O. & Razinkov, V. I. High throughput thermostability screening of monoclonal antibody formulations. *J Pharm Sci* **99**, 1707-1720 (2010).
296 Wang, F. *et al.* Somatic hypermutation maintains antibody thermodynamic stability during affinity maturation. *Proc Natl Acad Sci U S A* **110**, 4261-4266 (2013).
297 Wu, S. J. *et al.* Structure-based engineering of a monoclonal antibody for improved solubility. *Protein Eng Des Sel* **23**, 643-651 (2010).
298 Spencer, S., Bethea, D., Raju, T. S., Giles-Komar, J. & Feng, Y. Solubility evaluation of murine hybridoma antibodies. *MAbs* **4**, 319-325 (2012).
299 Pepinsky, R. B. *et al.* Improving the solubility of anti-LINGO-1 monoclonal antibody Li33 by isotype switching and targeted mutagenesis. *Protein Sci* **19**, 954-966 (2010).
300 Kaleli, N. E., Karadag, M. & Kalyoncu, S. Phage display derived therapeutic antibodies have enriched aliphatic content: Insights for developability issues. *Proteins* **87**, 607-618 (2019).
301 Rabia, L. A., Desai, A. A., Jhajj, H. S. & Tessier, P. M. Understanding and overcoming trade-offs between antibody affinity, specificity, stability and solubility. *Biochem Eng J* **137**, 365-374 (2018).
302 Dobson, C. L. *et al.* Engineering the surface properties of a human monoclonal antibody prevents self-association and rapid clearance in vivo. *Scientific Reports* **6**, 38644 (2016).
303 van der Kant, R. *et al.* Prediction and Reduction of the Aggregation of Monoclonal Antibodies. *Journal of Molecular Biology* **429**, 1244-1261 (2017).
304 Mason, D. M. *et al.* Optimization of therapeutic antibodies by predicting antigen specificity from antibody sequence via deep learning. *Nature Biomedical Engineering* **5**, 600-612 (2021).
305 Makowski, E. K. *et al.* Optimization of therapeutic antibodies for reduced self-association and non-specific binding via interpretable machine learning. *Nature Biomedical Engineering* **8**, 45-56 (2024).
306 Parthiban, K. *et al.* A comprehensive search of functional sequence space using large mammalian display libraries created by gene editing. *MAbs* **11**, 884-898 (2019).
307 Bowers, P. M. *et al.* Mammalian cell display for the discovery and optimization of antibody therapeutics. *Methods* **65**, 44-56 (2014).
308 Leimu, L. *et al.* Epitope-specific antibody fragments block aggregation of AGelD187N, an aberrant peptide in gelsolin amyloidosis. *Journal of Biological Chemistry*, 107507 (2024).
309 Brockmann, E. C. *et al.* Synthetic single-framework antibody library integrated with rapid affinity maturation by VL shuffling. *Protein Eng Des Sel* **24**, 691-700 (2011).
310 Huovinen, T. *et al.* Two ScFv antibody libraries derived from identical VL-VH framework with different binding site designs display distinct binding profiles. *Protein Eng Des Sel* **26**, 683-693 (2013).
311 Söderberg, L. *et al.* Lecanemab, Aducanumab, and Gantenerumab - Binding Profiles to Different Forms of Amyloid-Beta Might Explain Efficacy and Side Effects in Clinical Trials for Alzheimer's Disease. *Neurotherapeutics* **20**, 195-206 (2023).

312 Jia, L. *et al.* Expression and purification of amyloid β-protein, tau, and α-synuclein in Escherichia coli: a review. *Crit Rev Biotechnol* **40**, 475-489 (2020).

313 Ree, R., Varland, S. & Arnesen, T. Spotlight on protein N-terminal acetylation. *Experimental & Molecular Medicine* **50**, 1-13 (2018).

314 Törnquist, M. *et al.* Secondary nucleation in amyloid formation. *Chem Commun (Camb)* **54**, 8667-8684 (2018).

315 O'Malley, T. T., Witbold, W. M., 3rd, Linse, S. & Walsh, D. M. The Aggregation Paths and Products of Aβ42 Dimers Are Distinct from Those of the Aβ42 Monomer. *Biochemistry* **55**, 6150-6161 (2016).

316 Maier, M. *et al.* A human-derived antibody targets misfolded SOD1 and ameliorates motor symptoms in mouse models of amyotrophic lateral sclerosis. *Sci Transl Med* **10** (2018).

317 Michalon, A. *et al.* A human antibody selective for transthyretin amyloid removes cardiac amyloid through phagocytic immune cells. *Nature Communications* **12**, 3142 (2021).

318 Nobuhara, C. K. *et al.* Tau Antibody Targeting Pathological Species Blocks Neuronal Uptake and Interneuron Propagation of Tau in Vitro. *Am J Pathol* **187**, 1399-1412 (2017).

319 Weihofen, A. *et al.* Development of an aggregate-selective, human-derived α-synuclein antibody BIIB054 that ameliorates disease phenotypes in Parkinson's disease models. *Neurobiol Dis* **124**, 276-288 (2019).

320 Hardy, J. A. & Higgins, G. A. Alzheimer's disease: the amyloid cascade hypothesis. *Science* **256**, 184-185 (1992).

321 Richards, D. B. *et al.* Therapeutic Clearance of Amyloid by Antibodies to Serum Amyloid P Component. *N Engl J Med* **373**, 1106-1114 (2015).

322 Emdin, M. *et al.* Monoclonal antibodies and amyloid removal as a therapeutic strategy for cardiac amyloidosis. *Eur Heart J Suppl* **25**, B79-b84 (2023).

323 Lambert, M. P. *et al.* Diffusible, nonfibrillar ligands derived from Abeta1-42 are potent central nervous system neurotoxins. *Proc Natl Acad Sci U S A* **95**, 6448-6453 (1998).

324 Agerschou, E. D. *et al.* An engineered monomer binding-protein for α-synuclein efficiently inhibits the proliferation of amyloid fibrils. *eLife* **8**, e46112 (2019).

325 Apetri, A. *et al.* A common antigenic motif recognized by naturally occurring human VH5-51/VL4-1 anti-tau antibodies with distinct functionalities. *Acta Neuropathol Commun* **6**, 43 (2018).

326 Aprile, F. *et al.* Selective targeting of primary and secondary nucleation pathways in Aβ42 aggregation using a rational antibody scanning method. *Sci Adv* **3** (2017).

327 Doherty, C. P. A. *et al.* A short motif in the N-terminal region of [alpha]-synuclein is critical for both aggregation and function. *Nature Structural and Molecular Biology* **27**, 249+ (2020).

328 Giasson, B. I., Murray, I. V. J., Trojanowski, J. Q. & Lee, V. M. Y. A Hydrophobic Stretch of 12 Amino Acid Residues in the Middle of α-Synuclein Is Essential for Filament Assembly. *Journal of Biological Chemistry* **276**, 2380-2386 (2001).

329 Bhopatkar, A. A. & Kayed, R. Flanking regions, amyloid cores, and polymorphism: the potential interplay underlying structural diversity. *Journal of Biological Chemistry* **299** (2023).

330 Mirecka, E. A. *et al.* Sequestration of a β-Hairpin for Control of α-Synuclein Aggregation. *Angewandte Chemie International Edition* **53**, 4227-4230 (2014).

331 Shah, D. K. & Betts, A. M. Antibody biodistribution coefficients: inferring tissue concentrations of monoclonal antibodies based on the plasma concentrations in several preclinical species and human. *MAbs* **5**, 297-305 (2013).

332 Diao, L. & Meibohm, B. Tools for predicting the PK/PD of therapeutic proteins. *Expert Opin Drug Metab Toxicol* **11**, 1115-1125 (2015).

333 Tabrizi, M. A., Tseng, C.-M. L. & Roskos, L. K. Elimination mechanisms of therapeutic monoclonal antibodies. *Drug Discovery Today* **11**, 81-88 (2006).

334 Igawa, T. *et al.* Antibody recycling by engineered pH-dependent antigen binding improves the duration of antigen neutralization. *Nat Biotechnol* **28**, 1203-1207 (2010).

335 Kamath, A. V. Translational pharmacokinetics and pharmacodynamics of monoclonal antibodies. *Drug Discov Today Technol* **21-22**, 75-83 (2016).
336 Lu, L. L., Suscovich, T. J., Fortune, S. M. & Alter, G. Beyond binding: antibody effector functions in infectious diseases. *Nat Rev Immunol* **18**, 46-61 (2018).
337 Igawa, T., Haraya, K. & Hattori, K. Sweeping antibody as a novel therapeutic antibody modality capable of eliminating soluble antigens from circulation. *Immunol Rev* **270**, 132-151 (2016).
338 Martin, P. *et al.* Alternative Strategies for Toxicity Testing of Species-Specific Biopharmaceuticals. *International journal of toxicology* **28**, 230-253 (2009).
339 Lynch, C. M., Hart, B. W. & Grewal, I. S. Practical considerations for nonclinical safety evaluation of therapeutic monoclonal antibodies. *mAbs* **1**, 2-11 (2009).
340 Bugelski, P. J. *et al.* Preclinical development of keliximab, a Primatized anti-CD4 monoclonal antibody, in human CD4 transgenic mice: characterization of the model and safety studies. *Hum Exp Toxicol* **19**, 230-243 (2000).
341 Verhelle, A. *et al.* Non-Invasive Imaging of Amyloid Deposits in a Mouse Model of AGel Using (99m)Tc-Modified Nanobodies and SPECT/CT. *Mol Imaging Biol* **18**, 887-897 (2016).
342 Davis, J. D. *et al.* Subcutaneous Administration of Monoclonal Antibodies: Pharmacology, Delivery, Immunogenicity, and Learnings From Applications to Clinical Development. *Clinical Pharmacology & Therapeutics* **115**, 422-439 (2024).
343 Dastjerdi, M. H. *et al.* Topical bevacizumab in the treatment of corneal neovascularization: results of a prospective, open-label, noncomparative study. *Arch Ophthalmol* **127**, 381-389 (2009).
344 Kim, S. W., Ha, B. J., Kim, E. K., Tchah, H. & Kim, T. I. The effect of topical bevacizumab on corneal neovascularization. *Ophthalmology* **115**, e33-38 (2008).
345 Bock, F., König, Y., Kruse, F., Baier, M. & Cursiefen, C. Bevacizumab (Avastin) eye drops inhibit corneal neovascularization. *Graefes Arch Clin Exp Ophthalmol* **246**, 281-284 (2008).
346 Koenig, Y. *et al.* Short- and long-term safety profile and efficacy of topical bevacizumab (Avastin) eye drops against corneal neovascularization. *Graefes Arch Clin Exp Ophthalmol* **247**, 1375-1382 (2009).
347 Ferrari, G. *et al.* Topical ranibizumab as a treatment of corneal neovascularization. *Cornea* **32**, 992-997 (2013).
348 Kessel, K., Mattila, J., Linder, N., Kivelä, T. & Lundin, J. Deep Learning Algorithms for Corneal Amyloid Deposition Quantitation in Familial Amyloidosis. *Ocular Oncology and Pathology* **6**, 58-65 (2020).
349 Gu, H. *et al.* Deep learning for identifying corneal diseases from ocular surface slit-lamp photographs. *Scientific Reports* **10**, 17851 (2020).
350 Hiltunen, T. *et al.* Finnish type of familial amyloidosis: cosegregation of Asp187----Asn mutation of gelsolin with the disease in three large families. *Am J Hum Genet* **49**, 522-528 (1991).
351 Mishra, S. & Venkatesh, M. P. Rare disease clinical trials in the European Union: navigating regulatory and clinical challenges. *Orphanet Journal of Rare Diseases* **19**, 285 (2024).
352 Du, Q. *et al.* Process optimization and protein engineering mitigated manufacturing challenges of a monoclonal antibody with liquid-liquid phase separation issue by disrupting inter-molecule electrostatic interactions. *mAbs* **11**, 789-802 (2019).
353 Mieczkowski, C. *et al.* Characterization and Modeling of Reversible Antibody Self-Association Provide Insights into Behavior, Prediction, and Correction. *Antibodies (Basel)* **10** (2021).
354 Makowski, E. K. *et al.* Co-optimization of therapeutic antibody affinity and specificity using machine learning models that generalize to novel mutational space. *Nature Communications* **13**, 3788 (2022).
355 Orand, T. & Jensen, M. R. Binding mechanisms of intrinsically disordered proteins: Insights from experimental studies and structural predictions. *Current Opinion in Structural Biology* **90**, 102958 (2025).

356 Simons, J. F. *et al.* Affinity maturation of antibodies by combinatorial codon mutagenesis versus error-prone PCR. *MAbs* **12**, 1803646 (2020).
357 Huhtinen, O., Prince, S., Lamminmäki, U., Salbo, R. & Kulmala, A. Increased stable integration efficiency in CHO cells through enhanced nuclear localization of Bxb1 serine integrase. *BMC Biotechnol* **24**, 44 (2024).
358 Liberis, E., Velickovic, P., Sormanni, P., Vendruscolo, M. & Liò, P. Parapred: antibody paratope prediction using convolutional and recurrent neural networks. *Bioinformatics* **34**, 2944-2950 (2018).
359 Bauer, J. *et al.* Rational optimization of a monoclonal antibody improves the aggregation propensity and enhances the CMC properties along the entire pharmaceutical process chain. *mAbs* **12**, 1787121 (2020).

TURUN
YLIOPISTO
UNIVERSITY
OF TURKU

Painosalama, Turku, Finland 2025

ISBN 978-952-02-0146-3 (PRINT)
ISBN 978-952-02-0147-0 (PDF)
ISSN 0355-9483 (Print)
ISSN 2343-3213 (Online)